ISOTOPE HYDROLOGY AND SUSTAINABILITY OF HIGH PLAINS GROUNDWATER IN NORTHEASTERN NEW MEXICO

by

Victoria Ann Blumenberg

A thesis submitted to the faculty of
The University of North Carolina at Charlotte
in partial fulfillment of the requirements
for the degree of Master of Science in
Earth Sciences

Charlotte

2018

Approved by:

_____
Dr. David Vinson

_____
Dr. Craig Allan

_____
Dr. Kate Zeigler

ABSTRACT

VICTORIA ANN BLUMENBERG. Isotope hydrology and sustainability of High Plains groundwater in northeastern New Mexico. (Under the direction of Dr. DAVID VINSON)

Observable increases in depth to water in wells throughout the High Plains Aquifer have led to growing concerns regarding the sustainability of groundwater in the High Plains region. Previous studies have pointed to overuse and the presence of paleowaters as factors contributing to the rapid declines that have been recorded. Because the High Plains Aquifer is not present or is too thin to be a productive hydrostratigraphic unit in most of northeast New Mexico, little research has been conducted on the status of groundwater there. This study aimed to fill an existing knowledge gap by analyzing 85 groundwater samples from a four-county study area in northeast New Mexico. Samples were anlalyzed for $\delta^{18}O$, δD, DIC, $\delta^{13}C$-DIC, and major ion concentrations to evaluate geochemistry and the possibility that paleowaters are present.

With the exception of one sample (M8), samples in this study did not exhibit characteristics of potential paleowaters. Therefore, a unique isotopic signature of paleowaters was not identified within the study area. Isotopic composition seems to be driven instead by the elevation effect, calculated to have a lapse rate of -0.31‰ per every 100m of elevation increase for all samples. Isotopic composition also appears to match seasonal patterns observed in nearby studies (winter-dominated recharge), but seasonal contributions could not be definitively determined by this study.

Four main hydrostratigraphic units were identified throughout the study area, three of which exhibit typical groundwater evolution behavior. The shallower, younger, alluvial unit contains enriched, high salinity groundwater, indicating high rates of evaporation after precipitation, but prior to recharge. Major ion analysis yielded 42 samples of the Ca^{2+} $Mg^{2+}HCO_3^-$ type, making this the most common type in the study area, followed by the Na^+ HCO_3^- type with

25 samples. Evidence of modern recharge was found by way of high nitrate concentrations in three locations in the western and southwestern portion of the study area.

Three locations were selected for tritium analysis to test the hypothesis that recharge occurs along watercourses and focused points at the mountain front. This data was combined with previously unpublished data to expand the discussion of modern recharge in this region. Locations along watercourses were found to contain tritium, but locations along the mountain front were not. Ultimately, locations that do not have detectable amounts of tritium were deemed to be unsustainable and are representative of groundwater mining. The finding of this study that tritium is not present in mountain front waters, where recharge is expected to occur in this setting, highlights the need for further research investigating recharge processes in northeastern New Mexico.

ACKNOWLEDGMENTS

TABLE OF CONTENTS

LIST OF TABLES

LIST OF FIGURES

1   Introduction

1.1   Water availability and its relationship to regional geology and hydrology

Water shortages have the potential to cause food shortages, famine, massive loss of life, or military conflicts. Despite the increasing need for water and growing threat of a food crisis, the GRACE mission, launched by NASA in 2001, has shown significant reductions in water storage throughout the world. Globally, 85% of groundwater extraction is for agricultural purposes (Harrington et al., 2007), closely related to food and livestock production. The most drastic changes in storage have been observed in highly populated and/or semi-arid to arid areas, with semi-arid regions that receive little recharge being the most vulnerable (Richey et al., 2015). In order to prevent food shortages, famine, massive loss of life, and/or military conflicts, a more thorough understanding of change of storage is necessary, with emphasis on the aquifers that are the most heavily utilized. Although satellite estimates are helpful, they provide estimates that only work for shallow groundwater. A greater understanding of deeper groundwater characteristics can be achieved through regional groundwater data collection, which can be pieced together in an effort to understand and responsibly manage this resource.

The High Plains region is roughly 450,000 km^2, lying beneath what are now eight states in the U.S.: New Mexico, Texas, Oklahoma, Colorado, Kansas, Wyoming, Nebraska, and South Dakota (Scanlon et al., 2012). The geologic history of the High Plains region, shown in **Error! eference source not found.**, is marked by alternating periods of deposition and erosion resulting in a suite of sedimentary rock layers. During the Permian Period, 290-240 million years ago (Ma), most of what is now the High Plains was covered by an inland sea (Gutentag et al., 1984) surrounded by granitic uplifts that were part of the Ancestral Rocky Mountains orogeny. Material from the Ancestral Rocky Mountains was carried into the surrounding basins, forming river and alluvial deposits known as the Sangre De Cristo Formation. As this ancient sea retreated, the Glorieta Sandstone was deposited. The latest Permian and Early to Middle Triassic Period (240-205 Ma) is represented by an unconformity caused by a period of erosion, meaning

that time interval is absent from the rock record. In the Late Triassic Period, rivers and streams flowing toward present-day Nevada deposited the Dockum Group, aka Chinle Formation. This depositional period was followed by the breakup of Pangea and a subsequent disconformity in which an estimated 30 million years are missing from the geologic record (New Mexico Bureau of Geology and Mineral Resources, 2003).

Following the rifting event that broke up Pangea roughly 200 million years ago, desert formation of a large dunefield in the region, represented today by the Exeter Sandstone, filled in over the folded Dockum Group. The Bell Ranch Formation was deposited next and is a deposit rich in gypsum resulting from playas developing as the dune field retreated. These are followed by deposition of fluvial mudstones and sandstones as well as lacustrine limestones in the Morrison Formation that can negatively affect carbon dating of the groundwater because of the ^{14}C-free carbonate content of limestones. The late Cretaceous Period (96 – 63 million years ago) saw the return of an interior seaway that brought deposition of the Lytle Sandstone, Glencairn Formation, Dakota Sandstone, and Niobrara Group. The Dakota Sandstone is a thick deposit of sand resulting from the first transgression of the Cretaceous Interior Seaway and is one of the primary hydrologic units in the study area. The Niobrara Group was deposited when the seaway returned and the entire region was under water. The Niobrara Group is primarily shale, and wells drawing water from it are high in sulfate. From the Late Cretaceous to Early Miocene, there is a disconformity in which the second and third transgressions of the interior seaway are missing. At the same time, mountain building in the west began (the Laramide Orogeny).

As the Rocky Mountains were uplifted in the west, a rain shadow developed, triggering a transition to an arid climate (Gutentag et al., 1984). This period of mountain building also led to stream incision and erosion adjacent to the mountain front (Gutentag et al., 1984). As more material became available from the mountains, streams began to transport large volumes of sediment and deposit them as alluvial fans, filling in the eroded landscape (Gutentag et al., 1984). This is the most productive lithostratigraphic unit of the High Plains region – the Miocene -

Pliocene Ogallala Formation, which overlies the Triassic, Jurassic, and Cretaceous units described above (Becker et al., 2002). The Ogallala Formation consists of clays, silts, sands, and gravels (Gutentag et al., 1984). Younger alluvial sediments are hydraulically connected to the Ogallala Formation, together representing a hydrostratigraphic unit known as the High Plains Aquifer (HPA) shown in Figure 2 (Becker et al., 2002). Saturated thickness of the HPA, which determines maximum possible pumping rates, is estimated to range from 0m to 305m (Dennehy et al., 2002). Haccker et al. (2016) determined that saturated thickness less than 9m is indicative of transmissivity that cannot withstand high-capacity irrigation wells, thereby rendering that part of the aquifer depleted.

Younger volcanics armor the complex topography in the area between Raton and Clayton, including basalts and dacites related to the Raton-Clayton volcanic field, the Ocate volcanic field and Sierra Grande (Sayre and Ort, 2011). These rocks range from eight million years to 40,000 years in age and create a landscape of inverted topography (Sayre and Ort, 2011). Much of these volcanic rocks now strongly control the elevation differences across the study area.

System	Series	Geologic unit	Thickness, in feet	Physical character
QUATERNARY	Pleistocene and Holocene	Valley-fill deposits	0 to 60	Stream-laid deposits of gravel, sand, silt, and clay associated with the most recent cycle of erosion and deposition along present streams. Forms part of High Plains aquifer where hydraulically connected to underlying Quaternary and Tertiary deposits.
		Dune sand	0 to 300	Fine to medium sand with small amounts of clay, silt, and coarse sand formed into hills and ridges by the wind. Forms part of High Plains aquifer where saturated.
		Loess	0 to 250	Silt with lesser amounts of very fine sand and clay deposited as windblown dust.
	Pleistocene	Unconsolidated alluvial deposits	0 to 550	Stream-laid deposits of gravel, sand, silt, and clay locally cemented by calcium carbonate into caliche or mortar beds. Forms part of High Plains aquifer where hydraulically connected laterally or vertically to Tertiary deposits.
TERTIARY	Miocene	Ogallala Formation	0 to 700	Poorly sorted clay, silt, sand, and gravel generally unconsolidated; forms caliche layers or mortar beds when cemented by calcium carbonate. Includes units equivalent to the locally used terms "Ash Hollow," "Kimball," "Sidney Gravel," and "Valentine" Members or Formations assigned to the Ogallala Formation or "Group," and Delmore and Laverne Formations. Ogallala comprises large part of High Plains aquifer where saturated.
		Arikaree Group	0 to 1000	Predominantly massive very fine to fine-grained sandstone with localized beds of volcanic ash, silty sand, siltstone, claystone, sandy clay, limestone, marl, and mortar beds. Includes units assigned to the Hemingford Group of Lugn (1938), Marsland Formation, Rosebud Formation used in South Dakota by Harksen and Macdonald (1969), and Sheep Creek Formation. Also includes units equivalent to Gering Formation, Harrison Sandstone, and Monroe Creek Sandstone. Forms part of the High Plains aquifer.
	Oligocene	White River Group	0 to 700	Upper unit, Brule Formation, predominantly massive siltstone containing sandstone beds and channel deposits of sandstone with localized lenticular beds of volcanic ash, claystone, and fine sand. The Brule Formation is considered part of the High Plains aquifer only where it contains saturated sandstones or interconnected fractures. Lower unit, Chadron Formation, mainly consists of varicolored, bentonitic, loosely to moderately cemented clay and silt that contains channel deposits of sandstone and conglomerate.
CRETACEOUS	Upper Cretaceous	Undifferentiated rocks	0 to 8000	Shales, chalks, limestones, and sandstones. Upper part may contain lignite and coal beds. Unit includes Belle Fourche and Carlile Shales, Codell and Fox Hills Sandstones, Frontier Formation, Graneros Shale, Greenhorn Limestone, Lance Formation, Niobrara Chalk or Formation, and Pierre Shale.
	Lower Cretaceous	Undifferentiated rocks	0 to 700	Fine- to medium-grained, thin-bedded to massive cliff-forming sandstone interbedded with shale. Black and varicolored shale and thin- to thick-bedded limestone. Includes units equivalent to Fredericksburg and Washita Groups; Dakota and Purgatoire Formations; Antlers Sand of Hill (1894), Cheyenne, Fall River, Lakota, Mesa Rica, and Newcastle Sandstones; and Fuson, Kiowa, Mowry, Skull Creek, and Tucumcari Shales.
JURASSIC	Middle and Upper Jurassic	Undifferentiated rocks	0 to 600	Varicolored shale, fine- to very coarse grained sandstone, limestone, dolomite, and conglomerate. Includes units equivalent to Entrada and Exeter Sandstones, and Morrison and Sundance Formations.
TRIASSIC	Upper Triassic	Dockum Group	0 to 2000	Upper unit, Trujillo Formation, varicolored siltstone, claystone, conglomerate, fine-grained sandstone, and limestone. Lower unit, Tecovas Formation, varicolored fine- to medium-grained sandstone with some claystone and interbedded shale. Include units equivalent to Chinle and Redondo Formations, and Santa Rosa Sandstone.
PERMIAN	Lower and Upper Permian	Undifferentiated rocks	300 to 3000	Interbedded predominantly red-shale, siltstone, sandstone, gypsum, anhydrite, dolomite, bedded salt, and local limestone beds. Includes Artesia, Council Grove, Nippewalla Groups; Quartermaster Formation, Sumner and Whitehorse Groups.

Figure 1: General overview of geologic units of the High Plains region (Gutentag et al., 1984).

4
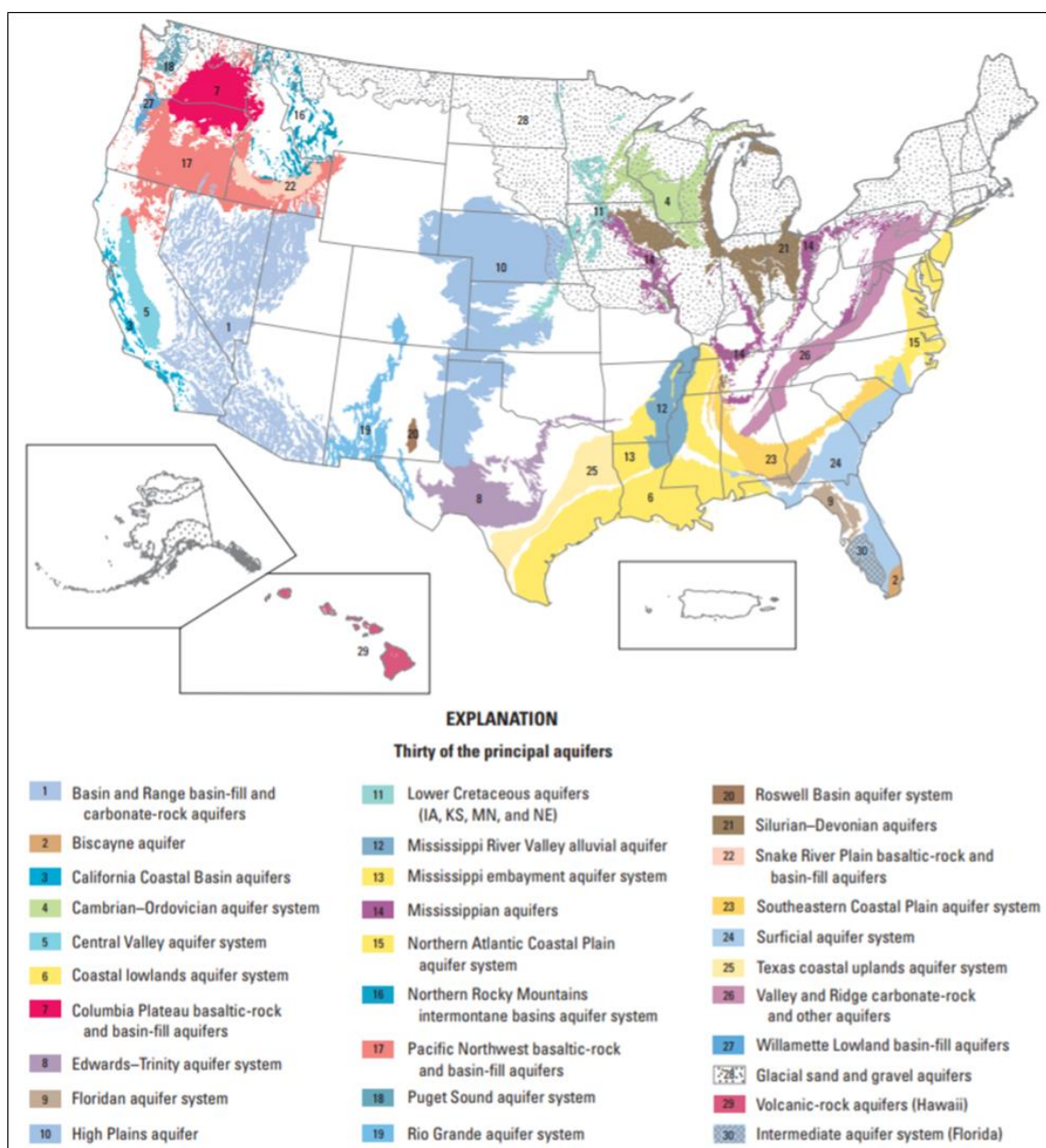
Figure 2: Map of the principal aquifers in the United States. Number 10 is the High Plains Aquifer (HPA), which extends into eastern New Mexico (Reilly et al., 2008).

Prior to the discovery of groundwater in this region, land use was limited by climate conditions, so rain-fed/dry-land agriculture was predominant (Harrington et al., 2007). Annual precipitation in the Central and Southern High Plains is roughly 406mm – 508mm (Becker et al., 2002), with an observable trend of lower precipitation in the west and higher precipitation in the

east (Nativ and Riggio, 1989). Nativ and Riggio (1989) found that the Gulf of Mexico produces most of the summer precipitation, while the eastern Pacific Ocean produces most of the winter precipitation in the region. Nativ and Riggio (1989) also found that roughly two thirds of annual precipitation falls during the summer months, when potential evapotranspiration rates are the highest.

Discovery and subsequent pumping of the HPA was the solution to the Dust Bowl in the 1930s (Steward and Allen, 2016). The seemingly endless supply of groundwater was used to supplement low amounts of precipitation, quickly repairing the damaged land and agriculture industry in the region. Irrigation wells first appeared in the south, and were developed in a northward trend over the next few decades, transforming the entire overlying area into a system dependent on groundwater (Harrington et al., 2007). Water withdrawals continued to grow as irrigation technology improved. Due to the high agricultural intensity and relatively low rainfall of the region, an estimated 23% (Butler et al., 2013) to 30% of the total groundwater pumped in the United States for irrigation now comes from the High Plains aquifer (Dennehy et al., 2002). Groundwater from the High Plains aquifer supports irrigated crops, crops for feed, and 82% of the people who live above it (Dennehy et al., 2002). "Of the total crop production in the United States, the High Plains Aquifer area accounts for about 19% of the wheat, 19% of the cotton, 15% of the corn and 3% of the sorghum," while also accounting for 18% of the cattle production (Dennehy et al., 2002). In fact, 93-97% of the crops grown in this region are grown for the purpose of feeding the cattle industry (Esnault et al., 2014). As a result, the High Plains region of the United States and its agricultural products were worth ~$35 billion in 2007 (Scanlon et al., 2012). Unfortunately, these crops have a high water footprint, resulting in higher rates of consumption which put more stress on the underlying aquifer (Esnault et al., 2014).

Increasing depths to water in wells were observed as early as 1940 in the High Plains region (Steward and Allen, 2016). An analysis cited by Haacker et al. (2016) found that "depth to water is one of the primary determinants of the price of irrigable farmland on the High Plains."

Concern over declining water levels in parts of the High Plains aquifer prompted the development

of a water-level monitoring program in 1984 (Dennehy et al., 2002). Since then, several studies

have attempted to quantify how much groundwater has been depleted in an effort to estimate

when it will fail. A common method used for these estimations is data interpolation based on

historical well measurements. Steward and Allen (2016) matched well depth measurements to a

logistic curve to interpolate backward in time, estimating pre-development levels of saturated

thickness throughout the aquifer. These estimates were compared to depletion rates to project

forward to the year 2110. The authors ultimately estimated that by 2110 there will be significant

decreases of saturated thickness in the southern and central High Plains aquifer. Texas will be the

most impacted, reaching 61% depletion. New Mexico will also be severely impacted with an

estimated 49% depletion from pre-development conditions (Steward and Allen, 2016).

Haacker, et al. (2016), in an effort to generate a more accurate predevelopment map of

water levels in the High Plains aquifer, modified previous methods of data interpolation using

well depth measurements. The resulting map indicates much larger volumes of predevelopment

storage than previously thought, or 4230 km^3. Comparing a higher estimate of predevelopment

volume to today's estimated volume suggests that humans have depleted more over time than

other studies have previously calculated. Using this new rate of depletion, future projections

were recalculated. This study found that water storage values in the southern and central High

Plains were low to begin with, and are experiencing the most rapid changes. While they estimate

that 40% of the aquifer will no longer be suitable for agriculture by 2100, they believe that large

portions in the southern and central High Plains will be depleted within decades (Haacker et al.,

2016). Scanlon et al. (2012) claimed that only 8% has been depleted since predevelopment, but

also confirmed that depletion is not uniform, with roughly 1/3 of that occurring in only 4% of the

aquifer which is intensely irrigated but has little or no natural recharge.

The obvious implication of groundwater depletion is an eventual decline in food

production occurring at precisely the time more food is needed for a growing population. A case

study in Wichita County, Kansas found a direct correlation between high rates of depletion and high rates of land use change away from irrigation (Harrington et al., 2007). Steward et al. (2013) found that water reductions today can increase the lifespan of the aquifer, ultimately yielding more production over time. Unfortunately, this comes at the cost of reducing production today. Steward et al. (2013) show that an 80% reduction in water use, while comparable to recharge rates, can only produce enough feed to support 12% of the current cattle population. Still, water reductions today may extend the lifespan of the aquifer until we gain a better understanding of this region and find a way to match depletion rates with recharge rates while maintaining production (Steward et al., 2013).

The goal of water management in this region is not to refill the aquifer, but to manage what is left in such a way that withdrawals, both from groundwater abstraction and discharge to support stream flow, are equal to recharge. This would effectively put an end to depletion and ensure a sustainable water future. With pre-development volume and depletion rate estimates available, recharge (defined as water reaching the water table) is studied to assist in water management decisions (Hiscock and Bense, 2014). Low precipitation rates, coupled with high potential evapotranspiration rates, suggests low recharge dominated by winter precipitation (Nativ and Riggio, 1989). In general, three types of studies are used to estimate the amount of recharge to the water table or the rate at which water moves through the unsaturated zone: stable isotopes in precipitation, isotope patterns of evaporation, and peak displacement and mass balance equations (Koeniger et al., 2016). Recharge rates in this region are highly variable, with Becker et al. (2002) estimating 1 – 47mm/year, Nativ and Riggio (1989) estimating 0 – 41mm/year, and Nativ and Riggio (1989) estimating 13 – 82mm/year near playas. There is still a debate as to the role that playas play in providing recharge (Nativ and Riggio, 1989).

Rosenberg et al. (1999), Ng et al. (2010), Crosbie et al. (2013) and Thomas et al. (2016) all bring to light that precipitation intensity (the amount of precipitation that falls over the duration of a storm event) may also have an impact on recharge, noting the episodic patterns of recharge

observed in the High Plains region. Thomas et al. (2016) concluded that "small changes in precipitation intensity result in magnified changes in groundwater recharge" and Crosbie et al. (2013) estimated a 2% change in recharge for every 1% change in precipitation.

Changes in recharge are thought to be the result of a combination of variables, notably the ability for excess runoff to escape evapotranspiration and vegetation in higher intensity events (Ng et al., 2010). Variables affecting recharge have received a lot of attention as we attempt to predict climate change patterns. Although global circulation models (GCMs) generally predict an increase in precipitation with an increase in global temperatures, predictions on a regional scale are highly uncertain (Ng et al., 2010). Rosenberg et al. (1999) predicted decreased recharge in all scenarios because of increased potential evapotranspiration, Ng et al. (2010) predicted a -75% - +35% change in recharge, and Crosbie et al. (2013) predicted a median of -3% and -10% change in recharge in the Central and Southern High Plains, respectively. Ultimately, uncertainties in the future of groundwater recharge lie in the uncertainty of climate change models and the uncertain nature of the response of recharge to changes in precipitation (Ng et al., 2010).

1.2 Groundwater residence time

Separate from, but related to, recharge, is the concept of groundwater residence time since recharge, often simplified to groundwater "age." Whereas recharge estimates describe the amount of water reaching the water table (Hiscock and Bense, 2014), Suckow (2014) defines idealized groundwater age as "the time difference that a water parcel needs to travel from the groundwater surface to the position where the sample is taken." The concept of age is complicated by mixing processes below the groundwater surface – groundwater molecules each move along different paths that result in mixing of waters of differing ages and waters from different recharge zones (Dutton, 1995; Clark and Fritz, 1997; Bethke and Johnson, 2002; Suckow, 2014). For the purpose of this study, "age" is referred to as residence time and is represented by the average amount of time since recharge for the total molecules in each sample (Bethke and Johnson, 2002). Estimates of residence time distinguish between groundwater resources that are replenishing quickly

enough to be consumed sustainably and groundwater resources that are not, abstraction of which is referred to as water mining.

Water molecules themselves cannot be used to calculate long residence times (Suckow, 2014), although tritium is itself part of the water molecule and can be used to calculate very short residence times of waters recharged within the last ~70 years. Several different approaches have been developed to measure long residence times, each of which yields different clues as to recharge conditions, sources of recharge, and subsurface flow paths (McGuire et al., 2005; Suckow, 2014). One main approach, and the focus of this study, is to compare the isotopic composition of groundwater samples to that of modern day precipitation, discussed in section 1.2.1 (Craig, 1961; Rozanski et al., 1993; Dutton, 1995; Clark and Fritz, 1997; Plummer et al., 2004; Dutton et al., 2005; Hiscock and Bense, 2014). Other approaches include analyzing hydrochemical facies and groundwater evolution, measuring dissolved inorganic carbon (DIC) and $\delta^{13}C$, and measuring dissolved gases such as tritium and ^{14}C, discussed in section 1.2.2 (Clark and Fritz, 1997; McMahon et al., 2004; Plummer et al., 2004; Suckow 2014)

1.2.1 Stable Isotopes

Isotopes are variations of the same element that have equal protons but a different number of neutrons, resulting in differences in atomic mass (Clark and Fritz, 1997). The stable isotopes in precipitation are ^{1}H, ^{2}H, ^{18}O, and ^{16}O. Isotopes require different amounts of energy to separate them because of the differences in bond strength (Clark and Fritz, 1997). Heavier isotopes have a stronger bond that requires more energy to break than lighter isotopes with weaker bonds (Clark and Fritz, 1997). Different energy requirements result in preferential evaporation of ^{1}H and ^{16}O into vapor and preferential condensation of ^{2}H and ^{18}O into precipitation, known as fractionation (Clark and Fritz, 1997). As mentioned previously, the difference in atomic mass causes proportional fractionation between H and O isotopes. Fractionation causes spatial variation in the isotopic signature of meteoric waters based on

latitude, continentality, elevation, rain-out, seasonality, and climate change (Clark and Fritz, 1997; Dutton et. al, 2005).

When an air mass cools, fractionation condenses heavier isotopes into precipitation which are then expelled from the vapor first (Clark and Fritz, 1997). As the air mass moves further from its source it gradually loses the heavier isotopes and becomes isotopically depleted, a process known as "rain-out" (Clark and Fritz, 1997). Therefore, air masses that have moved toward higher latitudes or further inland tend to have more negative $\delta^{18}O$ and δD values (Clark and Fritz, 1997). Rain-out also occurs when an air mass is orographically uplifted and cools adiabatically (Clark and Fritz, 1997). Known as the elevation effect, isotopically depleted precipitation is delivered to higher elevations, meaning more negative $\delta^{18}O$ values can be found in mountainous regions (Rozanski et al., 1993; Clark and Fritz, 1997). Clark and Fritz (1997) showed that depletion of $\delta^{18}O$ generally varies between -0.15 and -0.5‰ for every 100 meter rise in elevation. A study conducted by Dutton et al. (2005) found that the rate for North America is -0.29‰ for every 100 meter rise in elevation. The rate was calculated using data heavily based in the western United States, providing a reasonable comparison for this study (Dutton et al., 2005). Seasonal changes in temperature at the vapor source can also result in different isotopic compositions of winter and summer precipitation, while seasonal changes at the point of precipitation determine how much is lost to evapotranspiration (Clark and Fritz, 1997).

These variables show that the isotopic composition of meteoric water is dependent on temperature and amount of precipitation, thereby producing unique isotopic signatures of climatic conditions at the time of the precipitation event. The unique isotopic signatures are then recorded in the water that escapes runoff and evapotranspiration, reaching the water table and becoming groundwater recharge. A useful method of assessing potential influences on groundwater isotopic data is to map it and analyze the spatial distribution. Figure 3 provides an example of this method from a study conducted by Plummer et al. (2004) in the Rio Grande Basin, New Mexico.
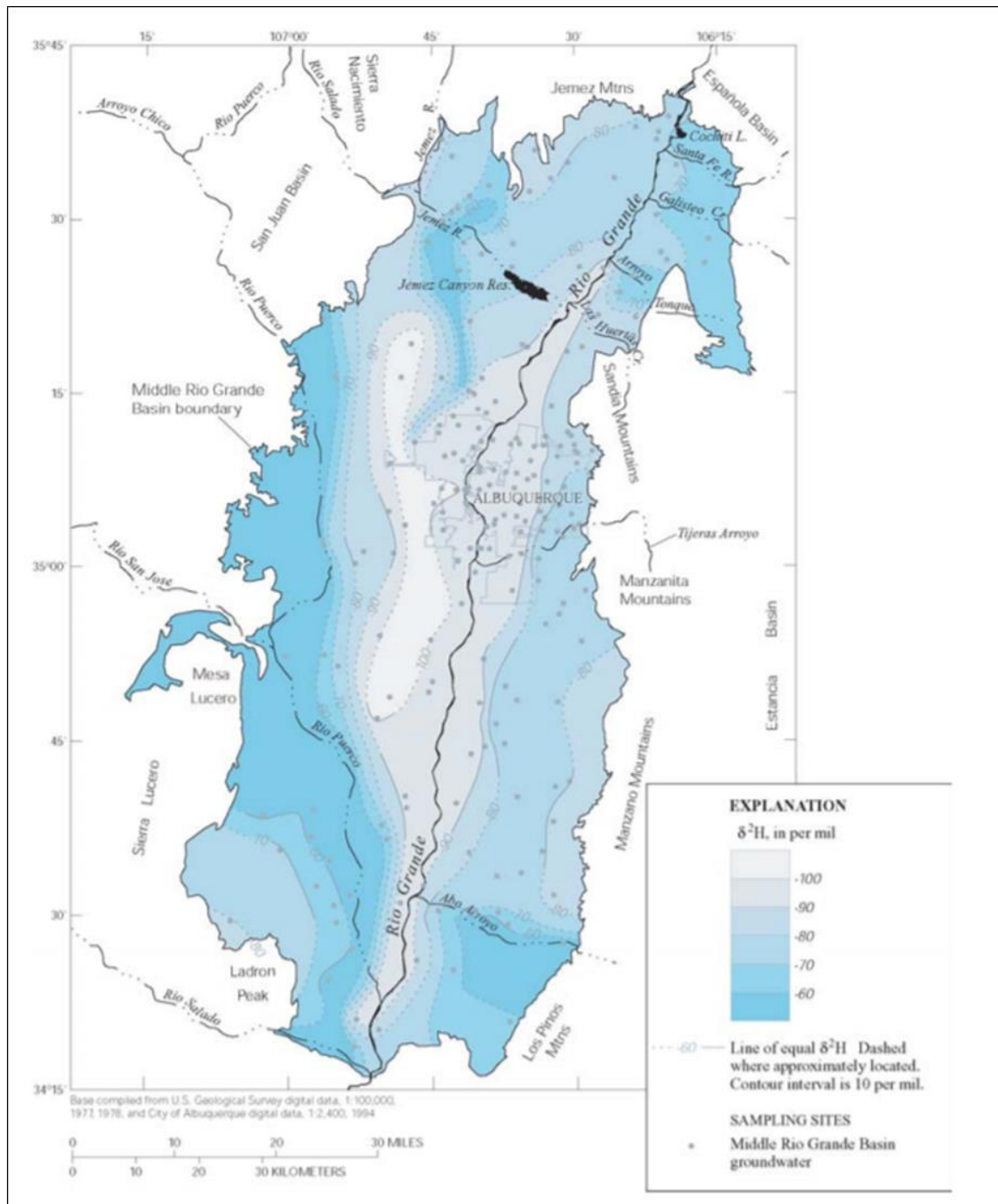
Figure 3: Example of mapping the spatial distribution of stable isotope data with interpolated contours of equal δD as a method of data interpretation (Plummer et al., 2004).

In 1961 a global program to analyze the isotopic composition of precipitation was instituted by the International Atomic Energy Agency (IAEA) and the World Meteorological Organization (WMO) (Rozanski et al., 1993). Long term averages of the isotopic data collected

from stations within this monitoring network found a predictable and linear relationship between δ^2H and $\delta^{18}O$ known as the Global Meteoric Water Line (GMWL). This relationship has been calculated as $\delta^2H = (8.17 \pm 0.06)\delta^{18}O‰ + (10.35 \pm 0.65)$ ‰ VSMOW (Rozanski et al.,1993), $\delta^2H = 8.13\delta^{18}O‰ + 10.8‰$ VSMOW by Clark and Fritz (1997), and commonly simplified to $\delta^2H = 8\delta^{18}O‰ + 10‰$ VSMOW (Craig, 1961; Rozanski et al., 1993; Clark and Fritz, 1997). δ values, expressed in parts per thousand (permil), represent the difference from the Vienna Standard Mean Ocean Water (VSMOW) reference, and are calculated using the following equation (Clark and Fritz, 1997):

$$\delta^{18}O_{sample} = ((({}^{18}O/{}^{16}O)_{sample} / ({}^{18}O/{}^{16}O)_{reference}) - 1) \times 1000 ‰ \text{ VSMOW}$$

The creation of the GMWL provided a base for comparison with graphs generated by the isotopic composition of groundwater samples. Comparing groundwater samples to precipitation data can result in important interpretations: (1) the slope and intercept of the line when δD is plotted against $\delta^{18}O$ (meteoric water lines); (2) the location of data points along these meteoric water lines, representing cooler or warmer conditions (i.e. winter vs. summer precipitation or differences in climate conditions); and (3) the effects of evaporation which causes a predictable excursion from the lines (lower slope than the GMWL). These interpretations can assist in determining if groundwater matches recent precipitation or that of a different paleoclimate (Hiscock and Bense, 2014). Because fractionation is temperature dependent, cold regions have depleted precipitation, falling at lower points along the GMWL, while warm regions have enriched precipitation, falling at higher points on the GMWL (Clark and Fritz, 1997). Groundwaters recharged under cooler climatic conditions are therefore typically found to be isotopically depleted compared to modern precipitation, falling at more negative values along the GMWL or having a displaced line altogether, as seen in arid regions (Clark and Fritz, 1997).

Figure 4 illustrates an example of comparing a large set of groundwater samples to the GMWL, taken from Plummer et al. (2004). This figure illustrates the importance of analyzing the relationship of the samples to the GMWL itself, as well as their position along the line. Dutton (1995) also used these interpretations to compare unconfined and confined aquifers throughout the High Plains (Figure 5). Studies using a multi-tracer approach conducted by Dutton (1995) and Plummer et al. (2004) identified paleowaters that fall at more negative values along the GMWL but do not deviate from the line (Figure 4 and Figure 5). This study applies a similar technique used by Plummer et al. (2004) and Dutton (1995) in northeastern NM.

While the GMWL is a useful tool for comparing groundwater isotopes to modern precipitation, it is a composite of the annual averages of many LMWLs. The slope and y-intercept of the GMWL differ from regional and local patterns (Clark and Fritz, 1997). Variations at the source of water vapor such as humidity, salinity, wind speed, and sea surface temperature, as well as variations in elevation, seasonality, latitude, and continentality at the site of precipitation all affect the LMWL (Clark and Fritz, 1997). Because local meteoric waters can differ greatly from global averages, use of a LMWL for detailed groundwater analysis yields more accurate comparisons (Clark and Fritz, 1997).
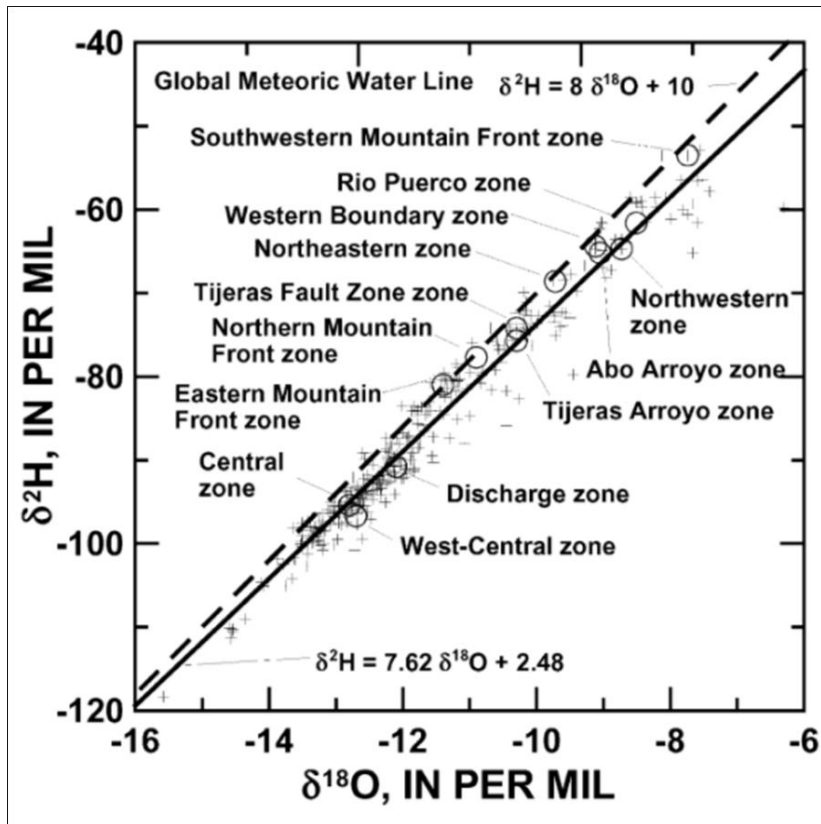
Figure 4: Example of plotting groundwater samples (solid line) in comparison to the Global Meteoric Water Line (dashed line) to analyze proximity to, and position along, the line. Plummer et al. (2004) analyzed samples taken in the Rio Grande Basin, New Mexico.
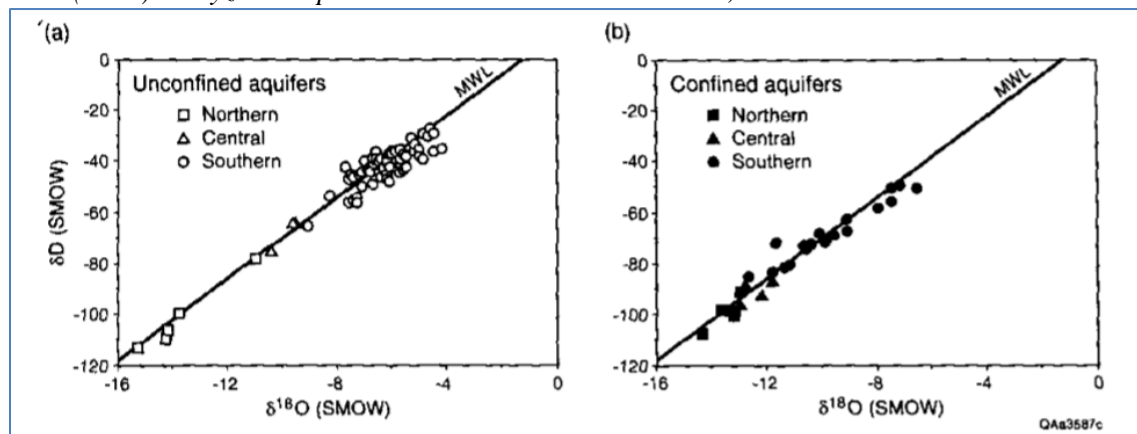
Figure 5: Example of plotting groundwater samples in comparison to the Global Meteoric Water Line to analyze proximity to, and position along, the line. Dutton (1995) compared water samples in unconfined and confined aquifers in the northern, central, and southern High Plains.

15

1.2.2   Other methods for estimating groundwater residence time

1.2.2.1   Hydrochemical facies

"A hydrochemical facies is a distinct zone of groundwater that can be described as having cation and anion concentrations with definite limits" (Hiscock and Bense, 2014). Hiscock and Bense (2014) list the principal cations in groundwater as Na^+, Ca^{2+}, Mg^{2+}, and the anions as Cl^-, HCO_3^-, and SO_4^{2-}. Hydrochemical analysis of these ions will not yield a numerical estimate of residence time, but will provide general clues because of the typical changes observed along groundwater flowpaths (Figure 6) (Hiscock and Bense, 2014). This evolutionary pattern was confirmed in a study in the Central High Plains by McMahon et al. (2004), recording a progression from low to high concentrations of SO_4^{2-} as water moved downgradient. Aside from analyzing the six major ions, the presence of elevated concentrations of nitrate (NO_3^-) has been linked to the use of fertilizers and excess animal waste (McMahon et al., 2004; Hiscock and Bense, 2014). In an area dominated by agricultural land use, elevated concentrations of nitrate could indicate the recent recharge is present (McMahon et al., 2004; Gurdak and Qi, 2006; Hiscock and Bense, 2014).
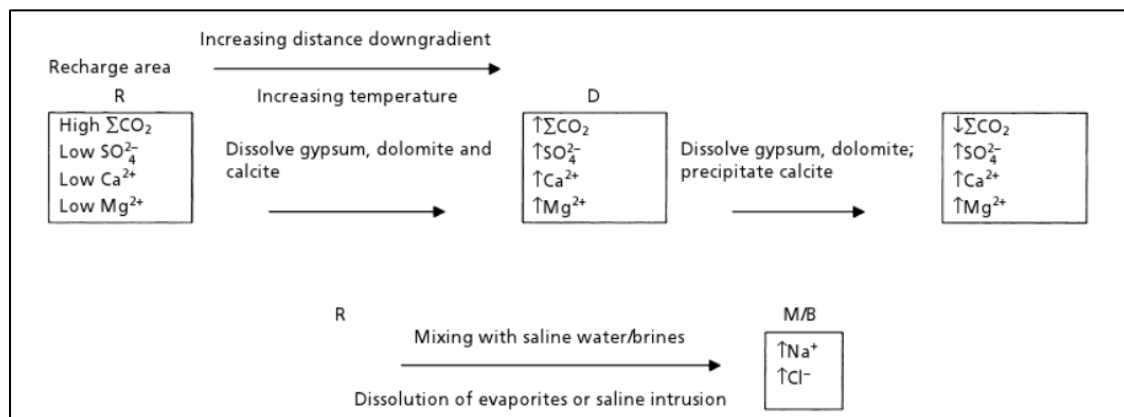
Figure 6: Model of chemical evolution of groundwater from Hiscock and Bense (2014).

1.2.2.2   DIC, $\delta^{13}C$, and ^{14}C

DIC is comprised of CO_2 (dissolved CO_2), H_2CO_3 (carbonic acid), HCO_3^- (bicarbonate), and CO_3^{2-} (carbonate) (Clark and Fritz, 1997). $\delta^{13}C$-DIC is the ratio of ^{13}C to ^{12}C in reference to the standard Vienna Pee Dee Belemnite (VPDB), a marine deposit defined to be 0‰ (Clark and Fritz, 1997). The atmospheric level of $\delta^{13}C$ is ~ -6.4‰ (Clark and Fritz, 1997). As precipitation percolates downward through the unsaturated zone, water encounters and dissolves CO_2 gas in soil pores (Clark and Fritz, 1997). CO_2 gas in soil has very negative values of $\delta^{13}C$-DIC, around -25‰, because it is the result of bacteria breaking down plant derived organic material with very negative values of $\delta^{13}C$-DIC (Clark and Fritz, 1997). The amount of CO_2 gas that is dissolved into the water is determined by pH, and together they form a weak carbonic acid that is capable of weathering rock (Clark and Fritz, 1997). When water reaches the water table, it has significantly negative values of $\delta^{13}C$-DIC (Figure 7) (Clark and Fritz, 1997). At the water table surface, water still has access to soil gas which will continue to dissolve and drive the $\delta^{13}C$-DIC values down (Clark and Fritz, 1997).

Once water descends below the water table surface, it no longer interacts with soil gas. The weak carbonic acid will dissolve calcium carbonate, a process that consumes carbonate acidity, buffering pH (Clark and Fritz, 1997). The reaction shifts the distribution of carbon species in DIC from CO_2 and H_2CO_3 to HCO_3^-, and CO_3^{2-}. Calcium carbonate also has $\delta^{13}C$-DIC values closer to zero, so carbonate dissolution moves groundwater $\delta^{13}C$-DIC to less negative values than those seen at the water table (Clark and Fritz, 1997).

In most situations, groundwater that has less negative $\delta^{13}C$-DIC values and relatively high concentrations of HCO_3^-, and CO_3^{2-} has likely been interacting with aquifer material for longer than groundwater with very negative $\delta^{13}C$-DIC values and relatively high concentrations of CO_2 and H_2CO_3. HCO_3^-, and CO_3^{2-} are also known to comprise carbonate alkalinity, so very alkaline water may have a longer residence time (Clark and Fritz, 1997).
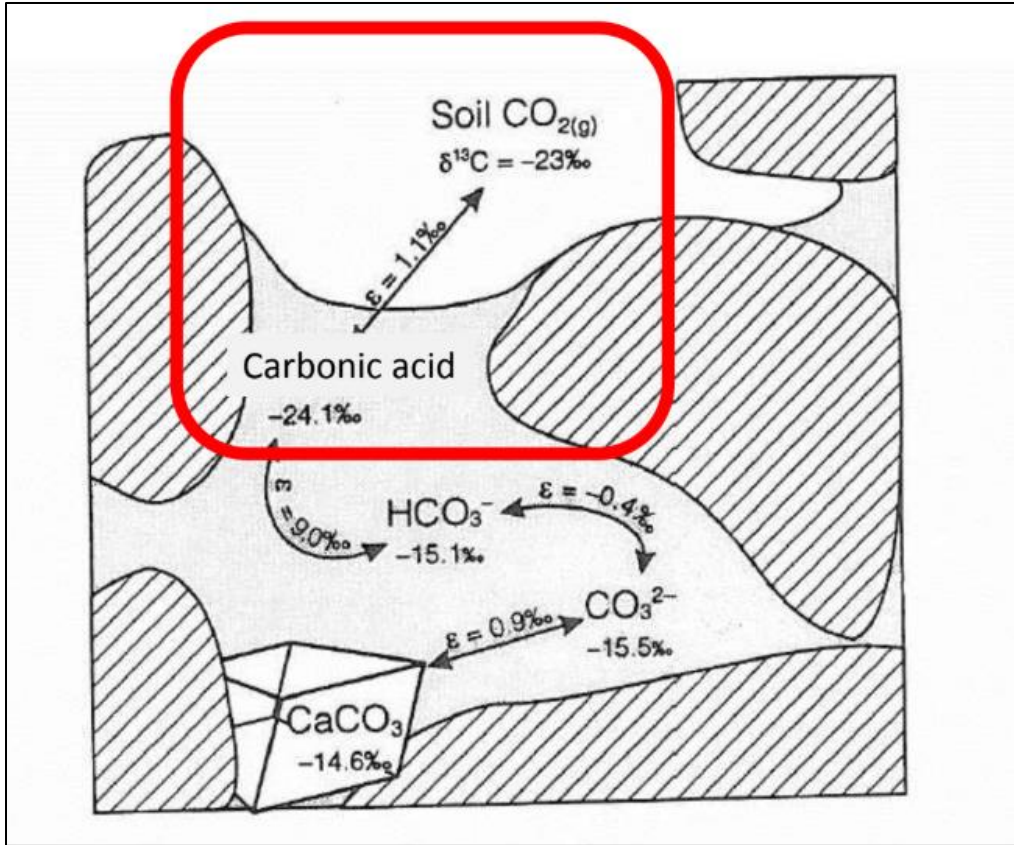
Figure 7: Diagram of δ¹³C-DIC progression as water moves from soil to deep in the aquifer, modified from Clark and Fritz, 1997.

A more direct way to estimate residence time of water using DIC is to measure the ^{14}C activity in DIC, known as radiocarbon dating. This process assumes that the initial ^{14}C concentration is known, and that the system is not open to subsequent gains or losses of ^{14}C (Clark and Fritz, 1997). Clark and Fritz (1997) report that at the surface, ^{14}C is approximately 100pmC (percent of modern carbon). Weapons testing in the 1950s and early 1960s released additional radiocarbon into the atmosphere, producing a peak that results in pmC values above 100 for groundwater younger than ~ 70 years (Clark and Fritz, 1997). Similar to ^{13}C in DIC, water traversing the unsaturated zone acquires additional ^{14}C from soil gas. Values of pmC once again reach roughly 100 at the groundwater surface and begin to decay (Clark and Fritz, 1997). From this point, assuming the system is closed, age can be calculated using its half-life of 5,730 years in a standard decay equation (Clark and Fritz, 1997).

Several processes can affect ^{14}C activity in aquifers, primarily the dissolution of calcite, a process that adds ^{14}C-free carbon to total DIC, thereby diluting the ^{14}C in the sample and resulting in an artificially "old" age (Clark and Fritz, 1997; Plummer et al., 2004). A study of the Middle Rio Grande Basin in New Mexico illustrates the relationship between $\delta^{13}C$ and ^{14}C, as shown in Figure 8 (Plummer et al., 2004). This graph illustrates two findings: 1.) groundwaters younger than 200 years have more negative values of $\delta^{13}C$-DIC (average -11.9 ± 2.0‰) and older waters have higher values of $\delta^{13}C$-DIC (average -8.2 ± 1.4‰), and 2.) the trend stabilized at $\delta^{13}C$ values of around -8‰, meaning there was no need for ^{14}C age correction among the older groundwaters in the study (Plummer et al., 2004). Figure 8 implies that measuring $\delta^{13}C$ can be used as a pre-screening and planning tool to further understand groundwater evolution and to target areas for radiocarbon dating. Figure 8 also shows that $\delta^{13}C$ data can be plotted against existing ^{14}C data to suggest whether an age correction may be necessary. Plummer et al. (2004) determined that age corrections are not likely to be necessary if calcite is precipitating because the $\delta^{13}C$ of the residual DIC in the groundwater is unaffected by calcite precipitation (Clark and Fritz, 1997). Calcite precipitation is a large component of dedolomitization, one of the processes inferred to occur in the High Plains by McMahon et al. (2004). Regardless, if the system is not fully closed and processes such as advection, dispersion, and diffusion are not taken into consideration, ^{14}C is subject to dilution, and radiocarbon dating will include some amount of error (Phillips et al., 1986; Clark and Fritz, 1997; Castro and Goblet, 2005).
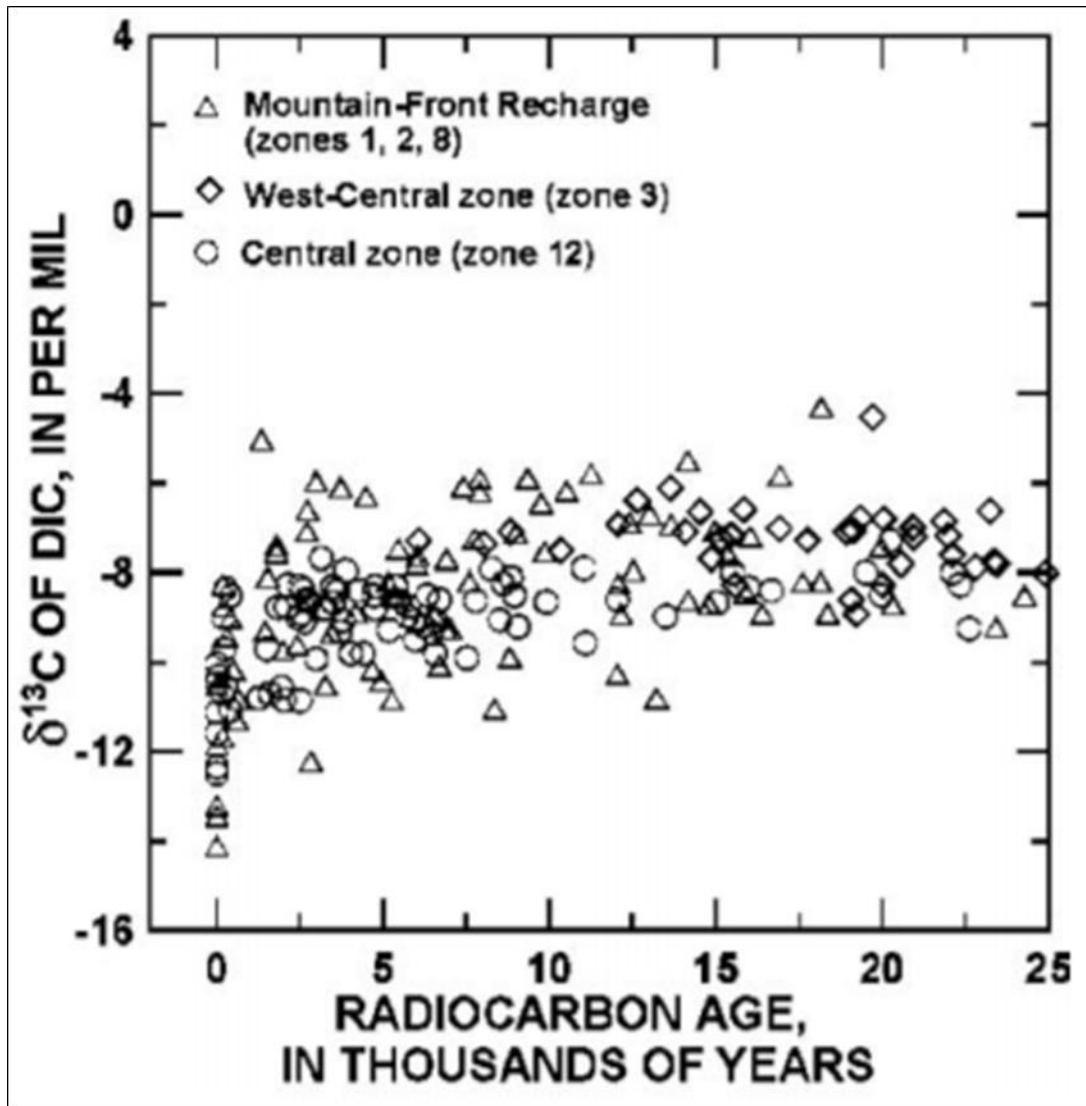
Figure 8: Example of plotting radiocarbon age vs. δ¹³C-DIC (Plummer et al., 2004). Note that the youngest waters exhibit more negative values of δ¹³C-DIC.

1.2.2.3   Tritium

Similar to ^{14}C, higher concentrations of tritium (^3H) were released into the atmosphere as a result of weapons testing in the 1950s (Clark and Fritz, 1997). Unlike ^{14}C, tritium occurs naturally in trace amounts and only has a half-life of 12.43 years (Clark and Fritz, 1997). Since discovery of high concentrations of this isotope in water, tritium has been used as an environmental tracer to locate sources of recharge, estimate recharge rates, and estimate residence times (Wood and

Sanford, 1994; Dutton, 1995; Clark and Fritz, 1997; McMahon, 2004; Castro, 2005; Gurdak and Qi, 2006; Gurdak and Roe, 2010; Estoe and Rodney, 2014; Koeniger, 2016).

The higher the value, measured in tritium units (TU), the less likely it is that the water has mixed with older waters or undergone extensive radioactive decay, indicating that the water is likely to have recharged recently. This concept was used to identify modern recharge in riparian zone wells near watercourses in Arizona (Wahi et al., 2008), beneath playas in the High Plains region (Gurdak and Roe, 2010), and in the Sacramento Mountains in New Mexico (Estoe and Rodney, 2014). Tritium has also been studied in the unsaturated zone to estimate recharge by measuring the distance from the surface to the 1963 peak tracer amount in the soil, relative to the amount of time that has passed (Wood and Sanford, 1994; Koeniger, 2016). Dutton (1995) found that in areas where the water table is deep, tritium activity is low, most likely because of the increased vertical travel time. Koeniger (2016) also found that the tritium peak can still be found in areas with very low recharge and thick soils. Unfortunately, tritium in the atmosphere has almost returned to pre-bomb concentrations, so this tracer is no longer used as frequently as it once was (Koeniger, 2016). With such low concentrations remaining, groundwater containing less than 0.5 TU is "pre-bomb recharge" and groundwater containing more than 0.5 TU has at least some water that has recharged since the 1950's (Gurdak and Qi, 2006). Although groundwater that has no tritium may only be a few hundred years old, groundwater that is tritium-free is not recharging within the average human lifespan and is therefore considered to be an unsustainable source of water.

1.3   Study Area

This project is the result of collaboration with Kate Zeigler, PhD of Zeigler Geologic Consulting (ZGC) LLC, who maintains groundwater monitoring contracts in the study area. This study focuses on groundwater in a four-county area in the High Plains region of northeastern New Mexico (Colfax, Mora, Union, and Harding counties – Figure 9).

The total area of these counties is 30,195.83 km^2 (11,658.67 mi^2) and elevation ranges from

1065.51m to 4016.32m (3495.77ft to 13,176.90ft), with elevation generally increasing from east

to west as seen in Figure 10. Precipitation values shown in Figure 11 range from 40.64cm -

76.2cm (12in - 30in). Precipitation values generally increase from the west to the east, but higher

values exist locally in relation to higher elevations in the west. As with the High Plains region in

general, summer precipitation originates in the Gulf of Mexico, while winter precipitation

originates in the eastern Pacific Ocean (Nativ and Riggio, 1989). Precipitation minus potential

evapotranspiration results in negative values of potential natural recharge, defined as infiltration

from precipitation and surface waters (Hiscock and Bense, 2014), for the majority of the study

area, as seen in Figure 12. Low precipitation and high potential evapotranspiration result in low

estimations of recharge, shown in Figure 13 to be 0.0cm/yr – 1.3 cm/yr (0.0in/yr – 0.5in/yr), for

the majority of the study area. The majority of the study area is oriented toward cattle production

because of the dry conditions. As access to more productive aquifer units increases, so does the

use of center-pivot irrigation. A west – east transition from ranchland farming to center-pivot

irrigation can be seen in Figure 14 via Google Earth satellite imagery.

An overview of surface geology is provided in Figure 15 with data from the New Mexico

Bureau of Geology and Mineral Resources (2003). Hydrostratigraphic units that were relevant to

this study are prominently displayed for reference. Within the study area, most of the Ogallala

Formation has been eroded away or presents as a thin surficial deposit of insufficient thickness to

be a hydrostratigraphic unit. The HPA is present in Union County (Figure 9 and Figure 15), but in

a strict sense, the HPA is absent as a hydrostratigraphic unit throughout the majority of the study

area because it is either too thin or absent altogether. The Groundwater Atlas of the United States

confirmed low saturated thickness and vast areas of discontinuous water table throughout the

study area (Robson and Banta, 1995). In these areas, the underlying bedrock aquifers are utilized

for groundwater abstraction. These aquifers share the same geographic and recharge setting, but

are not well studied or understood, and are thought to be less productive aquifers overall. The

most commonly utilized aquifers in the study area are alluvial sediments, Graneros Shale, Greenhorn Limestone, Dakota Sandstone, and the Dockum/Chinle Group.

Northeast New Mexico represents a challenging study area because of the seasonal difference in vapor sources, large elevation gradient, and heterogeneity of the subsurface geology. No precipitation collections have been analyzed to generate a meteoric water line specific to the study area that would allow for direct comparisons with groundwater samples. One study did analyze the isotopic composition of surface water for the United States, noting that "the steepest increases in δ values are found at the southeastern edges of the Colorado Plateau, towards southern Texas" (Kendall and Coplen, 2001). Figure 16 highlights the variability of the isotopic composition of surface water found in northeast New Mexico, exhibiting the heterogeneity present in the location of this study (Kendall and Coplen, 2001). Conducting isotopic research in this region not only adds information to the growing dataset of High Plains groundwater, but also serves to provide analysis on one of the most complex regions in the United States. The objective of this study is to gain a better understanding of the variables with the most influence on recharge processes.
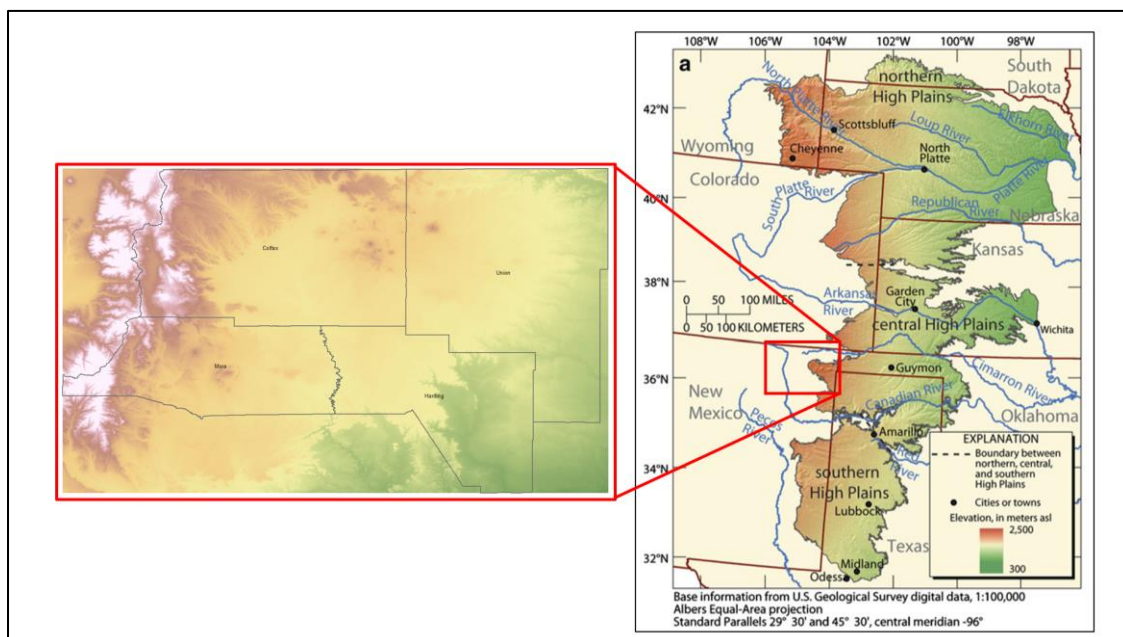
Figure 9: Overview of the High Plains Aquifer (Gurdak and Roe, 2010) and study area (DEM data for all generated maps is from USGS National Elevation Dataset).
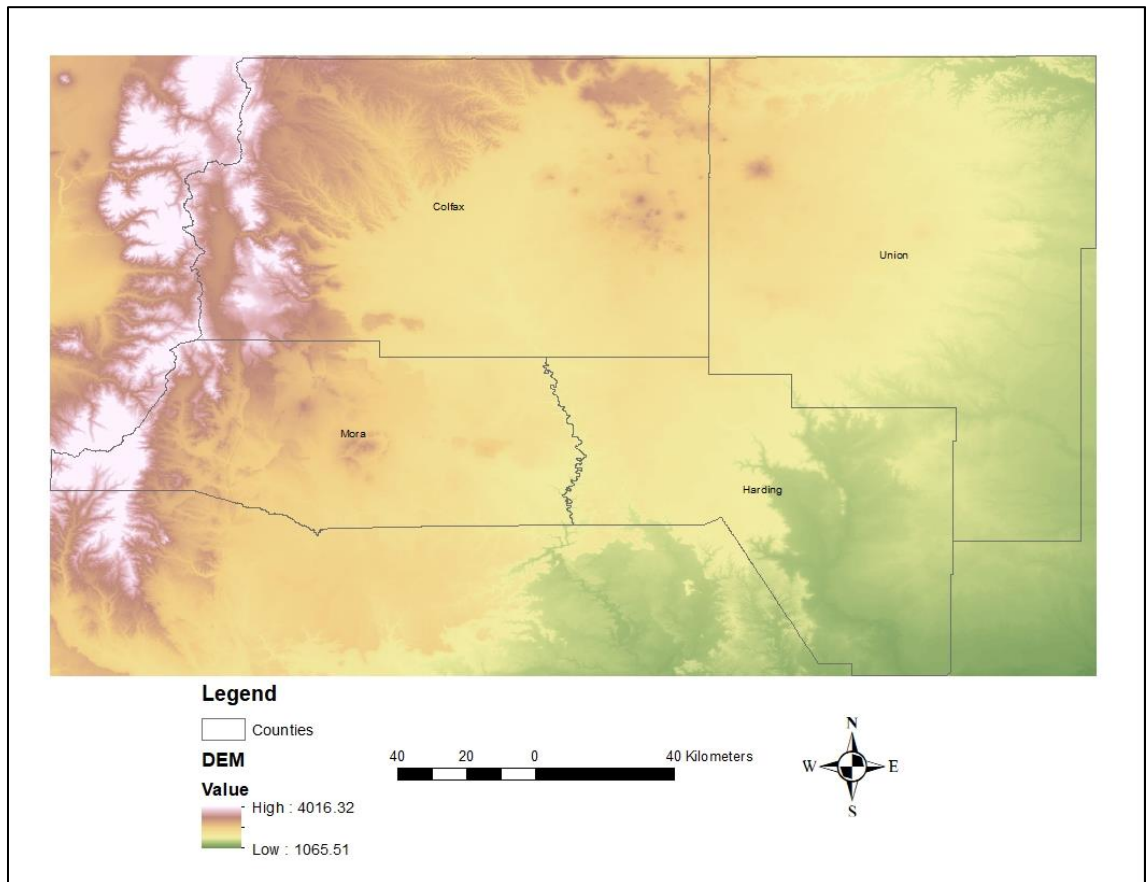
Figure 10: DEM of four-county study area. Elevations are in meters. DEM and County boundary shapefile provided by USGS.
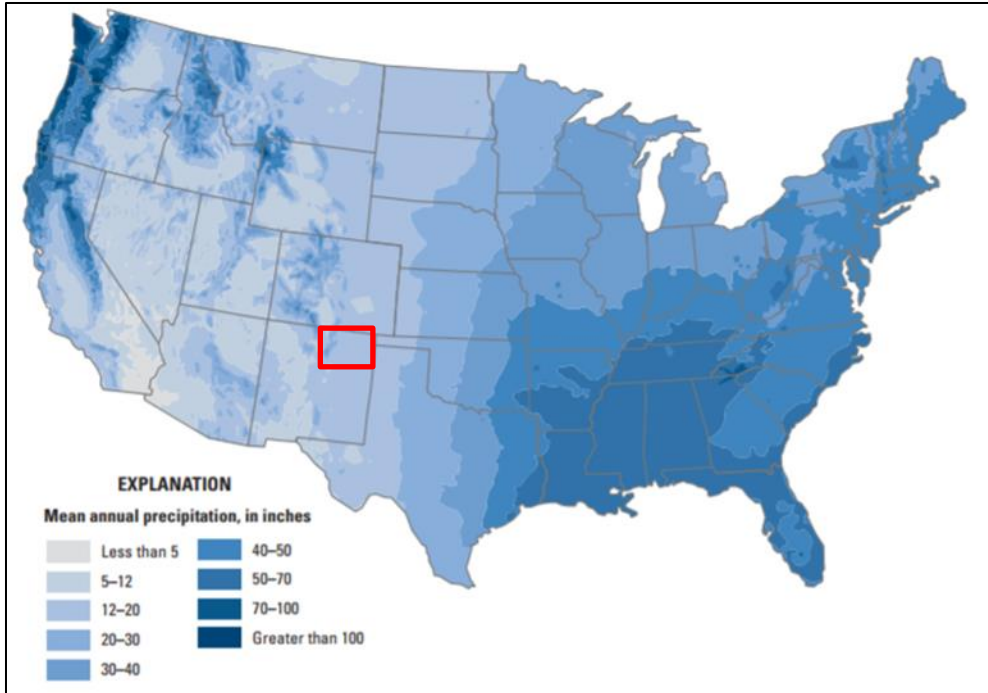
Figure 11: Mean annual precipitation (inches), with red box highlighting study area (Reilly et al., 2008).
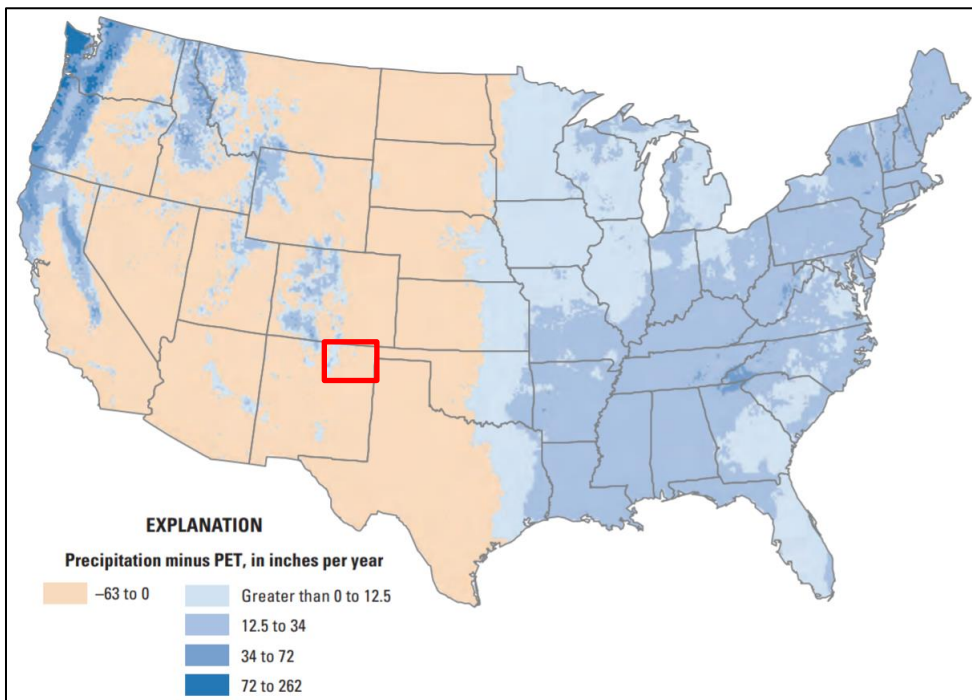
Figure 12: Precipitation minus potential evapotranspiration (inches), with red box highlighting study area (Reilly et al., 2008).
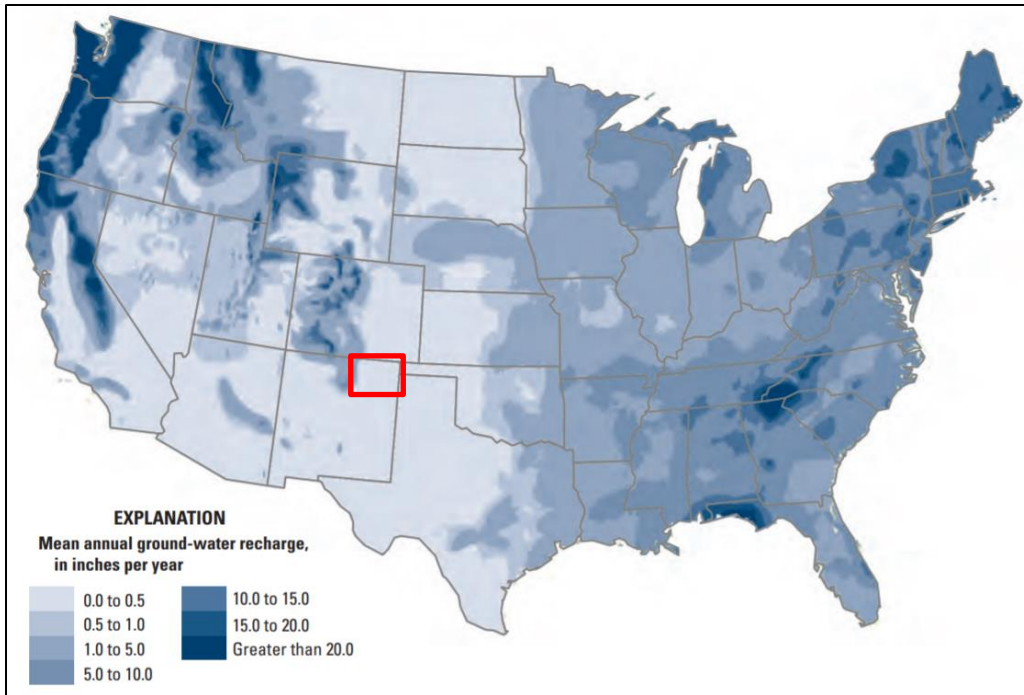
Figure 13: Estimated recharge (inches), with red box highlighting study area (Reilly et al., 2008).
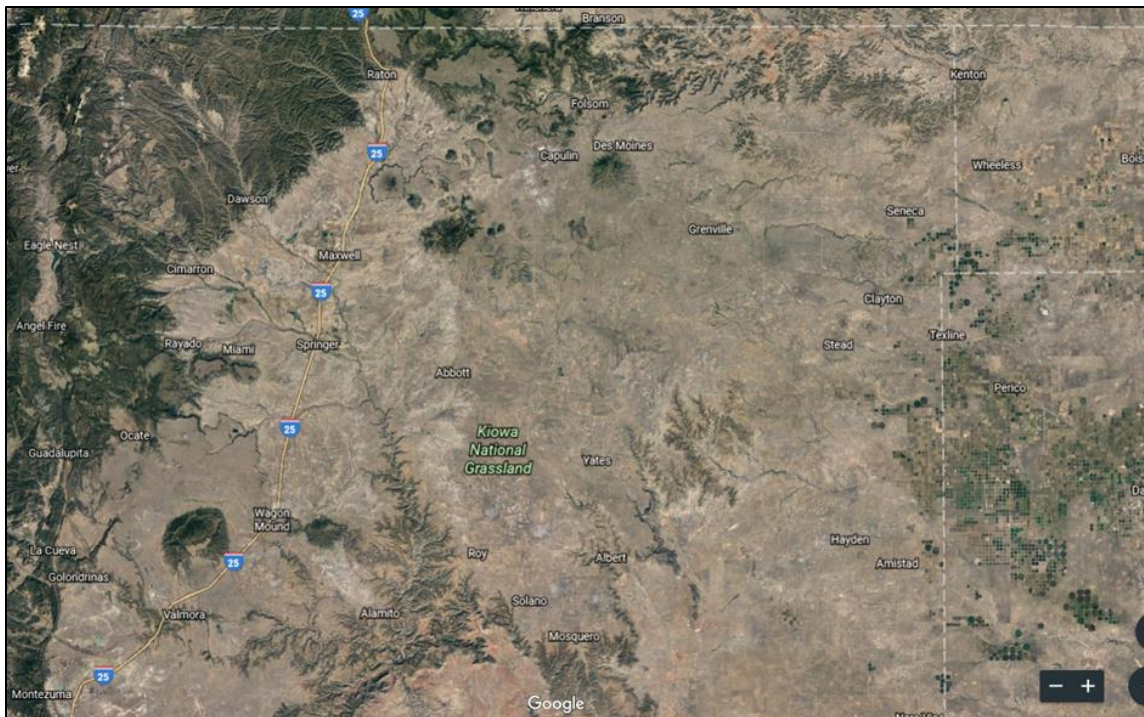
Figure 14: Google Earth satellite imagery of study area. Notice the transition from center-pivot irrigation in the east to ranchland farming in the west. View shown here is Union County, along with most of Colfax, Mora, and Harding counties. This view is roughly 125 miles across.
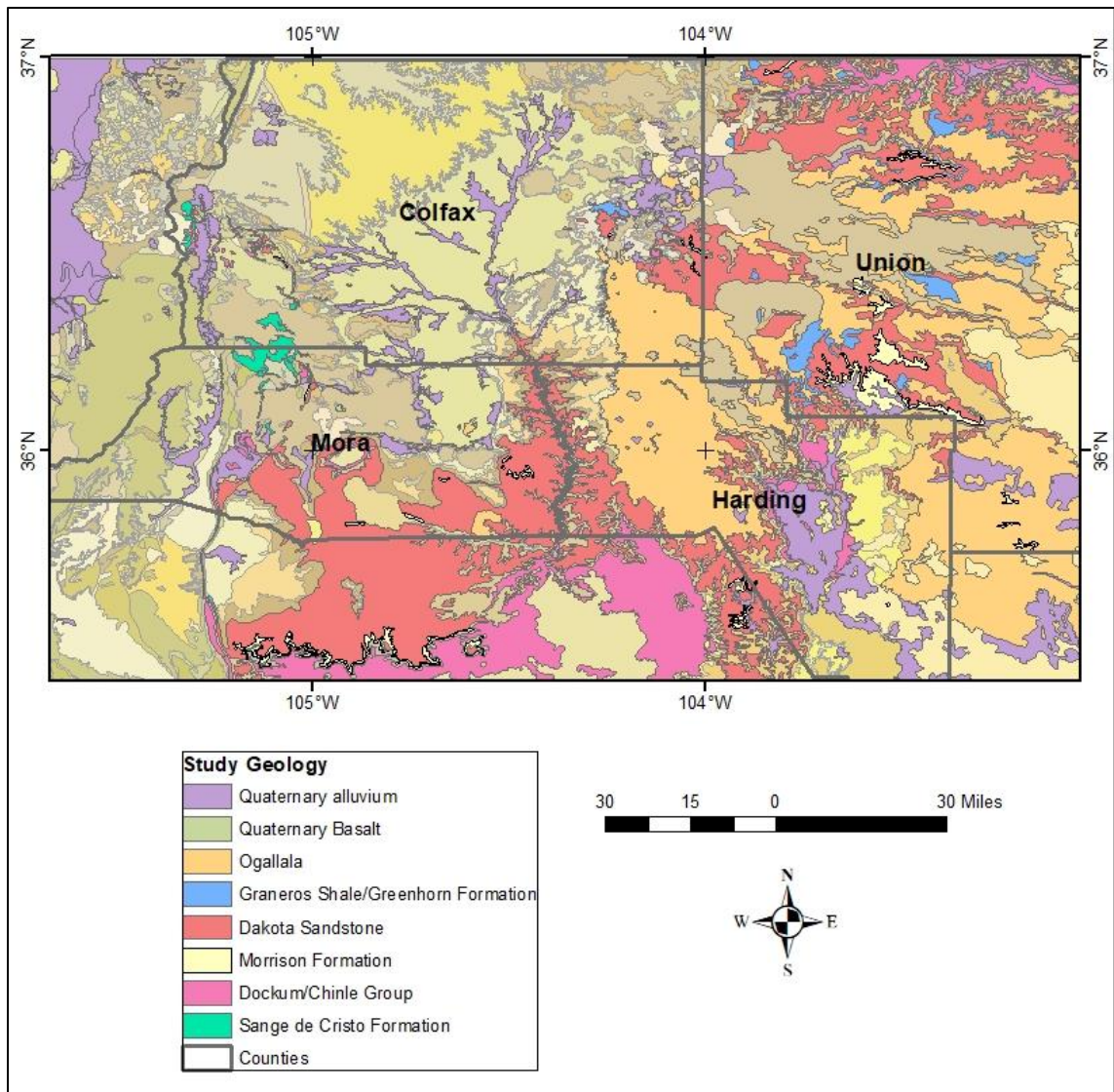
Figure 15: Geologic map of the study area with prominent units pertinent to this study displayed. Data is from the New Mexico Bureau of Geology and Mineral Resources (2003).
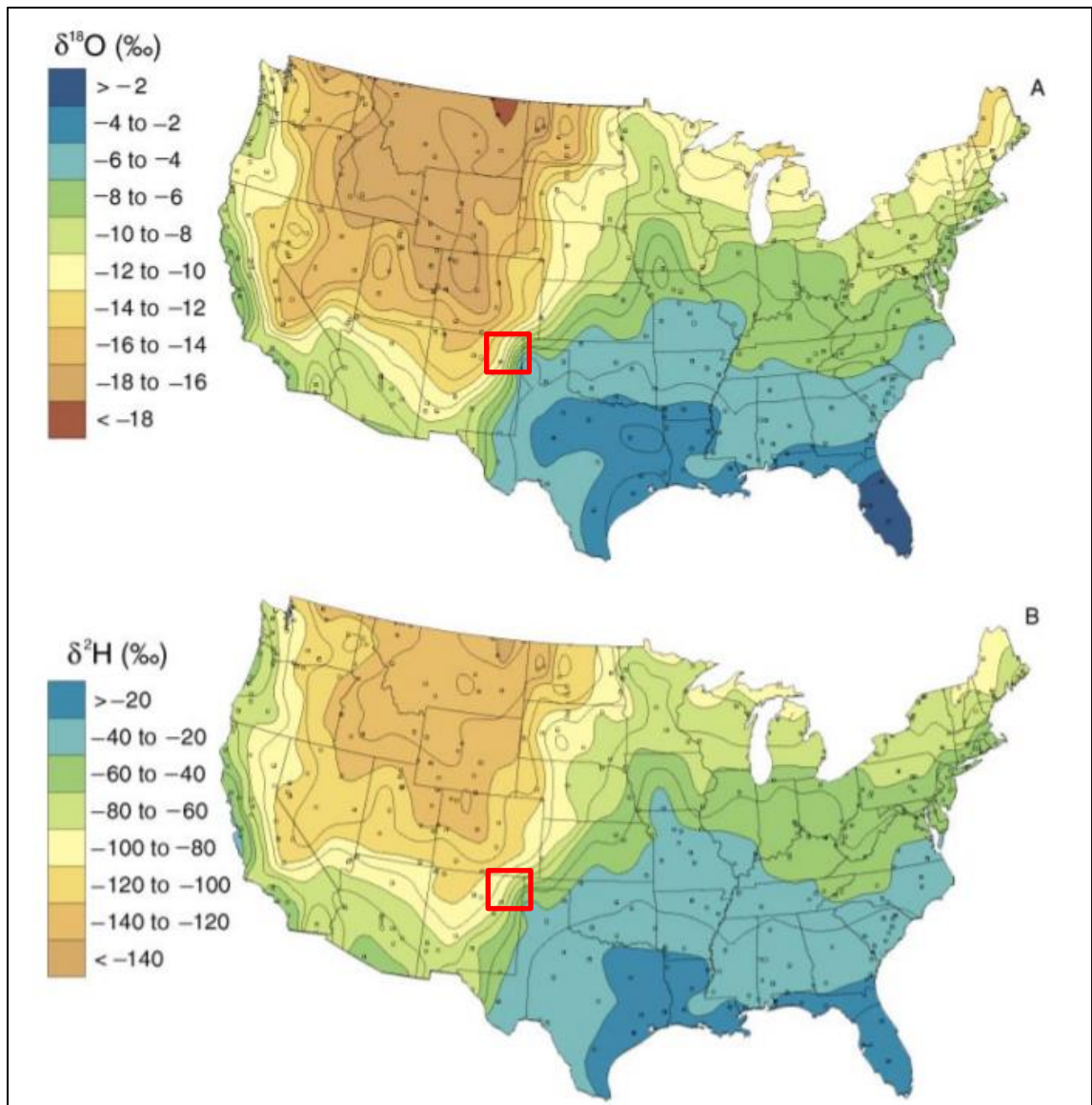
Figure 16: Map of spatial distribution of $\delta^{18}O$ and δD from a study conducted on surface water isotopic composition by Kendall and Coplen (2001). Note that northeastern New Mexico contains one of the steepest gradients of isotopic composition in surface water.

2   Hypotheses

Based on previous findings in the High Plains Region, it was hypothesized that:

- Water isotopes (oxygen and hydrogen) in groundwater samples throughout this region record conditions of recharge that may differ from the present day's recharge or a mix of winter vs. summer precipitation. Furthermore, modern waters will correlate with elevation of recharge.

- δ^{13}C-DIC will roughly correlate with carbon-14 activity where those data are available from other studies, and δ^{13}C-DIC can be used as a pre-screening tool for future carbon-14 analysis.

- Tritium analysis conducted at targeted locations near watercourses and points of accumulated runoff such as mountain fronts will identify locations of probable modern-day recharge.

3   Methods

3.1   Field Methods

Sample locations were intended to be taken at different elevations covering the extent of the study area, but were ultimately based on permission from the landowners. Some samples are located outside of the four county study area (Figure 17), but are from properties that straddle county lines. Because these landowners reside in the study area, all samples taken from their property were considered for analysis. In total, 85 samples were collected from wells and springs during scheduled site visits throughout 2017 and into early 2018.

A standard sampling protocol was used to ensure consistent data collection. If the well was not being pumped upon arrival at the site, it was allowed to pump water until a sufficient volume had been cleared from the well to remove any stagnant water in the well casing. Water was collected into a bottle that had been rinsed with water from the well at least three times. A syringe was also cleared with sampled water at least three times. The sample was then filtered using a syringe-tip 0.2 micron polyethersulfone (PES) filter into one 60mL crimp-top glass serum vial with no headspace, and into one 20mL borosilicate glass vial with no headspace and a cone-shaped cap. The cap threads were sealed with paraffin film. Tritium samples were collected in bottles that had been rinsed at least three times but not filtered, and not during precipitation events that could contaminate the sample. Standard field measurements (temperature, pH, dissolved solids, conductivity) were also recorded at the time of collection.

The samples were refrigerated until they were shipped to UNC Charlotte (UNCC), where they were once again refrigerated until lab analysis. Analysis was centered on hydrogen and oxygen isotopes, dissolved inorganic carbon, alkalinity, anion concentrations (chloride, fluoride, nitrate, and sulfate), and cation concentrations (calcium, sodium, magnesium, and potassium).

3.2 Laboratory Methods

Isotope analysis was performed on all 85 samples using a Los Gatos Research DLT-100 laser water analyzer. Samples were loaded using the IAEA-recommended protocol in which each 5 samples were bracketed by 3 working standards of known isotopic composition relative to VSMOW(IAEA, 2009). This loading pattern, along with analyzing duplicates of samples, was used to check for instrument drift during runs.

Dissolved inorganic carbon (DIC) concentrations and carbon isotope ratios of DIC were analyzed using a Picarro G2201-*i* carbon analyzer with AutoMate and Liaison peripherals for automated extraction and introduction of DIC. One sample had insufficient volume for DIC analysis and four additional samples were not able to be processed due to excessive DIC concentrations. Alkalinity concentrations were analyzed using the Gran titration method with 0.1 normal hydrochloric acid using an electronic titrator. Alkalinity and DIC concentrations together were used to confirm field-measured pH values using the acid dissociation constants of carbonic acid (Drever, 1997).

Major anions (fluoride, chloride, sulfate, and nitrate) and major cations (calcium, sodium, potassium, and magnesium) were analyzed using a Dionex DX-500 ion chromatograph.

4 Results

4.1 Isotopes

4.1.1 δ^{18}O, δD, and hydrostratigraphy

In total, groundwater samples represented 11 different hydrostratigraphic units throughout the study area. Figure 17 shows the locations and hydrostratigraphic units of each well that was

sampled. All 85 samples were analyzed for their isotopic composition (see Appendix A and B), with $\delta^{18}O$ values ranging from -13.71 to -4.42‰ and δD values ranging from -104.85 to -41.85‰.

Figure 18 shows the spatial distribution of $\delta^{18}O$ values. These values were contoured using kriging in ArcGIS and are displayed using the standard deviation method (degree of variance from the arithmetic mean). Without considering other variables such as well depth or aquifer sampled, an overall pattern can be observed. The most depleted isotope values are in the north, with values increasing to the west and transitioning into the least depleted groundwaters in the southeastern part of the study area. Figure 19 depicts the spatial distribution of δD values. These values were also mapped using kriging in ArcGIS and are displayed using the standard deviation method. The observable pattern in this map is similar to the pattern of $\delta^{18}O$ values, with the most depleted samples found in the north, and least depleted samples found in the southeast. $\delta^{18}O$ values and δD values were also plotted by hydrostratigraphic unit for comparison with the Global Meteoric Water Line, shown in Figure 20. The majority of the data fall along the line, grouped together between roughly -7 and -9. The alluvial and/or Dockum/Chinle Group is the only unit that noticeably deviates from this pattern. These data points are closely grouped, are the highest (most isotopically enriched) points in the study, and have a much lower slope and y-intercept than the Global Meteoric Water Line.

Of the 11 hydrostratigraphic units, only four were deemed to have an adequate sample size for individual unit analysis. These four, from youngest to oldest, are the alluvium and/or Dockum/Chinle Group, Graneros Shale/Greenhorn Limestone, Graneros Shale and/or Dakota Sandstone, and Dakota Sandstone. These four units have enough samples to generate individual maps and scatterplots, but the remaining seven units are included in the overall analysis and discussion.

31
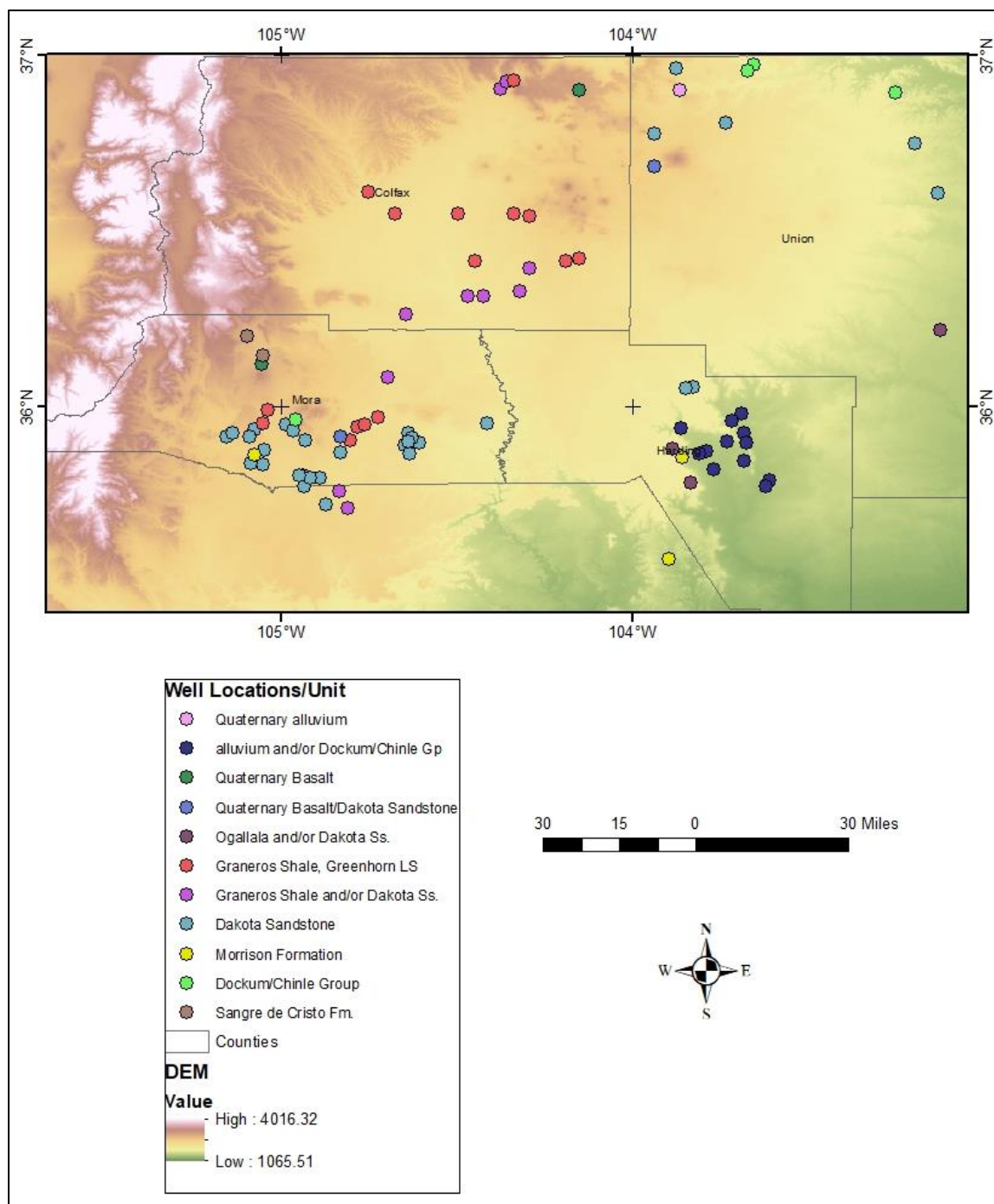
Figure 17: Map of all groundwater sample locations displayed by hydrostratigraphic unit.
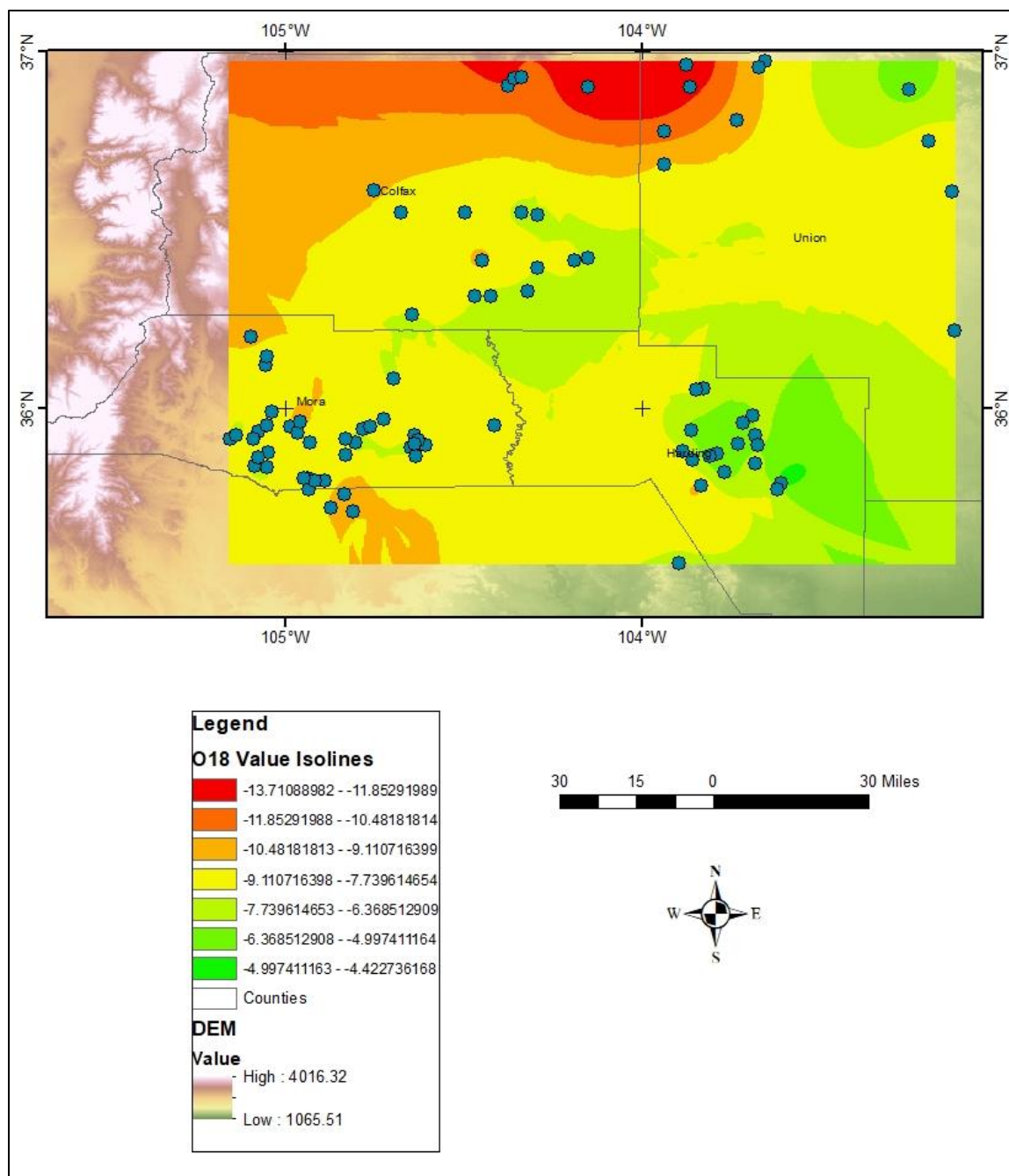
Figure 18: Map of locations of $\delta^{18}O$ values used to calculate and display isolines using the standard deviation method.
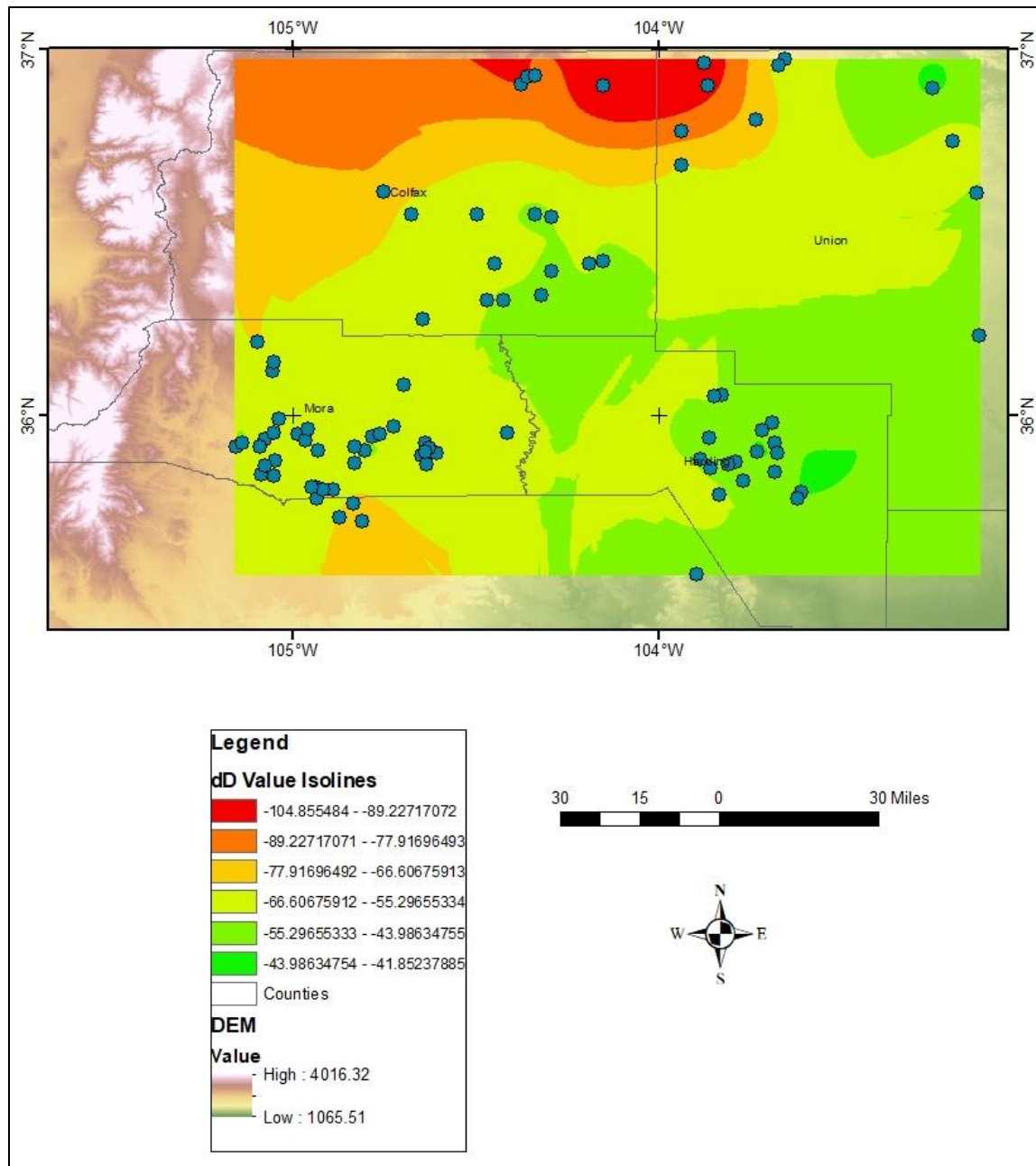
Figure 19: Map of locations of δD values used to calculate and display isolines using the standard deviation method.
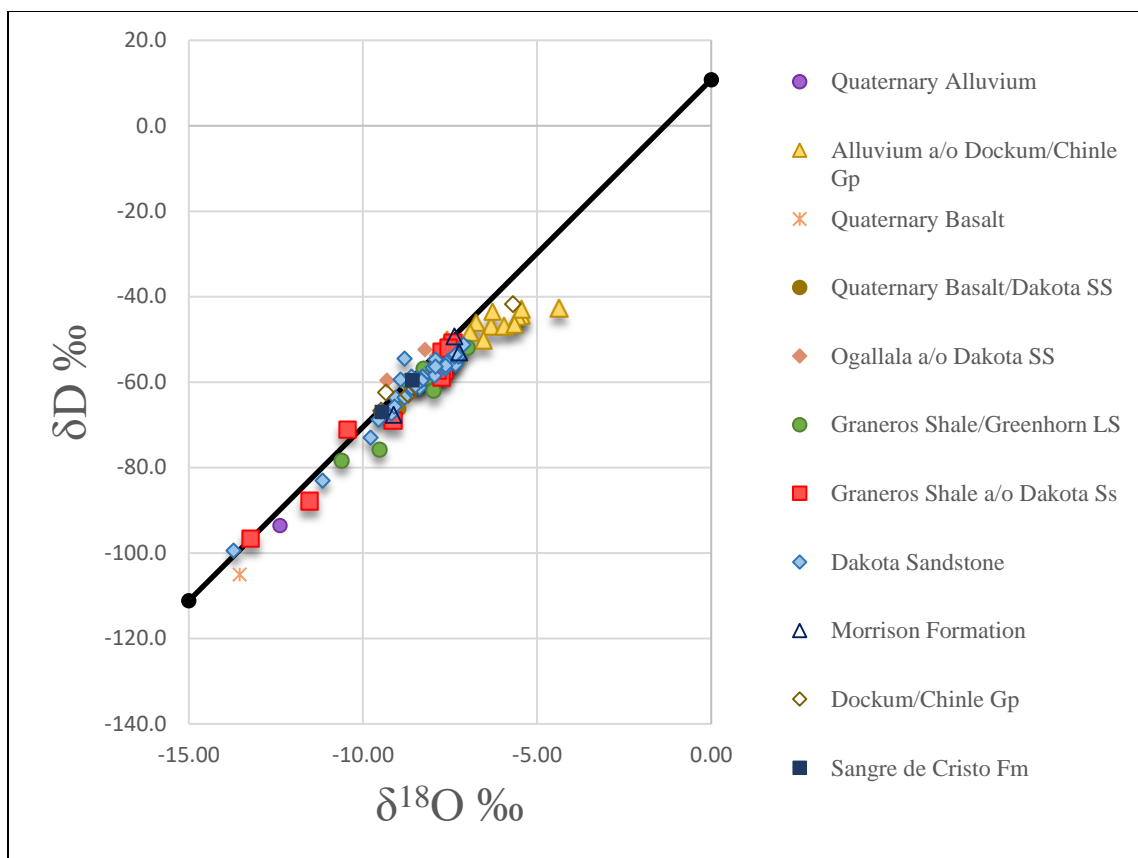
Figure 20: Scatterplot of all samples collected in this study relative to the GMWL (Clark and Fritz, 1997), plotted by hydrostratigraphic unit.

The first major hydrostratigraphic unit, alluvium and/or Dockum/Chinle Group (*n*=12), is shown in Figure 21, Figure 22, and Figure 23. The locations of these samples are geographically grouped in Harding County at land surface elevations ranging from 1337 to 1419m. $\delta^{18}O$ values shown in Figure 21 range from -7.58 to -4.37‰, with all but one near -7‰. δD values shown in Figure 22 range from -50.1 to -42.7‰. Although the values for this group of samples are grouped together, they exhibit a noticeable difference in distribution when compared to the Global Meteoric Water Line, shown in Figure 23 by moving to the right and away from the line. The trendline shown in Figure 23 has a lower slope and y-intercept than the GMWL with an equation of $\delta^2H = 2.37 \, \delta^{18}O - 31.70$‰ VSMOW versus the GMWL equation of $\delta^2H = 8.13\delta^{18}O + 10.8$‰ VSMOW (Clark and Fritz, 1997).
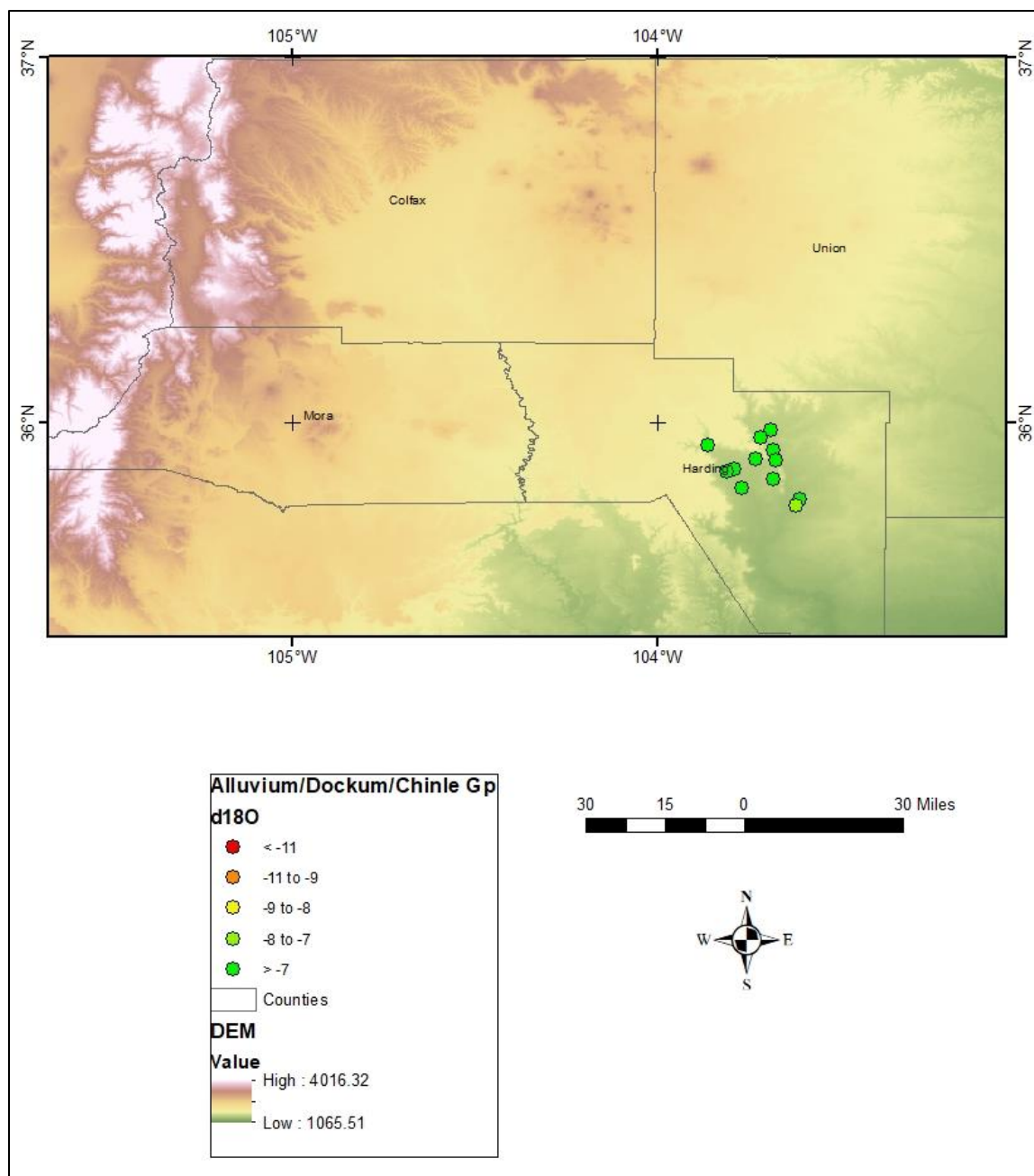
Figure 21: Map showing δ¹⁸O values for the alluvium and/or Dockum/Chinle Group unit only.
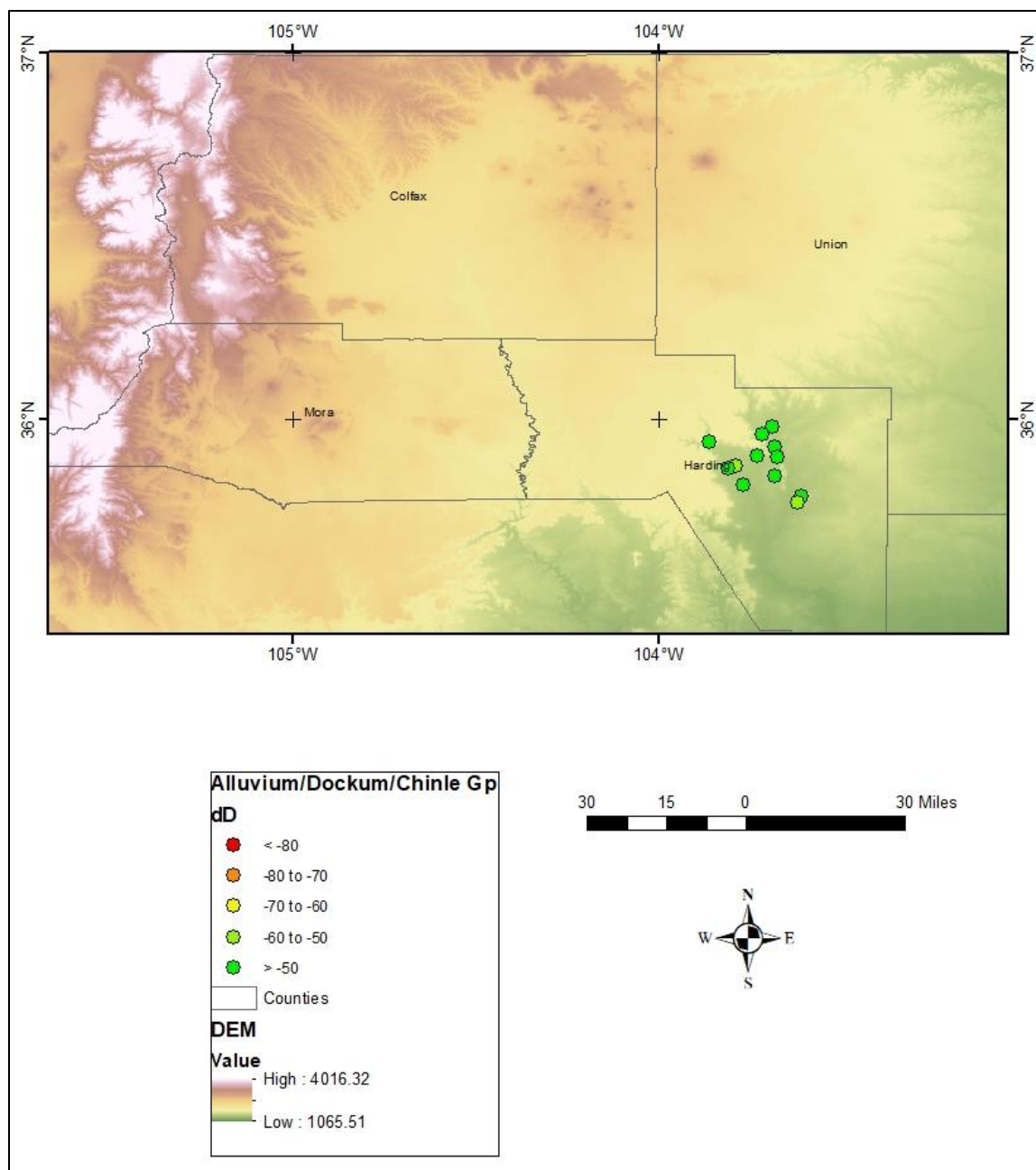
Figure 22: Map showing δD values for the alluvium/Dockum and/or Chinle Group unit only.
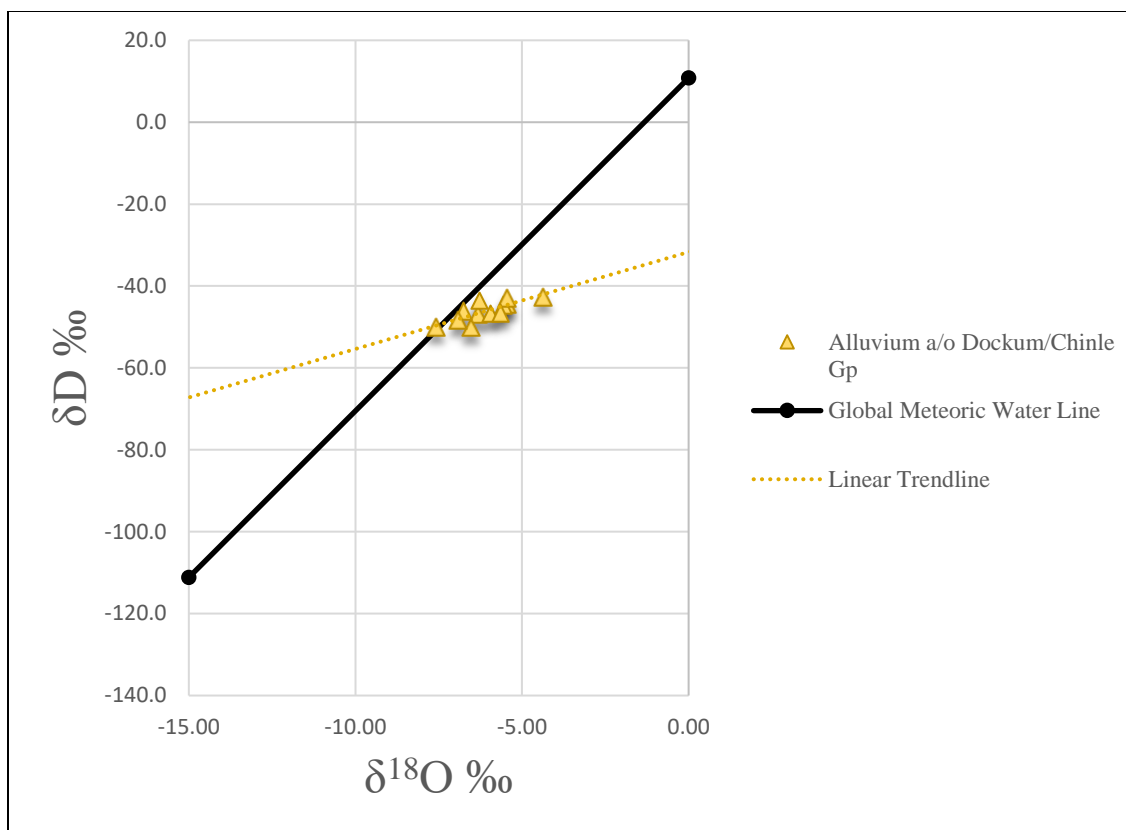
Figure 23: Scatterplot of GW samples in the alluvium and/or Dockum/Chinle Group hydrostratigraphic unit plotted against the GMWL (Clark and Fritz, 1997), with a linear trendline displayed (δ2H = 2.37 δ18O – 31.70‰ VSMOW).

The second hydrostratigraphic unit, Graneros Shale/Greenhorn Limestone (*n*=15), is shown

in Figure 24, Figure 25, and Figure 26. These samples are geographically spread throughout Mora

and Colfax Counties and have surface elevations ranging from 1832 to 2227 m. Figure 24 shows

the spatial distribution of $\delta^{18}O$ values, ranging from -10.62 to -6.99‰. There are no significantly

depleted values shown in Figure 24, but there are three moderately depleted values shown in

Colfax County (-10.62, -9.53, and -9.46‰), located north and west within the study area. δD

values shown in Figure 25 have a range of -78.3 to -51.8‰. The northern-most point in Colfax

County falls into the significantly negative range in this figure (-78.3‰). When plotted against

the GMWL in Figure 26, the values have a similar slope, but different y-intercept. This unit

yielded an equation of $\delta^2H = 7.52\delta^{18}O + 1.81$‰ VSMOW vs. the GMWL equation of $\delta^2H = 8.13\delta^{18}O + 10.8$‰ VSMOW (Clark and Fritz, 1997).
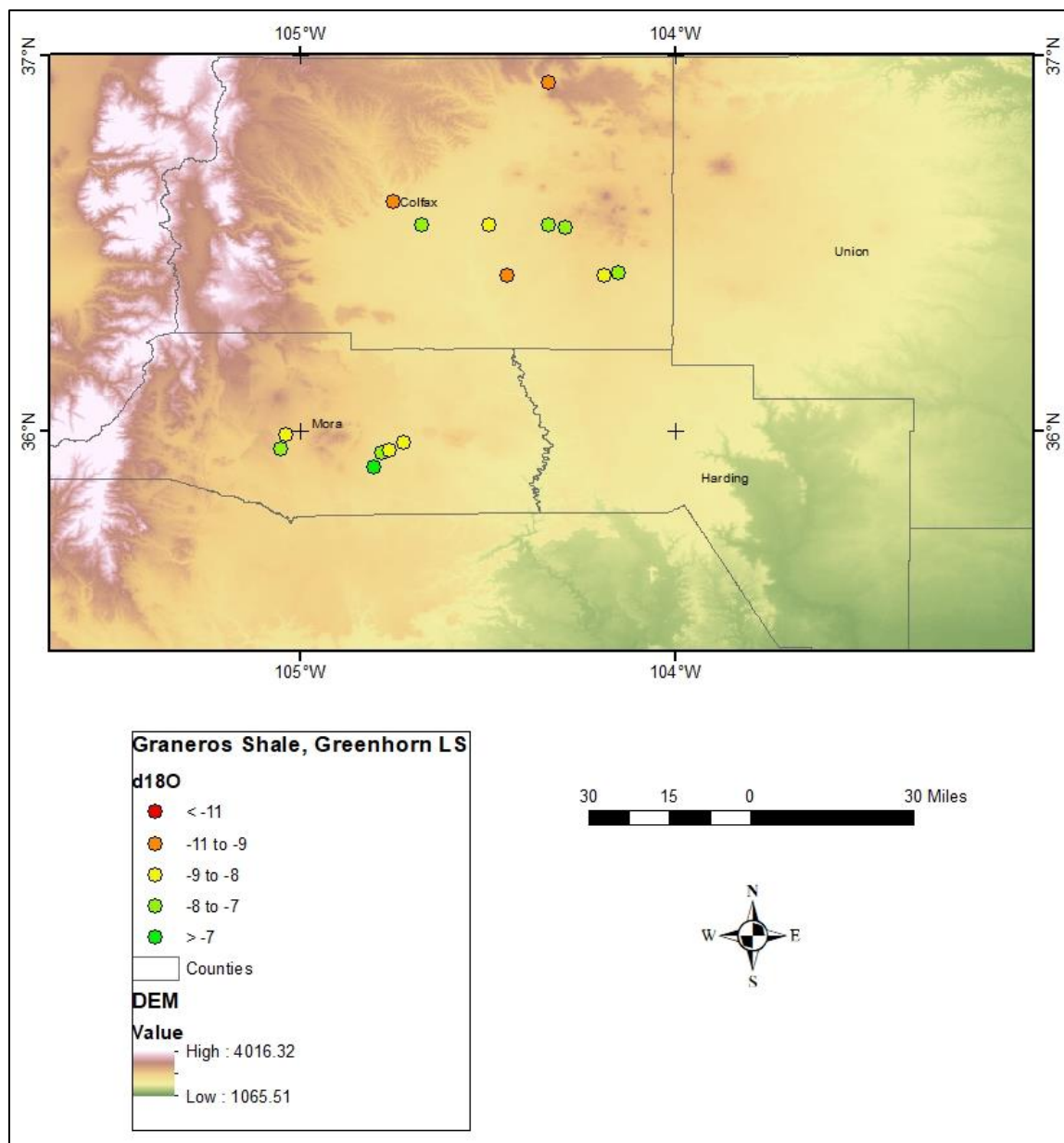
Figure 24: Map of $\delta^{18}O$ values for the Graneros Shale/Greenhorn Limestone unit only.
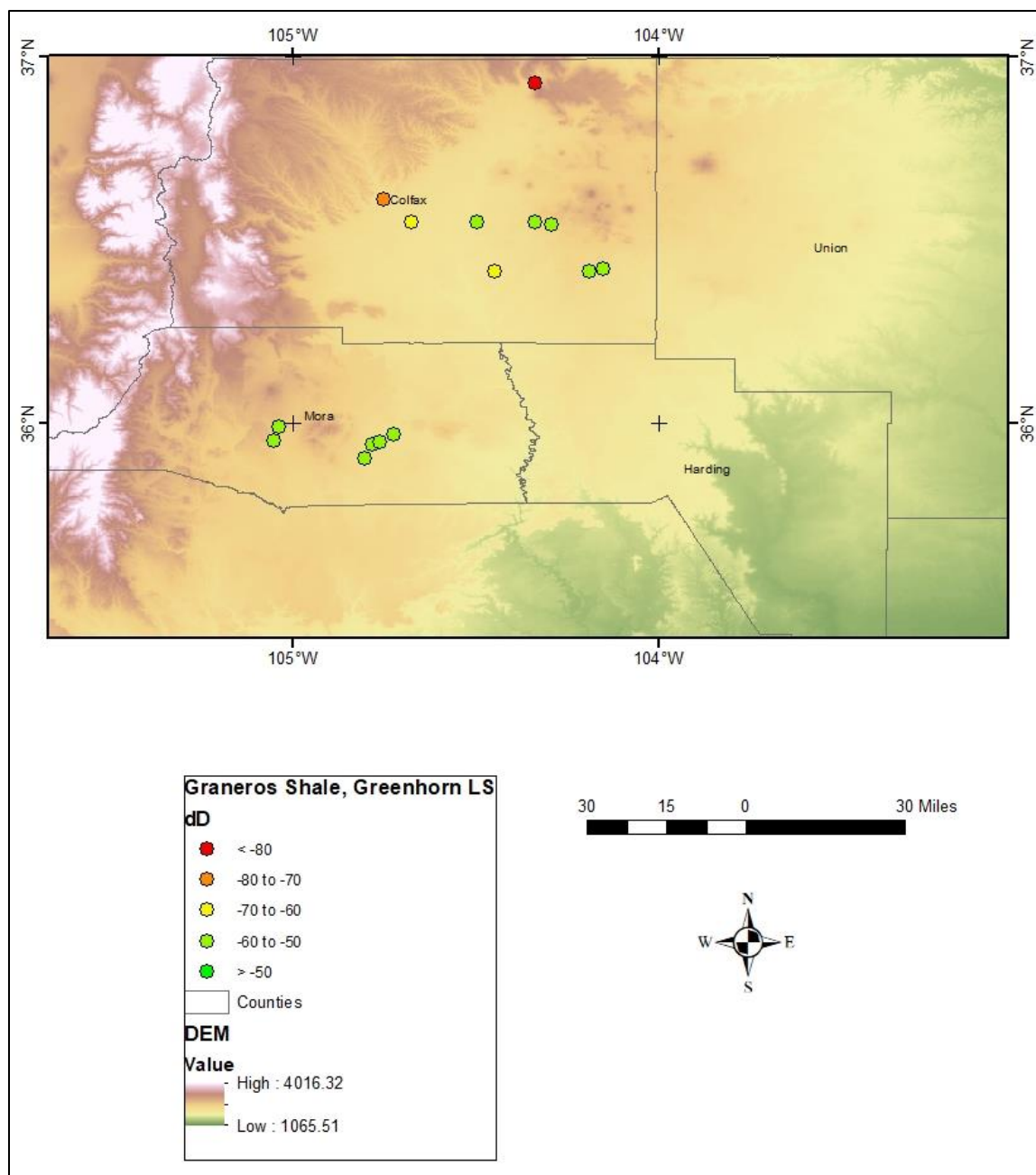
Figure 25: Map of δD values for the Graneros Shale/Greenhorn Limestone unit only.
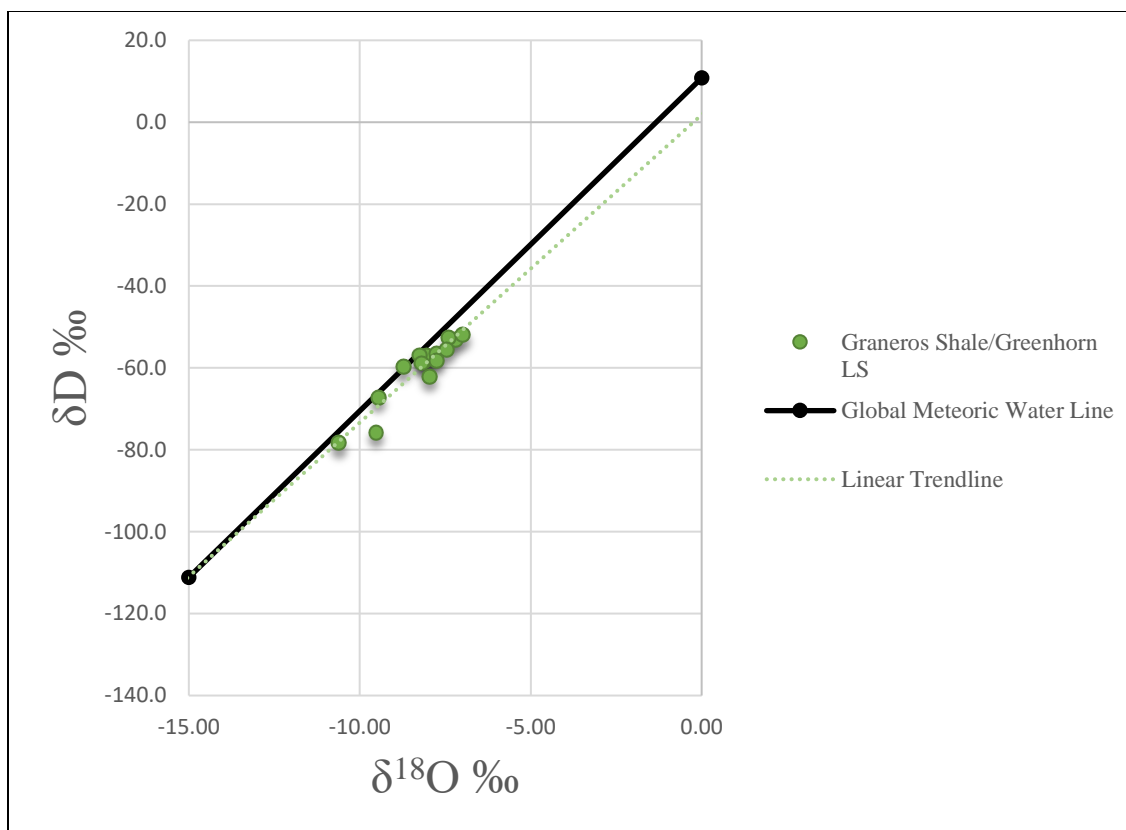
Figure 26: Scatterplot of GW samples in the Graneros Shale, Greenhorn Limestone hydrostratigraphic unit plotted against the GMWL (Clark and Fritz, 1997), with a linear trendline displayed ($\delta 2H = 7.52\delta 18O + 1.81‰$ VSMOW).

The third hydrostratigraphic unit, Graneros Shale and/or Dakota Sandstone (*n*=10), is shown in Figure 27, Figure 28, and Figure 29. These samples are geographically spread throughout Mora and Colfax Counties and have surface elevations ranging from 1785 to 2069m. $\delta^{18}O$ values shown in Figure 27 range from -13.23 to -7.41‰, with two very negative values shown in the northern part of Colfax County (-13.23 and -11.54‰). δD values shown in Figure 28 range from -96.5 to -50.7‰, with the same two locations having very negative values shown in the northern part of Colfax County (-96.5 and -87.80‰). These samples are spread along the GMWL, shown in Figure 29, and yielded an equation of $\delta^2H = 7.62\delta^{18}O + 3.51‰$ VSMOW, making this the unit with a trendline equation closest to that of the GMWL (Clark and Fritz, 1997).
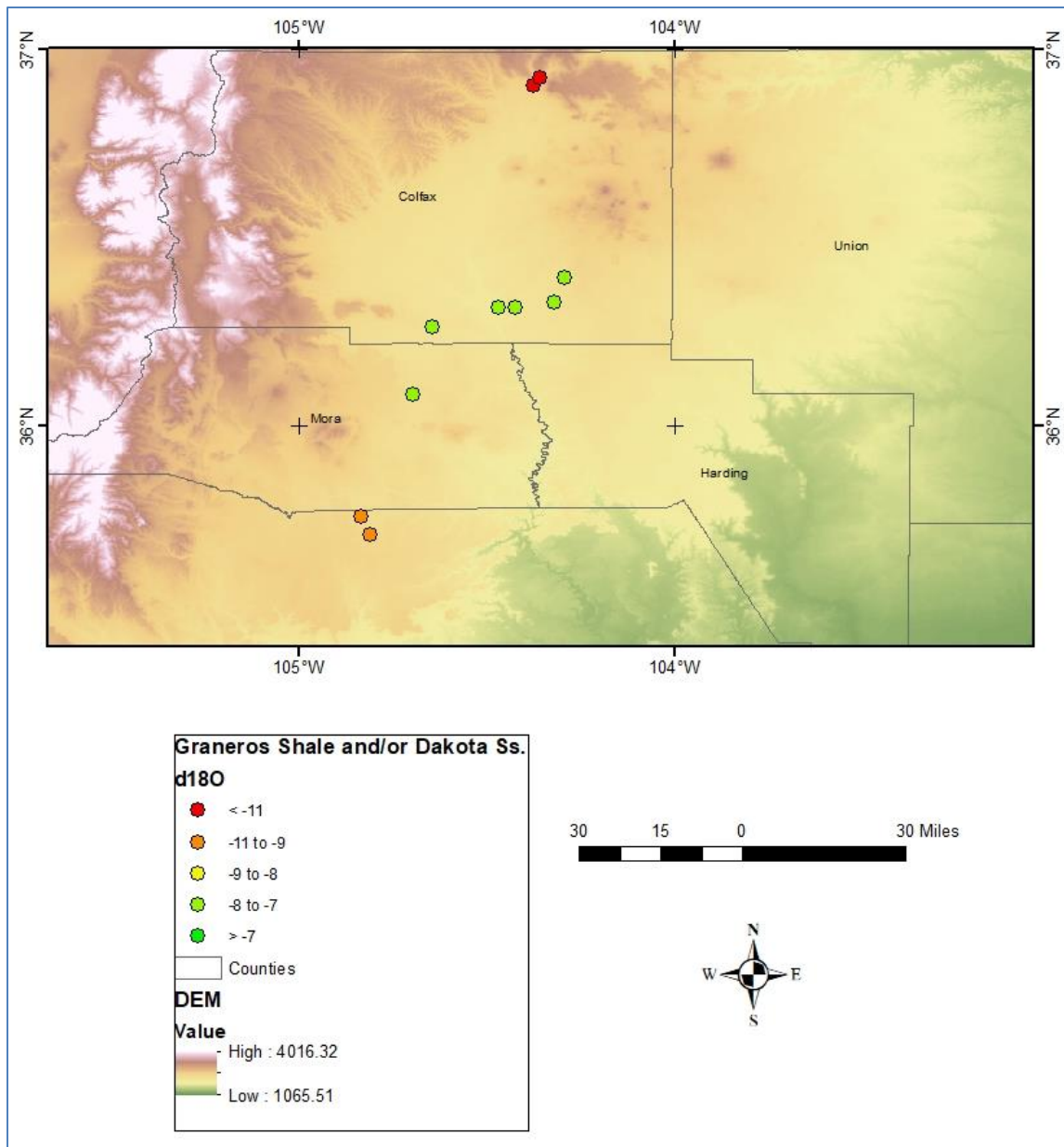
Figure 27: Map of δ^{18}O values for the Graneros Shale and/or Dakota Sandstone unit only.
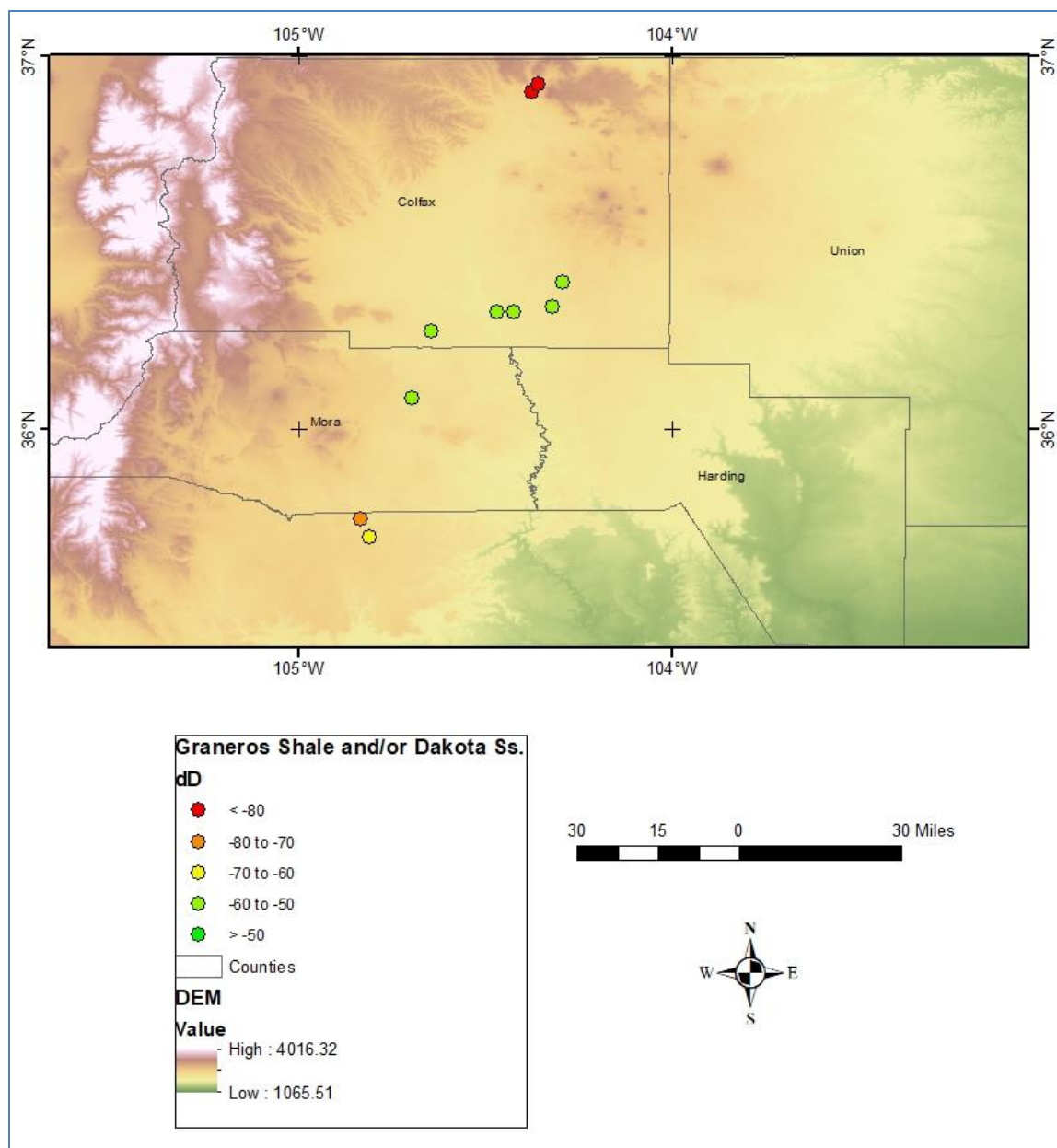
Figure 28: Map of δD values for the Graneros Shale and/or Dakota Sandstone unit only.
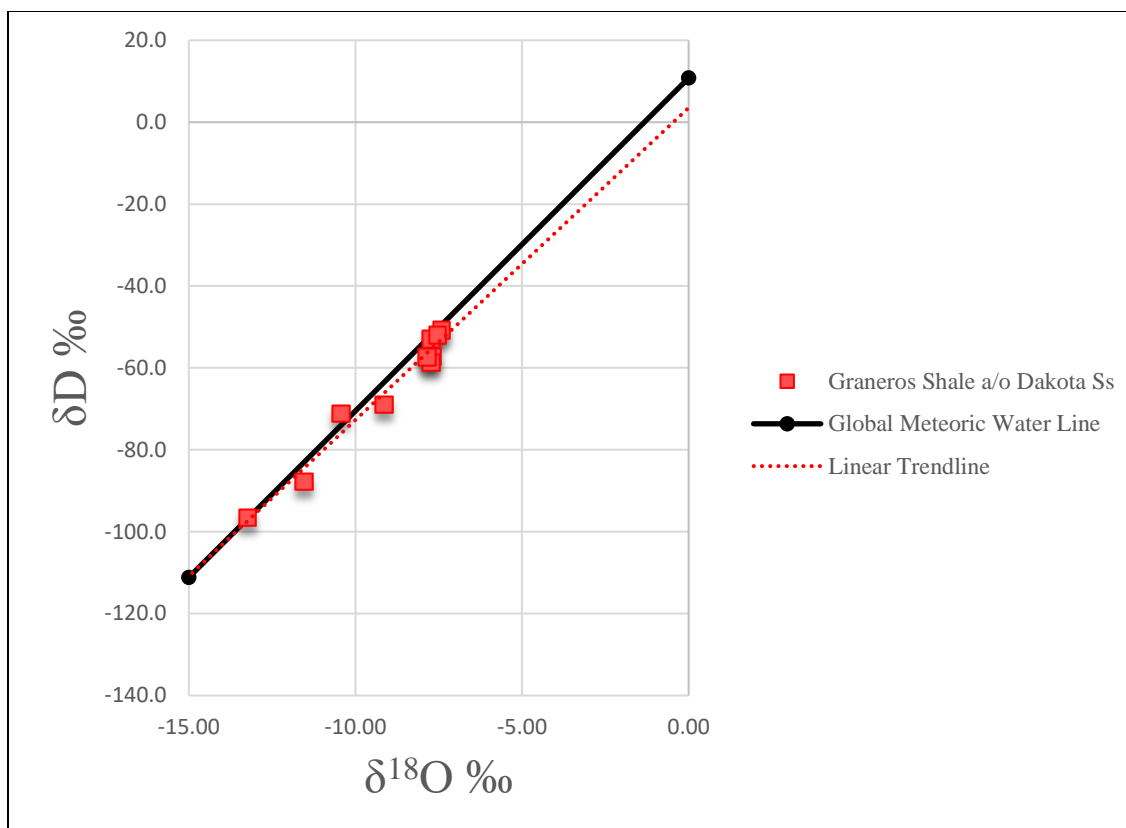
Figure 29: Scatterplot of GW samples in the Graneros Shale and/or Dakota Sandstone hydrostratigraphic unit plotted against the GMWL (Clark and Fritz, 1997), with a linear trendline displayed ($\delta 2H = 7.62\delta 18O + 3.51‰$ VSMOW).

The fourth and final major hydrostratigraphic unit that was analyzed individually, the Dakota Sandstone unit, has the largest sample size (*n=31*) and is shown in Figure 30, Figure 31, and Figure 32. Figure 30 and Figure 31 show that while the majority of these samples are grouped together in Mora County, there are five in Union County and two in Harding County. All of these samples were taken at locations with surface elevations higher than the alluvium and/or Dockum/Chinle Group samples (range 1517-2171 m). $\delta^{18}O$ values shown in Figure 30 range from -13.70 to -7.13‰, with two significantly depleted values in the northwest corner of Union County (-13.70 and -11.16‰) at relatively high elevations (1934 and 2062m, respectively). δD values shown in Figure 31 range from -99.4 to -51.1‰, again showing the two very negative values in Union County (-99.40 and -82.9‰). These samples fall along the center of, and just below, the GMWL (Figure 32). If not for a few samples that fall above the line, this line would

appear to be parallel to the GMWL. The results produced a trendline with the equation $\delta^2H = 7.23\delta^{18}O + 0.56‰$ VSMOW versus the GMWL equation of $\delta^2H = 8.13\delta^{18}O + 10.8‰$ VSMOW (Clark and Fritz, 1997).
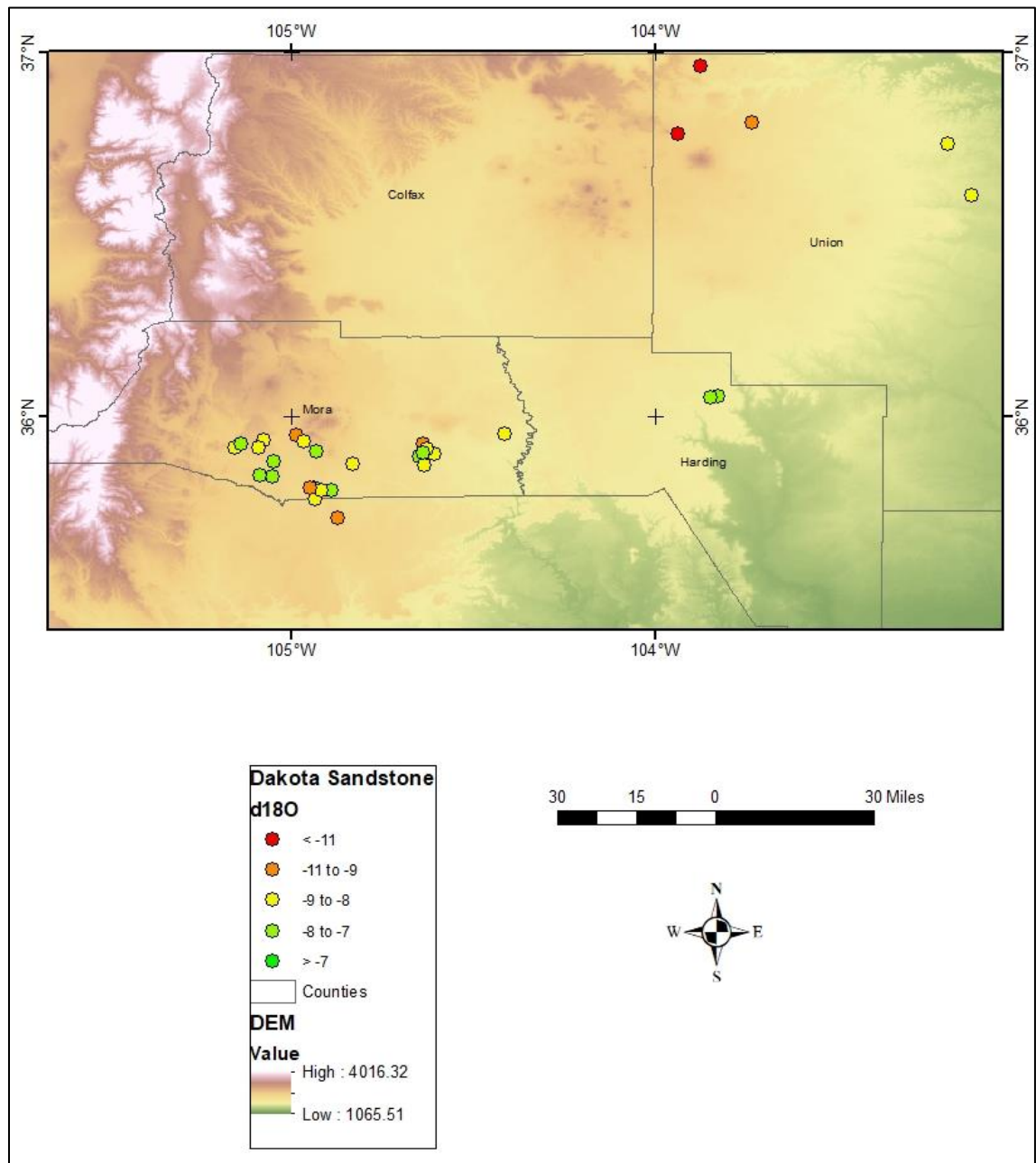
Figure 30: Map of $\delta^{18}O$ values for the Dakota Sandstone unit only.
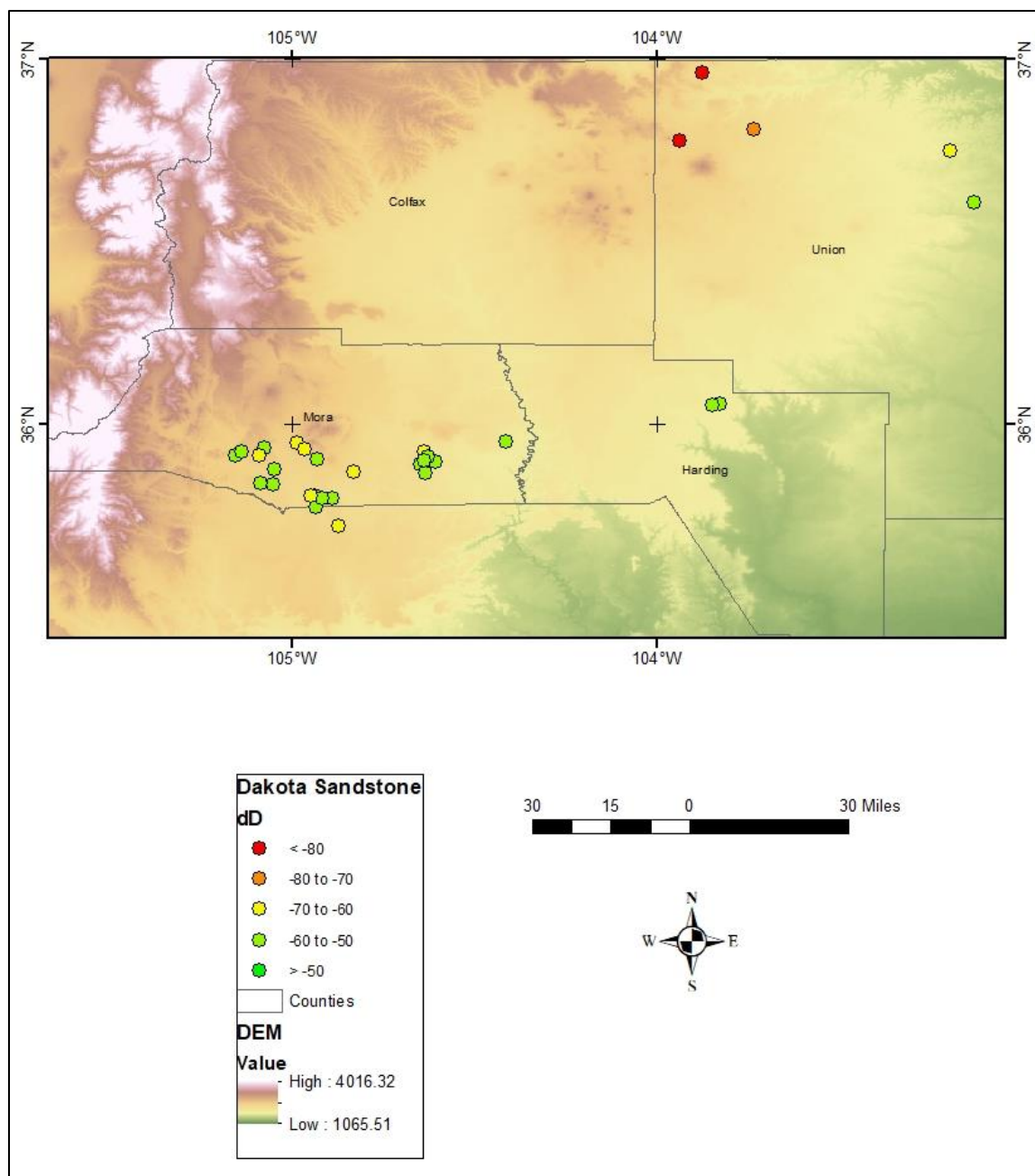
Figure 31: Map of δD values for the Dakota Sandstone unit only.
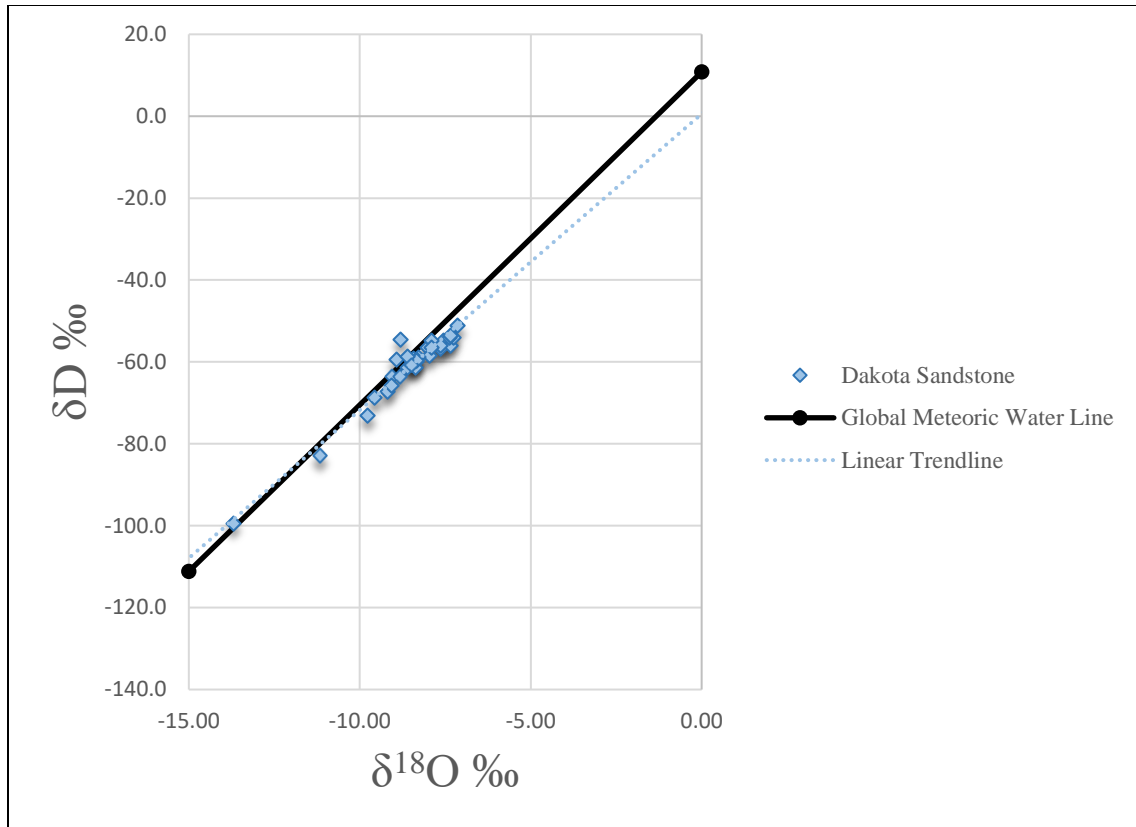
Figure 32: Scatterplot of GW samples in the Dakota Sandstone hydrostratigraphic unit plotted against the GMWL (Clark and Fritz, 1997), with a linear trendline displayed (δ2H = 7.23δ18O + 0.56‰ VSMOW).

4.1.2 δ¹⁸O and δD vs. elevation

Figure 33 and Figure 35 show the relationship between elevation and $\delta^{18}O$, and elevation and δD, respectively. Figure 33 shows that there is a slight relationship between $\delta^{18}O$ and elevation, with two groups of data that deviate notably from the overall trend. The first group is comprised mostly of samples from the alluvium and/or Dockum/Chinle Group and one sample from the Dockum/Chinle Group. This grouping falls above the overall trendline with high $\delta^{18}O$ values relative to their elevations. The second group highlighted in Figure 33 is comprised of samples from several different hydrostratigraphic units. These samples, found in Appendices A and B, are U9 from the Quaternary alluvium unit, C17 from the Quaternary Basalt unit, M8, C4, and C5 from the Graneros Shale and/or Dakota Sandstone unit, and U10 and U2 from the Dakota Sandstone unit. The locations of these outlying data points are shown in Figure 34. Figure 35

reveals a more noticeable relationship between δD and elevation, with the data more closely

grouped around a trendline than seen with the relationship between δ^{18}O and elevation. A few

samples still appear to deviate with significantly negative values relative to their elevation. These

samples (Appendix A) are U9 from the Quaternary alluvium unit, C17 from the Quaternary

Basalt unit, C9 and C15 from the Graneros Shale/Greenhorn Limestone unit, C4 and C5 from the

Graneros Shale and/or Dakota Sandstone unit, and U10, U11, and U2 from the Dakota Sandstone
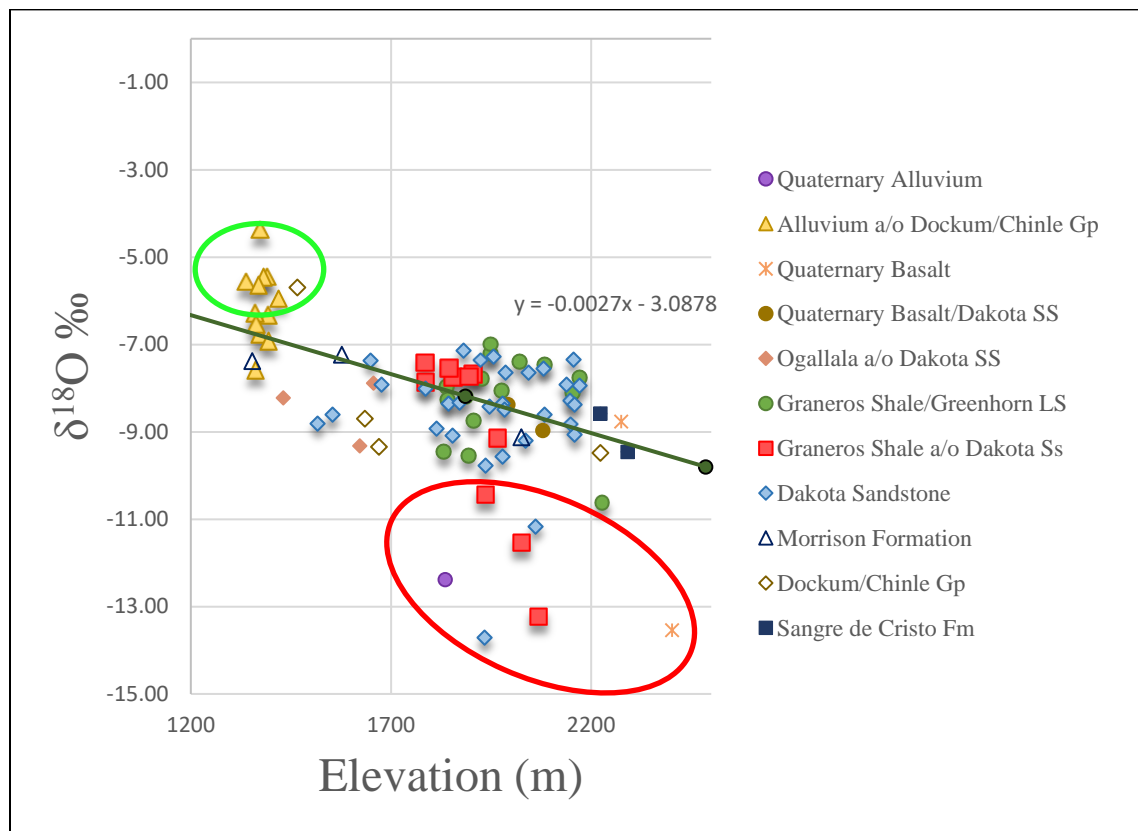
unit.

Figure 33: Scatterplot of δ^{18}O vs. elevation (m), plotted by hydrostratigraphic unit with a line of best fit shown for data excluding outlier groups, circled in green for more enriched and red for more depleted than the elevation trend.
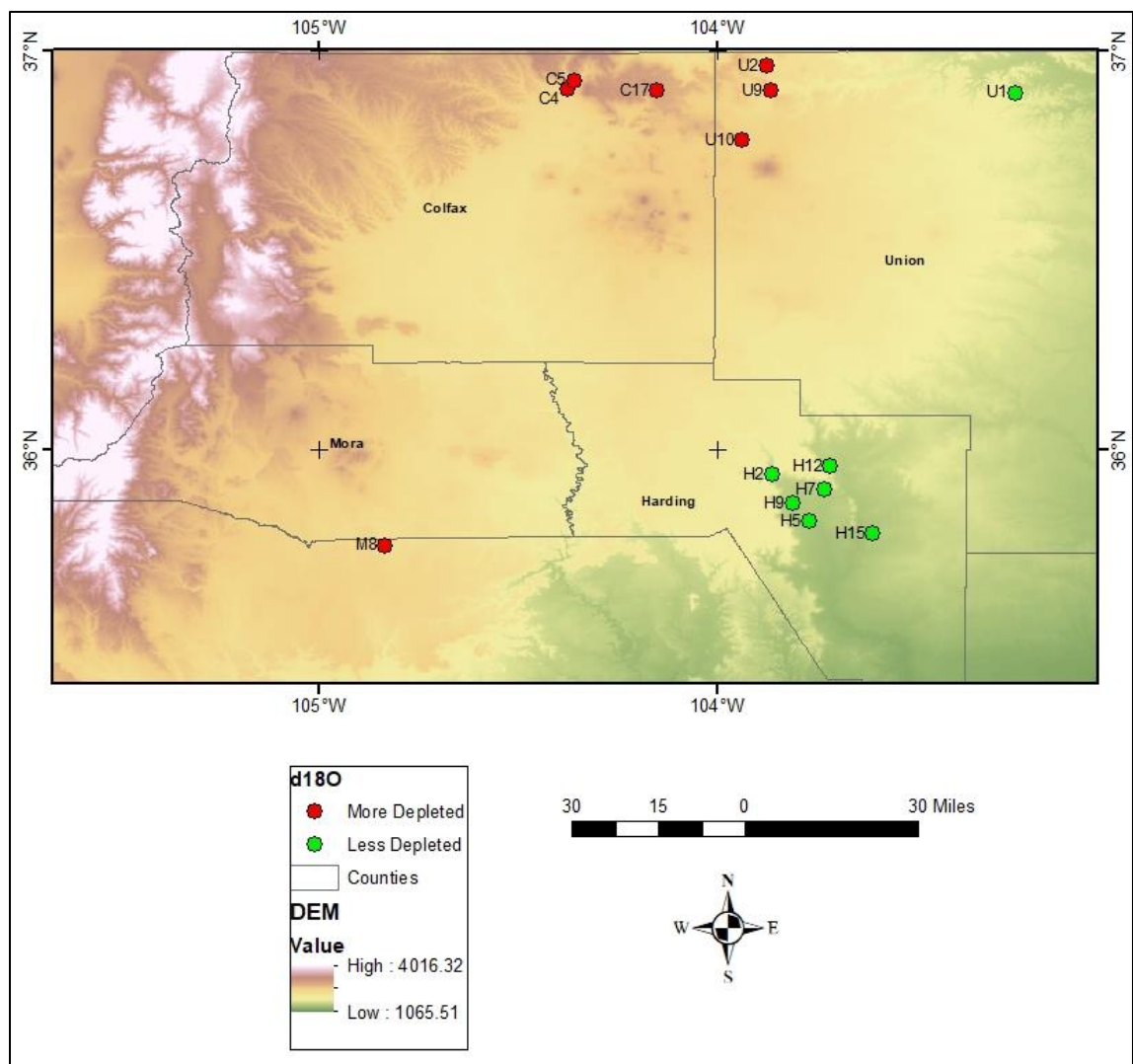
Figure 34: Map showing locations of δ¹⁸O values shown as outliers in Figure 33.
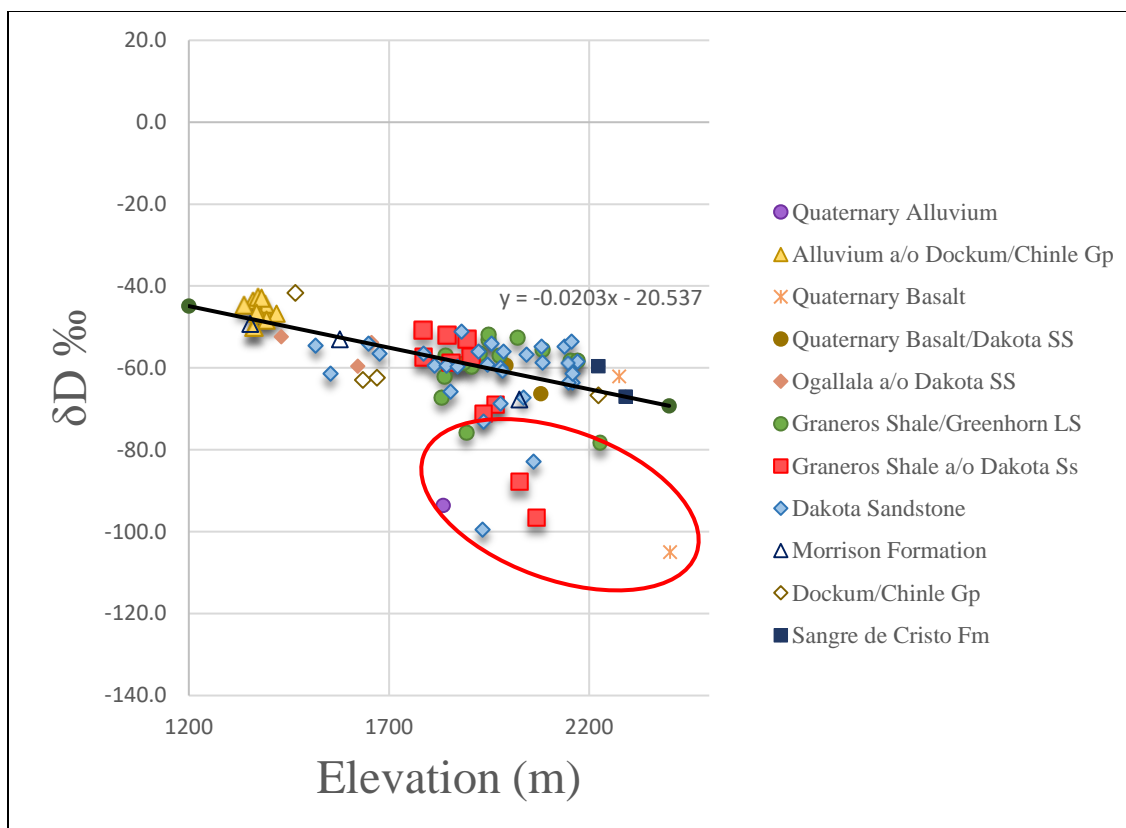
Figure 35: Scatterplot of δD vs. elevation (m), plotted by hydrostratigraphic unit with an approximate line of best fit and outlier data circled in red.

4.2 Major cation and anion concentrations

All cation and anion data can be found in Appendix A and Appendix B, with the exception

of samples M12, M13, M14, M16, and U1, which could not be analyzed for cations due to an

unknown matrix or interference issue. Data from all samples reveals the dominant cation is Ca^{2+},

while the dominant anion is HCO_3^- for the study area (Figure 36, Table 1). Cations and anion

concentrations were reported as meq/L and normalized to 100%. Any value above 50% was

determined to be the dominant cation and anion and were combined to determine the overall

hydrochemical facies for each sample. In the case of no ion registering above 50%, the facies was

determined to be "mixed." When Ca^{2+} is combined with Mg^{2+}, this dominant cation exceeds 50%

of total cations in all cases, resulting in no waters classified as "mixed cation." For the purpose of

this study, Ca^{2+} and Ca^{2+} - Mg^{2+} waters have been combined into the same category of

Ca^{2+} - Mg^{2+}. Spatial distribution of hydrochemical facies is provided in Figure 37.
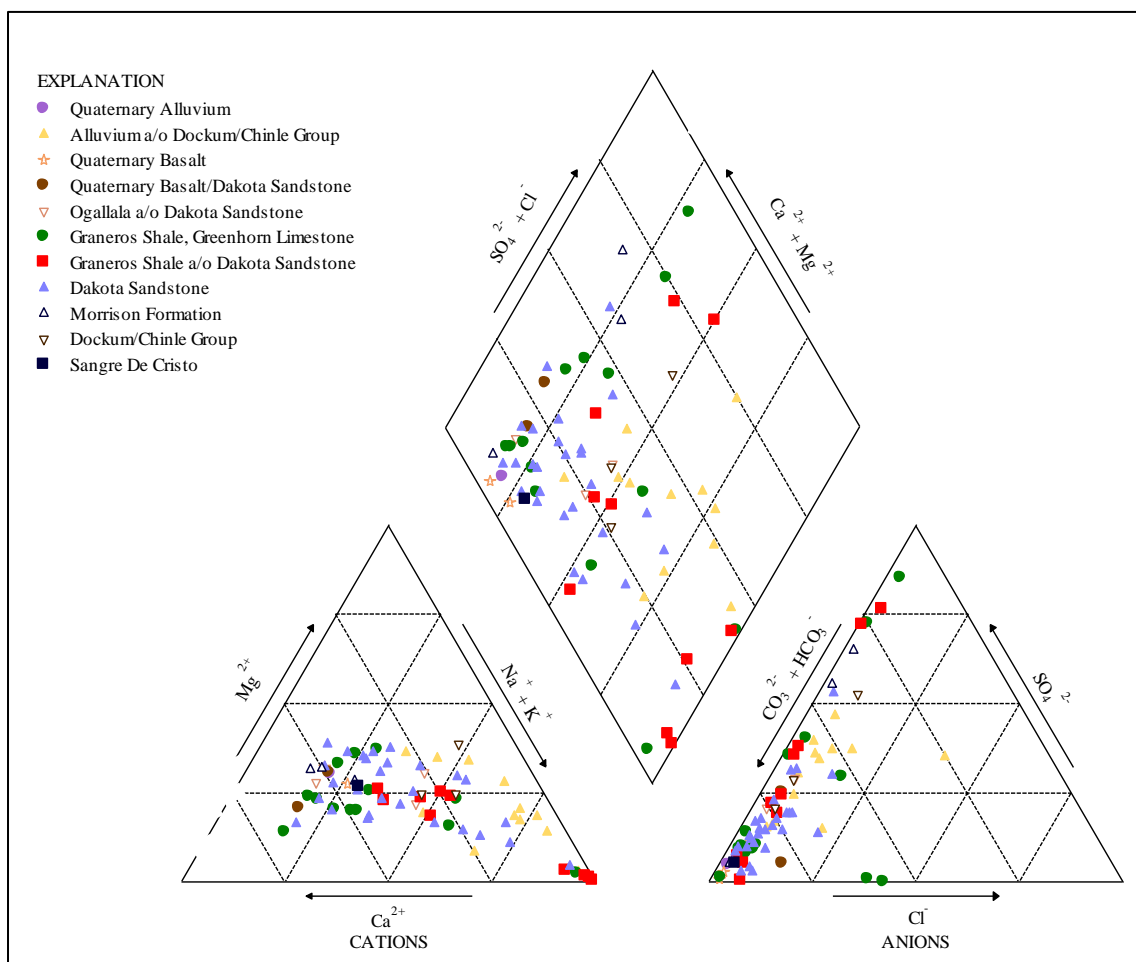
Figure 36: Piper diagram showing the major cations and ions of all samples.

Table 1: Table depicting number of samples in each hydrochemical facies, categorized by hydrostratigraphic unit. Hydrostratigraphic units: 11) Quaternary alluvium, 10) Alluvium and/or Dockum/Chinle Group, 9) Quaternary Basalt, 8) Quaternary Basalt and/or Dakota Sandstone, 7) Ogallala Formation, 6) Graneros Shale/Greenhorn Limestone, 5) Graneros Shale and/or Dakota Sandstone, 4) Dakota Sandstone, 3) Morrison Formation, 2) Dockum/Chinle Group, and 1) Sangre de Cristo Formation.

Hydrostratigraphic Unit	Ca-Mg – HCO_3	Ca-Mg – Mixed Anion	Ca-Mg – SO_4	Na – HCO_3	Na – Mixed Anion	Na – SO_4	Na – Cl-NO_3
11	1						
10	3			6	2		1
9	2						
8	2						
7	3						
6	8		2	4			
5	2		1	6		1	
4	18	1	1	8			
3	1		1	1			
2	1	1	1				
1	1						

Figure 37: Map depicting spatial distribution of hydrochemical facies.

A Piper diagram was created for each of the main hydrostratigraphic units for a determination of hydrochemical facies (Hiscock and Bense, 2014). The alluvium and/or Dockum/Chinle Group samples are a combination of Ca^{2+} $Mg^{2+}HCO_3^-$ type (*n*=3), Na^+ HCO_3^- type (*n*=6), mixed Na^+-mixed anion type (*n*=2), and Na^+ Cl^- NO_3^- type (*n*=1) (Table 1; Figure 38). Samples from the Graneros Shale/Greenhorn Limestone unit are a combination of Ca^{2+}

Mg^{2+}HCO$_3^-$ type (n=8), Ca^{2+} Mg^{2+} SO$_4^{2-}$ type (n=2), and Na$^+$HCO$_3^-$ type (n=4) (Table 1; Figure

39). The Graneros Shale and/or Dakota Sandstone samples are a combination of Ca^{2+} Mg^{2+}HCO$_3^-$

type (n=2), mixed Ca^{2+} Mg^{2+} SO$_4^{2-}$ type (n=1), Na$^+$HCO$_3^-$ type (n=6), and Na$^+$ SO$_4^{2-}$ type (n=1)

(Table 1; Figure 40). The last of the four major hydrostratigraphic units, Dakota Sandstone, is

comprised mostly of Ca^{2+} Mg^{2+}HCO$_3^-$ type (n=18), with one sample of Ca^{2+}Mg^{2+}-Mixed anion

type, one sample of Ca^{2+} Mg^{2+} SO$_4^{2-}$ type, and eight samples of Na$^+$HCO$_3^-$ type (Table 1; Figure

41).
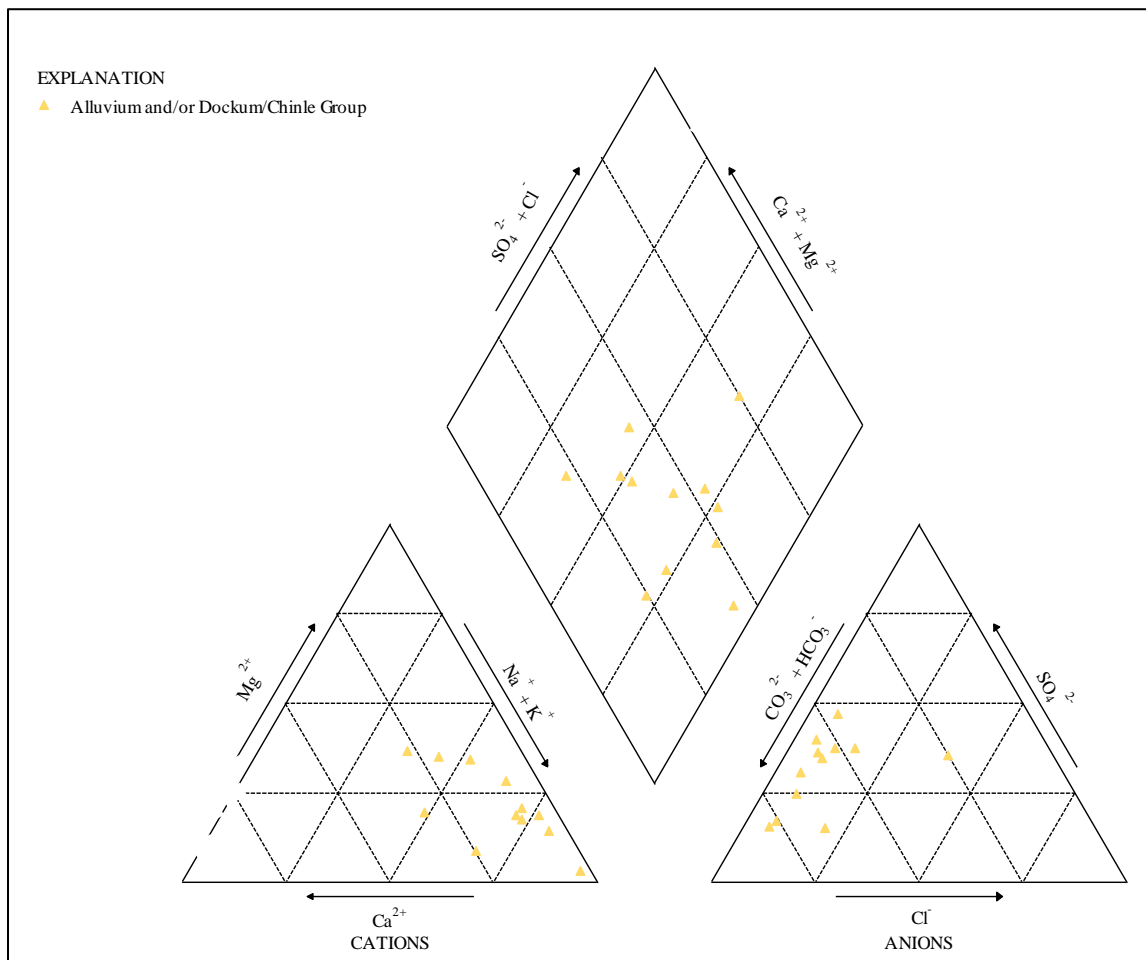
Figure 38: Piper diagram showing the major cations and ions of the alluvium and/or Dockum/Chinle Group hydrostratigraphic unit only.

54
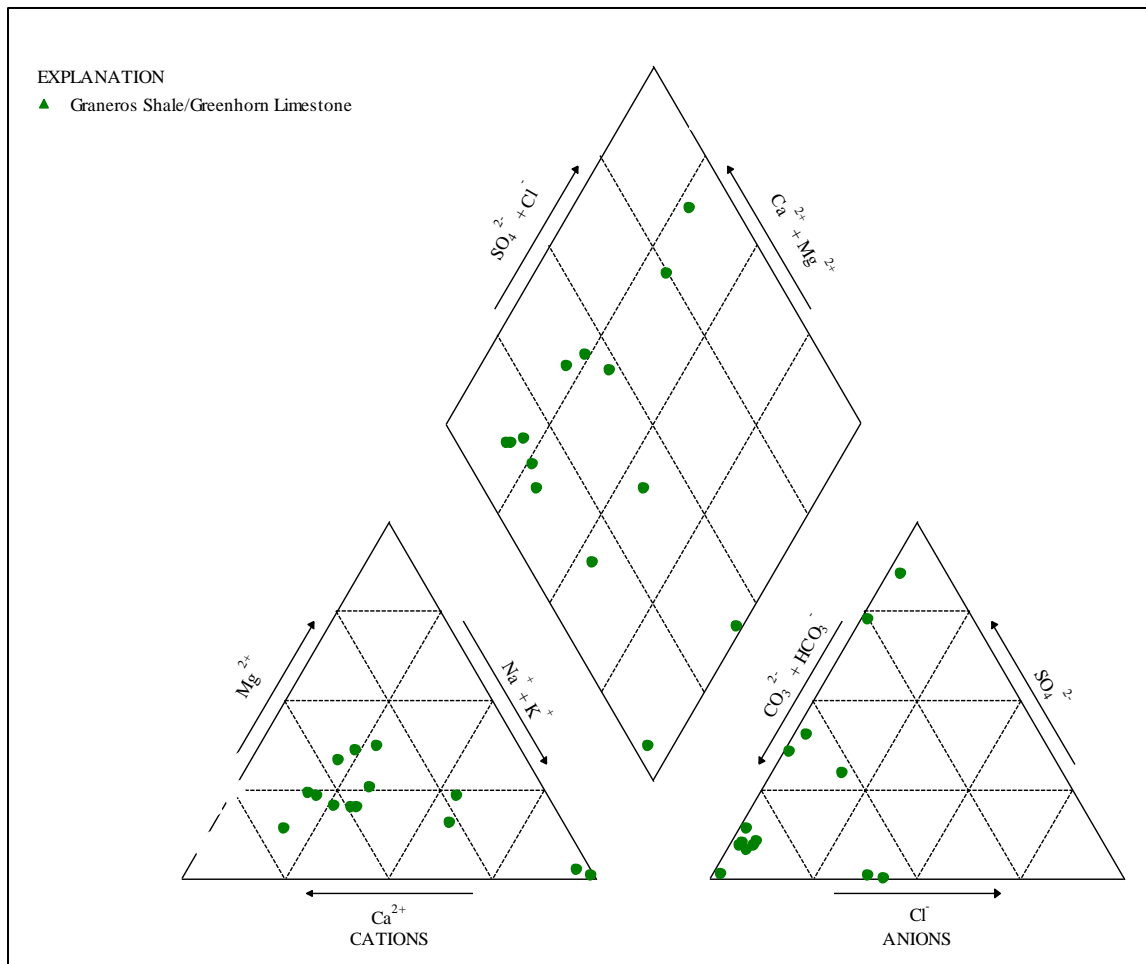
Figure 39: Piper diagram showing the major cations and ions of the Graneros Shale/Greenhorn Limestone hydrostratigraphic unit only.
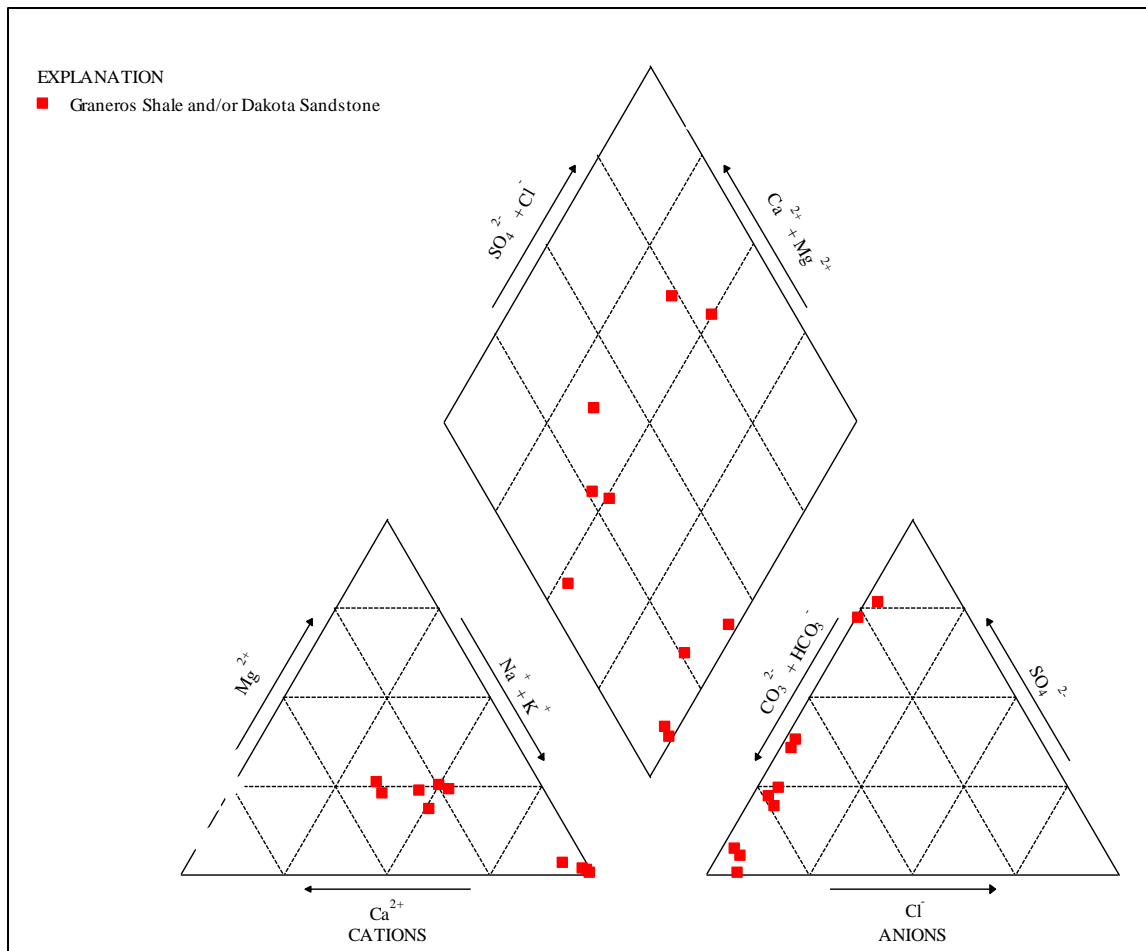
Figure 40: Piper diagram showing the major cations and ions of the Graneros Shale and/or Dakota Sandstone hydrostratigraphic unit only.
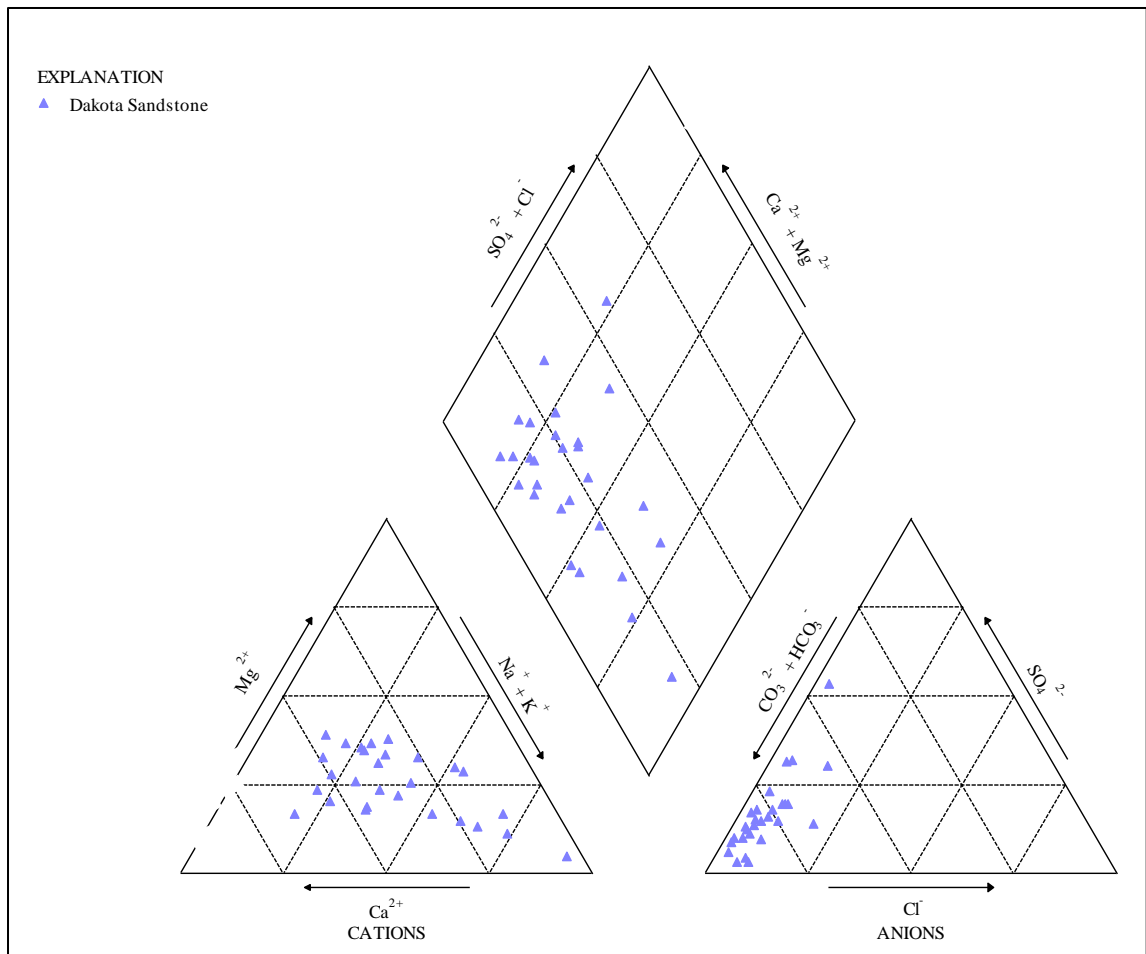
Figure 41: Piper diagram showing the major cations and ions of the Dakota Sandstone hydrostratigraphic unit only.

High concentrations of sulfate (SO_4^{2-}) were recorded in a few samples (Appendix B; Figure 36; Figure 42). High sulfate concentrations do not appear to be the signature of one specific unit, but instead occur broadly across units mostly containing Graneros Shale or the Dockum/Chinle Group (Figure 42). One exceptionally high sulfate concentration of 4,510 mg/L was recorded at C8 (Appendix B; Figure 42). High concentrations of nitrate (NO_3^-) were also recorded at three locations in the study area: H15 from the alluvium and/or Dockum Chinle

Group unit (12.5 mg/L), U5 from the Dakota Sandstone unit (6.7 mg/L), and U6 from the

Dockum/Chinle Group unit (12.6 mg/L) (Appendix B).
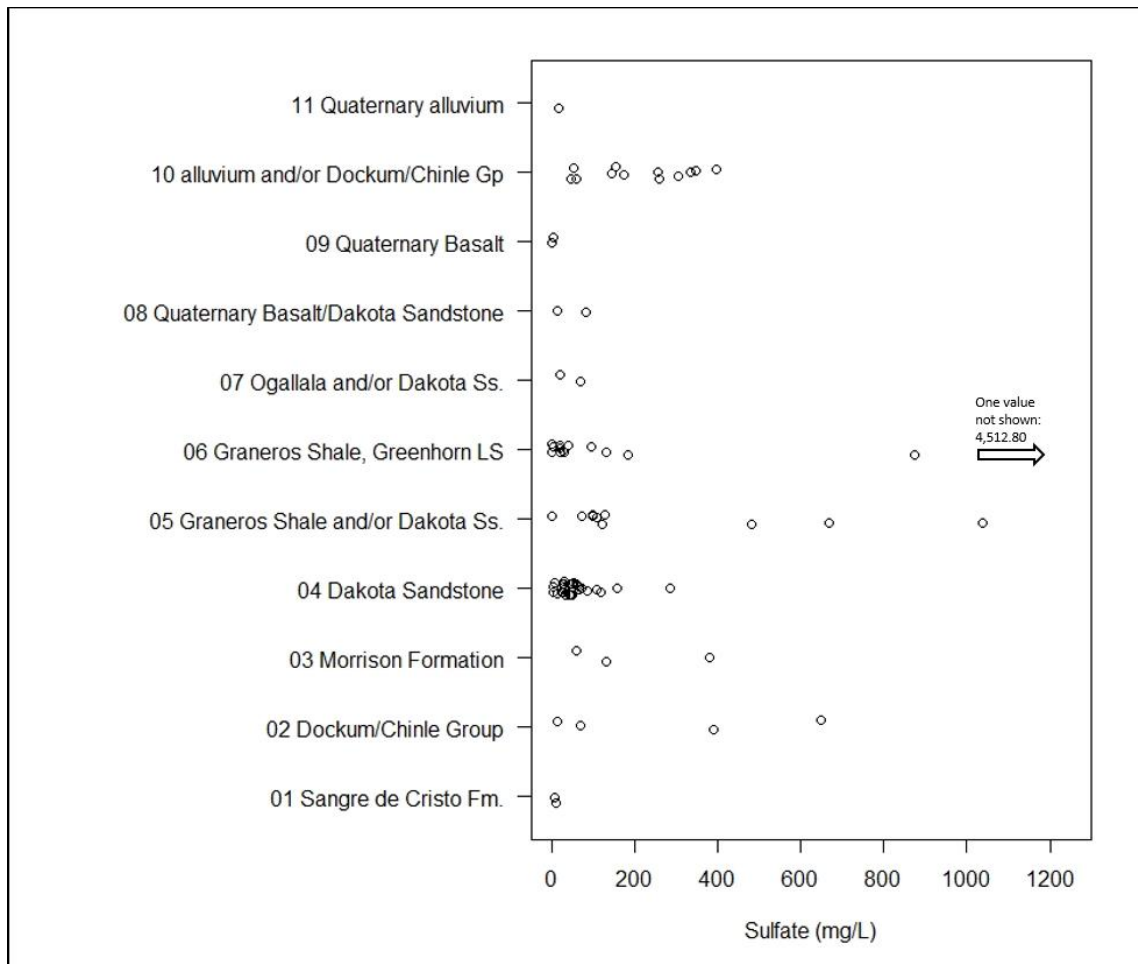
Figure 42: Dot plot of sulfate values for each hydrostratigraphic unit.

4.3   Dissolved Inorganic Carbon, alkalinity, and δ^{13}C-DIC

4.3.1   Dissolved inorganic carbon and alkalinity

Values for DIC, alkalinity, and pH calculated from DIC and alkalinity can be found in

Appendix B. For DIC analysis, one sample was not analyzed due to lack of volume of sample

(U1), and four (C2, C3, C10, and C13) could not be processed. DIC values range from 2.63 to

13.14 millimoles per liter (mM) with a median value of 5.50 mM, mean of 5.72 mM, and

standard deviation of 1.91 mM. All samples were analyzed for alkalinity concentration using the

Gran titration method with 0.1 normal hydrochloric acid using an electronic titrator. Alkalinity

values range from 2.62 to 37.57 millequivalents per liter (meq/L). Alkalinity is reported in meq/L because alkalinity is defined as the water sample's ability to neutralize H^+ from a strong acid, and therefore represents the combined effects of HCO_3^- and CO_3^{2-} ions. The four samples that were not quantified for DIC due to instrument range limitations, C2, C3, C10, and C13, represent the four highest alkalinity concentrations of 33.73, 37.57, 21.92, and 29.64 meq/L, respectively (Figure 43). Samples C2, C3, and C10 came from the Graneros Shale and/or Dakota Sandstone unit, while sample C13 came from the Graneros Shale/Greenhorn Limestone unit. Figure 44 is a scatterplot of the relationship between DIC and alkalinity plotted relative to the 1:1 ratio that exists when all alkalinity occurs as bicarbonate ion at neutral to slightly basic pH. Samples that could not be analyzed for DIC are not included in Figure 44.
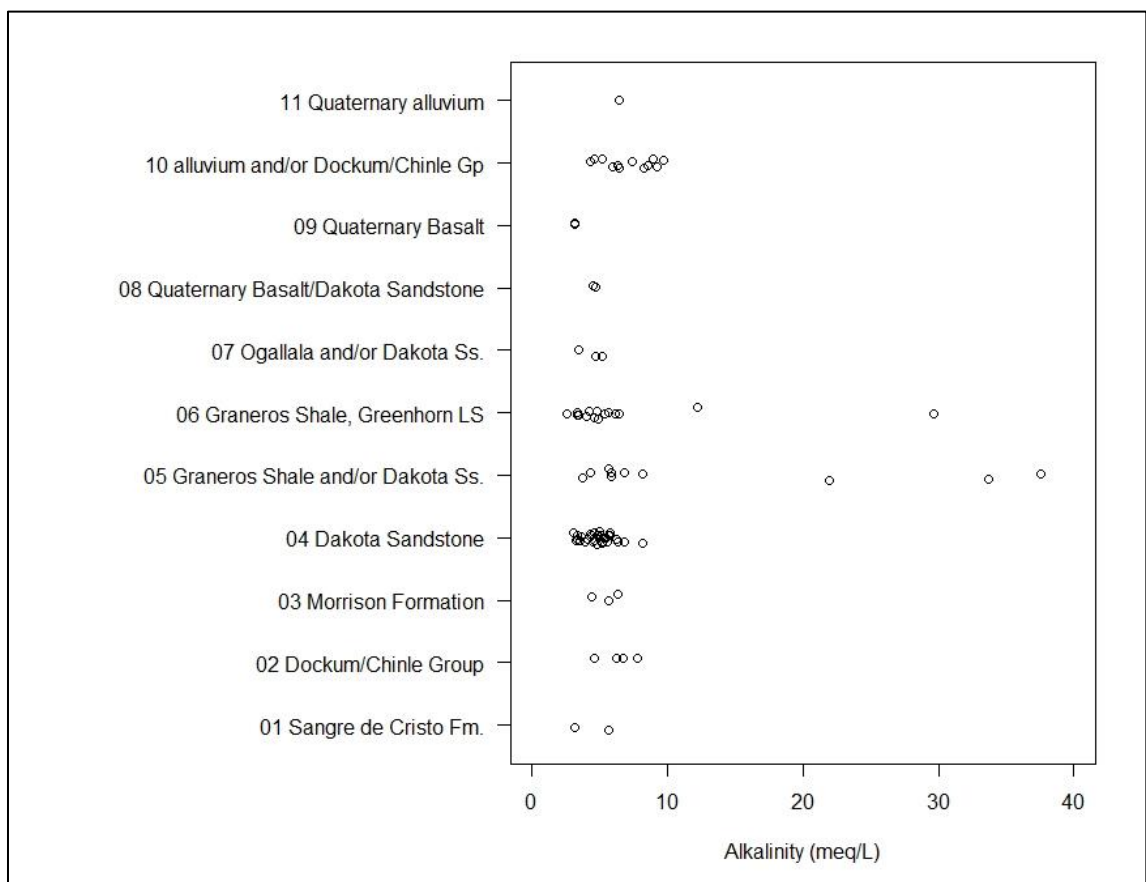
Figure 43: Dot plot of alkalinity values (meq/L) for each hydrostratigraphic unit.
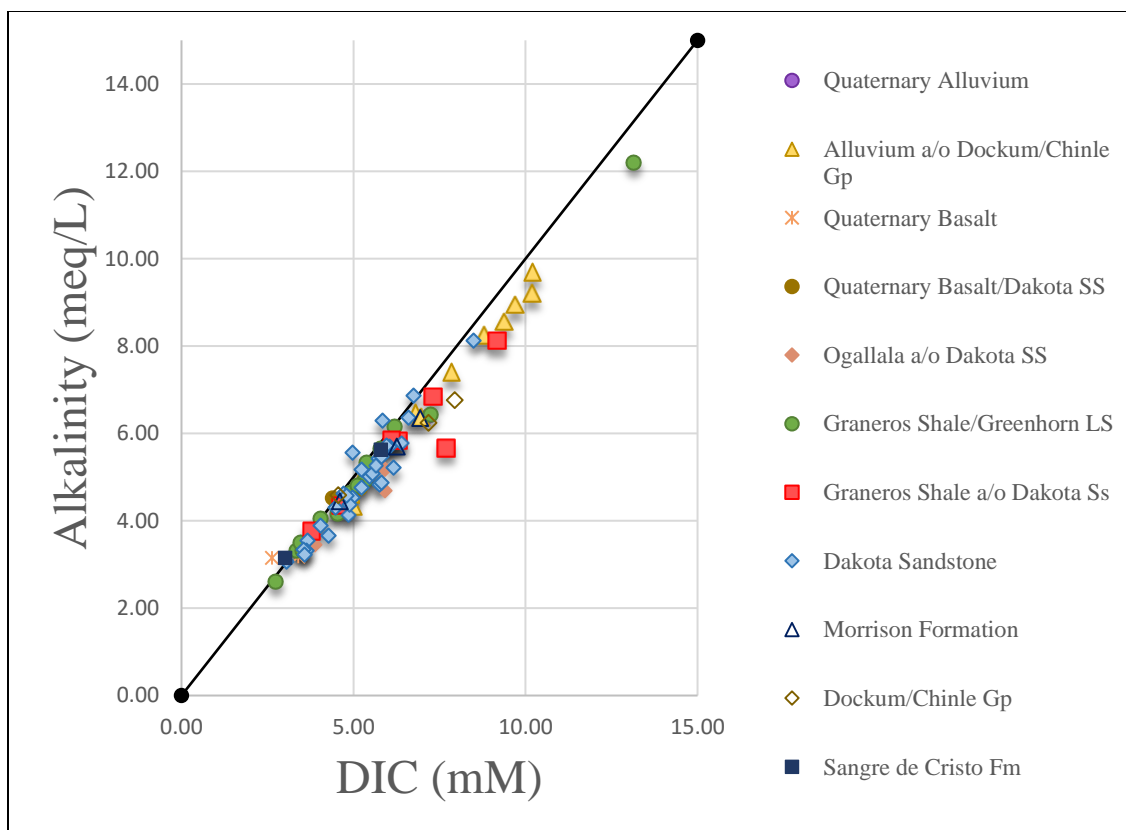
Figure 44: Scatterplot of alkalinity (meq/L) vs. DIC (mM) plotted by hydrostratigraphic unit. Solid line represents a 1:1 relationship between alkalinity and DIC which would occur when all alkalinity occurs as bicarbonate ion. Data lying slightly below the line correspond to a small proportion of DIC occurring as carbonic acid, which does not contribute to alkalinity.

Each of the four main hydrostratigraphic units is individually graphed in Figure 45,

Figure 46, Figure 47, and Figure 48. Samples from the alluvium and/or Dockum/Chinle Group

(Figure 45) fall slightly below the 1:1 line, with greater differences as DIC increases. The

majority of samples from the Graneros Shale/Greenhorn Limestone unit (Figure 46) fall directly

on the 1:1 line, with the two highest DIC values falling noticeably lower than the line. Sample C8

can be seen in Figure 44 and Figure 46 as the highest point, plotted at (13.14,12.21). Samples

from the Graneros Shale and/or Dakota Sandstone unit (Figure 47) appear to be the most different

from the 1:1 trend because of two data points (C1 and M5) falling significantly below the line.

Seen in Figure 44 and Figure 47, C1 is the farthest from a 1:1 relationship, plotted at (7.69,5.67).

Samples from the final unit, the Dakota Sandstone unit (Figure 48), fall mostly below the 1:1 line.

This unit would exhibit a trend parallel to the 1:1 line if not for three samples that fall above the
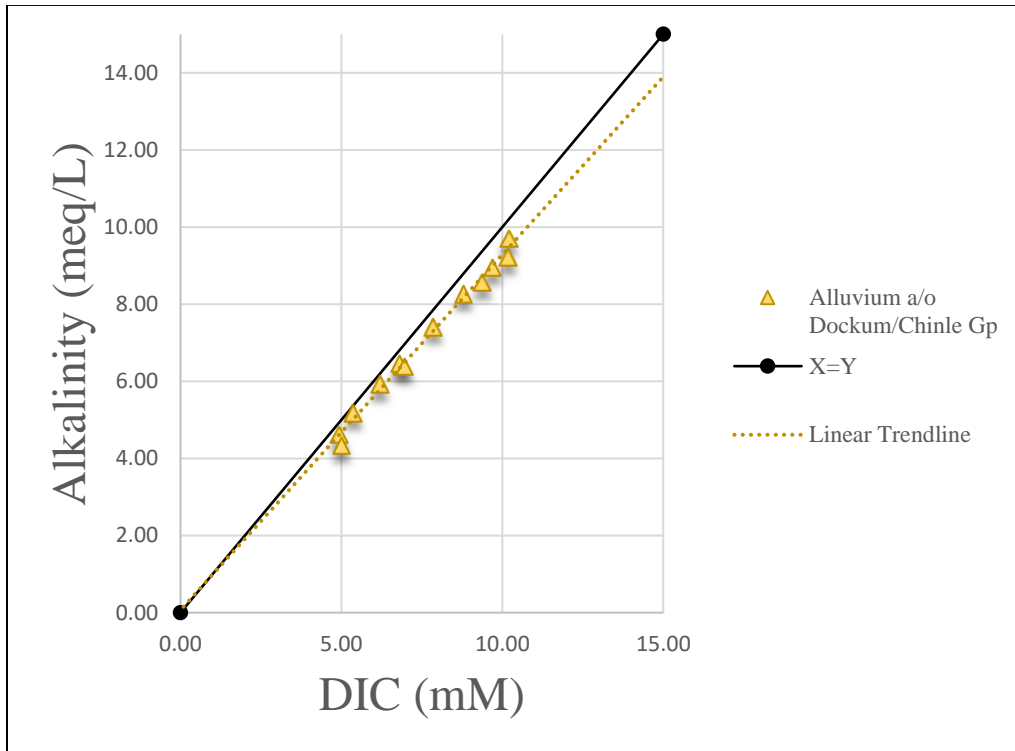
line.

Figure 45: Scatterplot of alkalinity vs. DIC plotted for the alluvium and/or Dockum/Chinle Group only. Solid line represents a 1:1 relationship between alkalinity and DIC.
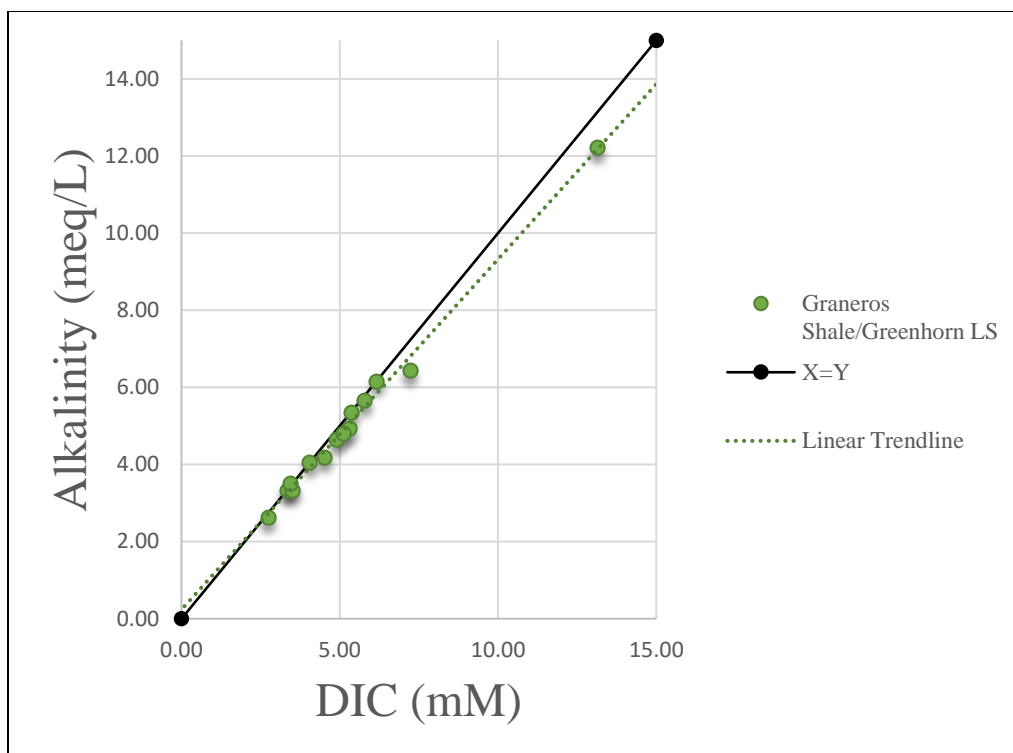
Figure 46: Scatterplot of alkalinity vs. DIC plotted for the Graneros Shale/Greenhorn Limestone unit only. Solid line represents a 1:1 relationship between alkalinity and DIC.
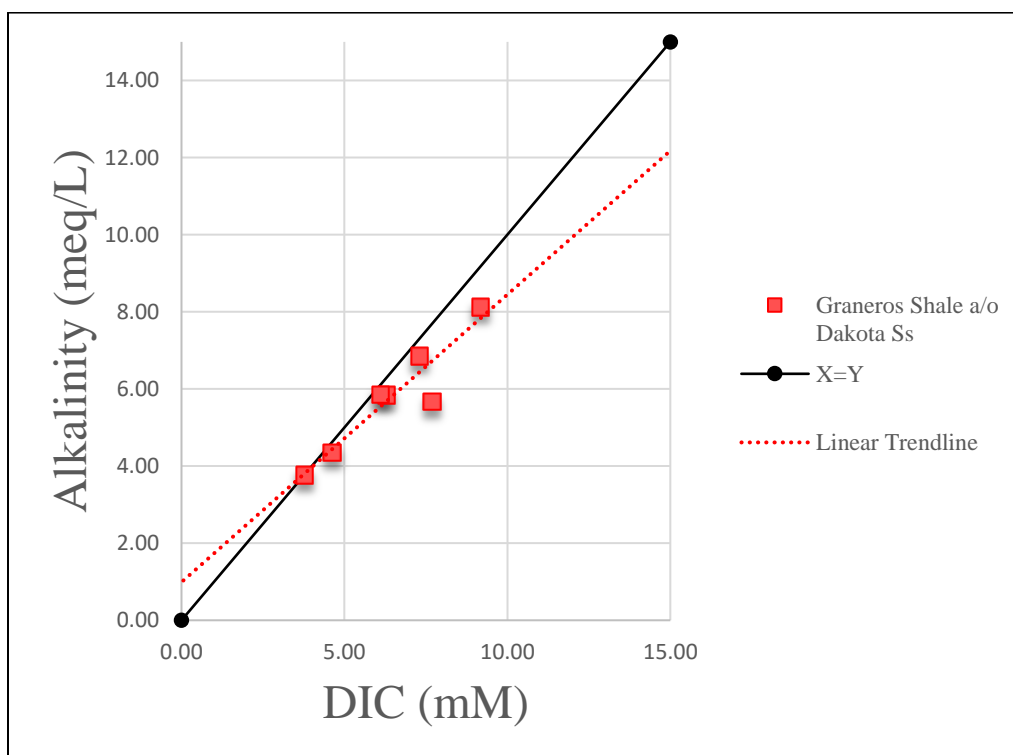
Figure 47: Scatterplot of alkalinity vs. DIC plotted for the Graneros Shale and/or Dakota Sandstone unit only. Solid line represents a 1:1 relationship between alkalinity and DIC.
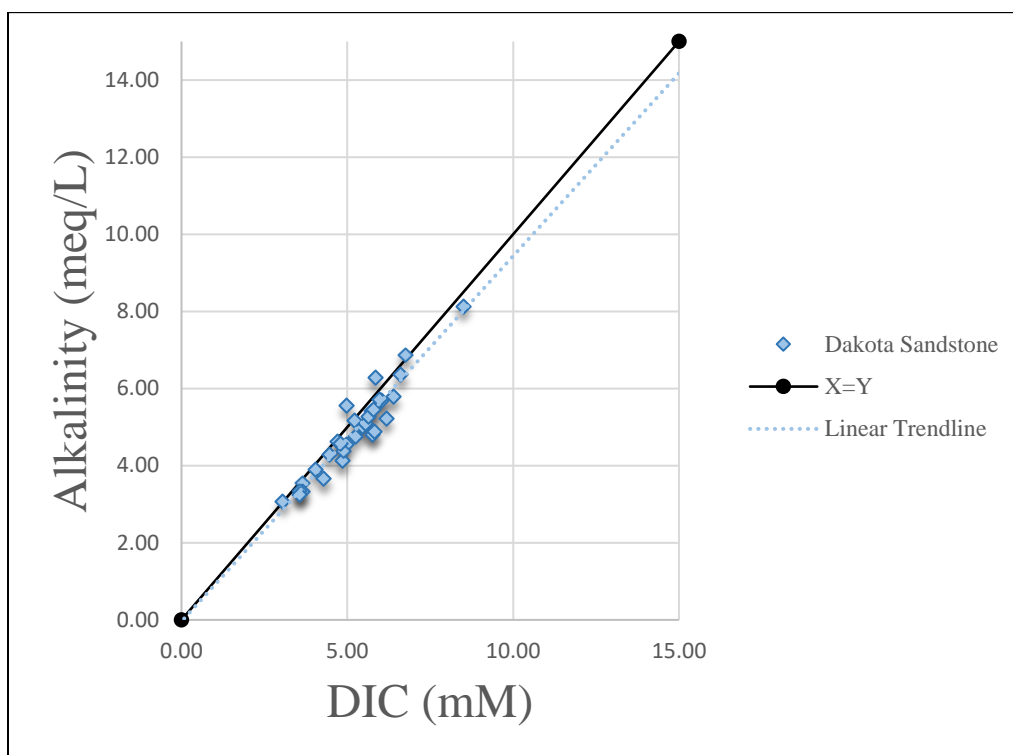
Figure 48: Scatterplot of alkalinity vs. DIC plotted for the Dakota Sandstone unit only. Solid line represents a 1:1 relationship between alkalinity and DIC.

4.3.2 δ¹³C-DIC

δ^{13}C-DIC values (Appendix B) range from -13.01‰ to -1.50‰ with an average value

of -7.41‰ and a standard deviation of 2.53‰. Data exhibit an approximately normal distribution,

with 80% of the data falling within one standard deviation and 94% of the data falling within two

standard deviations. Figure 49 is a dot plot depicting the data distribution of δ^{13}C-DIC values by

hydrostratigraphic unit. The alluvium and/or Dockum/Chinle Group ranges from -2.00

to -10.80‰, the Graneros Shale/Greenhorn Limestone unit ranges from -4.55 to -12.34‰, the

Graneros Shale and/or Dakota Sandstone unit ranges from -4.57 to -13.01‰, and the Dakota

Sandstone unit ranges from -1.50 to -12.96‰. δ^{13}C-DIC values were mapped to analyze any

potential spatial relationship, shown in Figure 50. More negative values of δ^{13}C-DIC roughly correlate with higher elevations and generally increase with distance from the mountains.

δ^{13}C-DIC values were plotted against pH values in Figure 51. Ranging from 6.83 to 9.77, pH values were calculated using alkalinity and DIC concentrations assuming that DIC > alkalinity at acidic pH because carbonic acid is a significant part of DIC, and DIC < alkalinity at basic pH because carbonate ions become a significant part of the DIC. Figure 51 reveals no overall trend. None of the major hydrostratigraphic units exhibit a noticeable relationship between δ^{13}C-DIC and pH when analyzed individually.
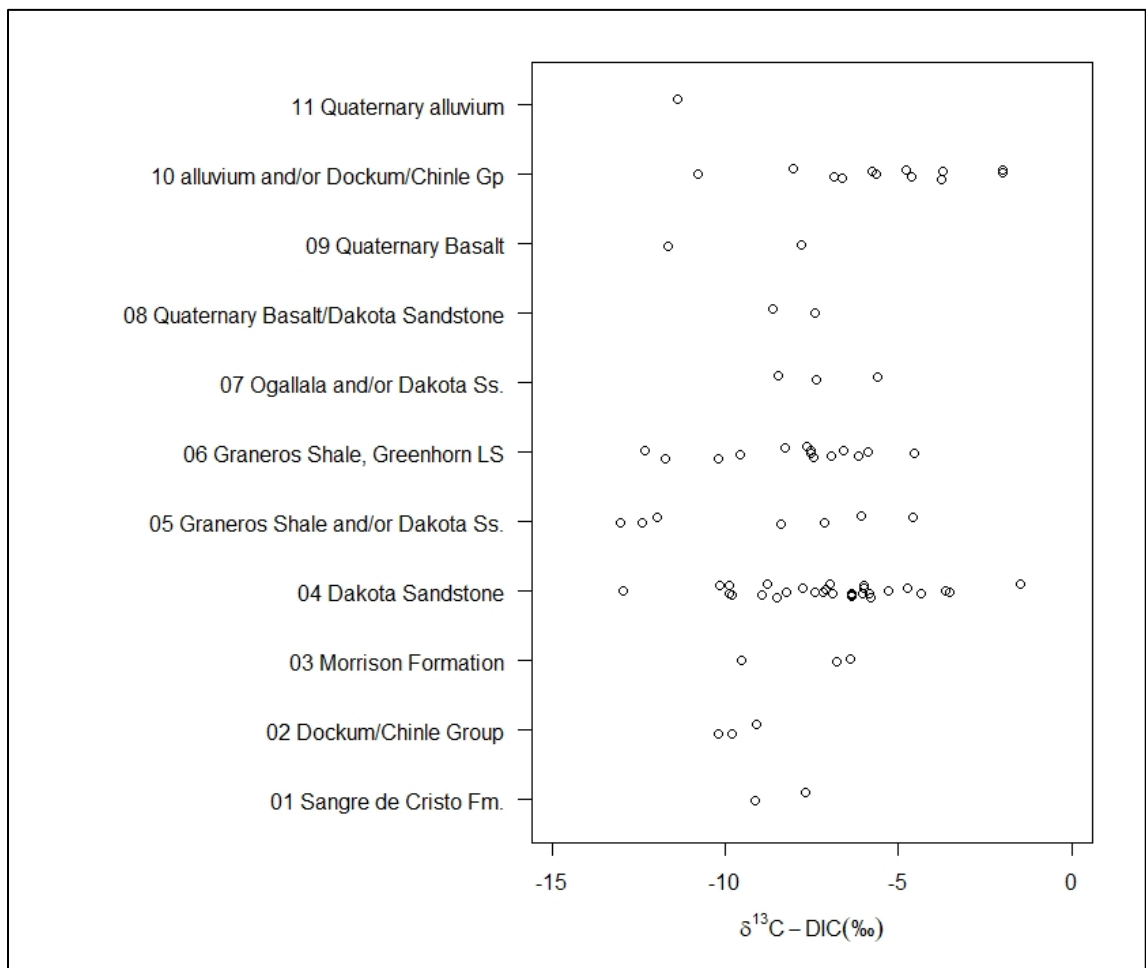
Figure 49: Dot plot of δ^{13}C-DIC values for each hydrostratigraphic unit.
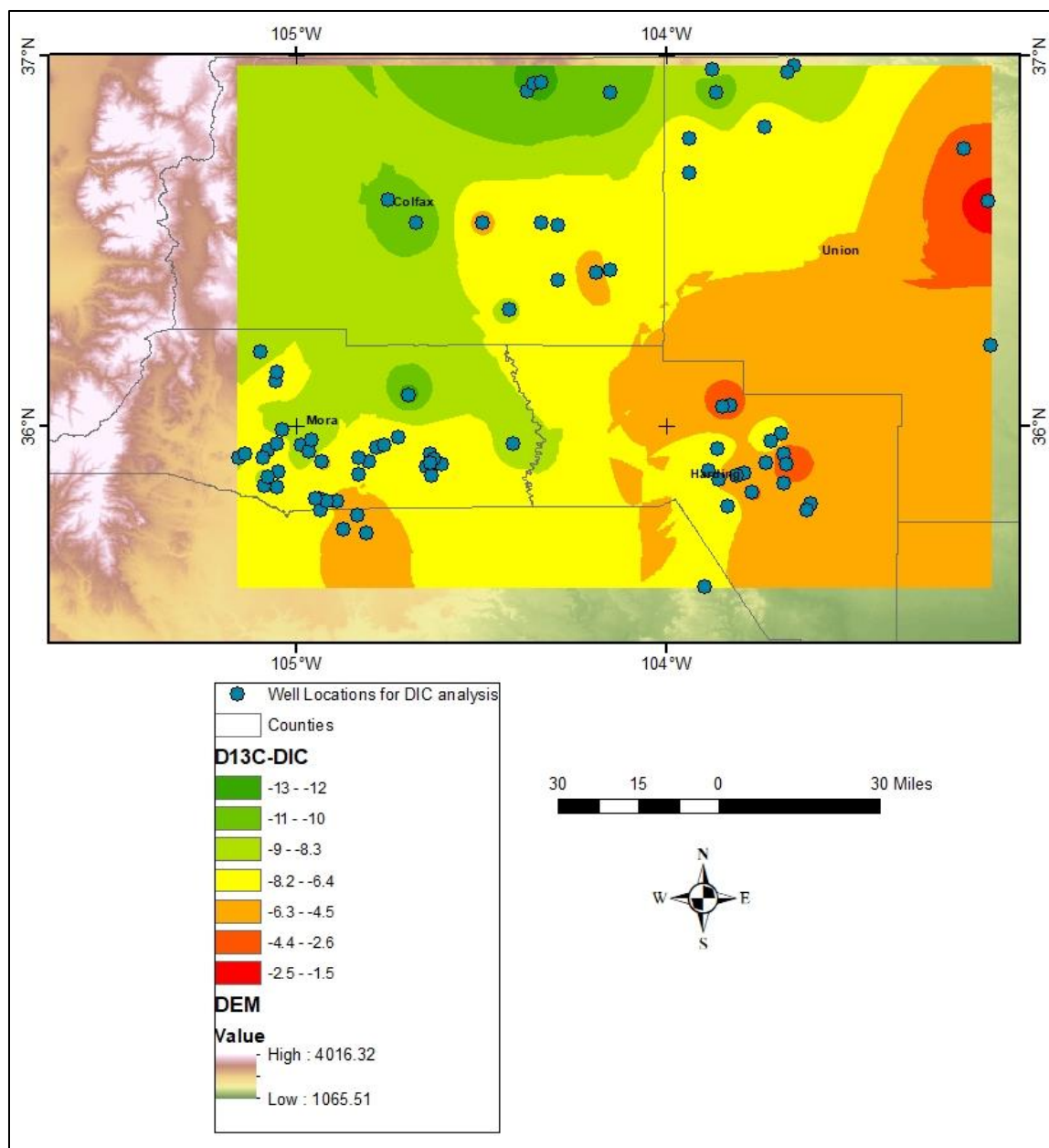
Figure 50: Map of δ¹³C-DIC values created using IDW method and displayed by standard deviation.
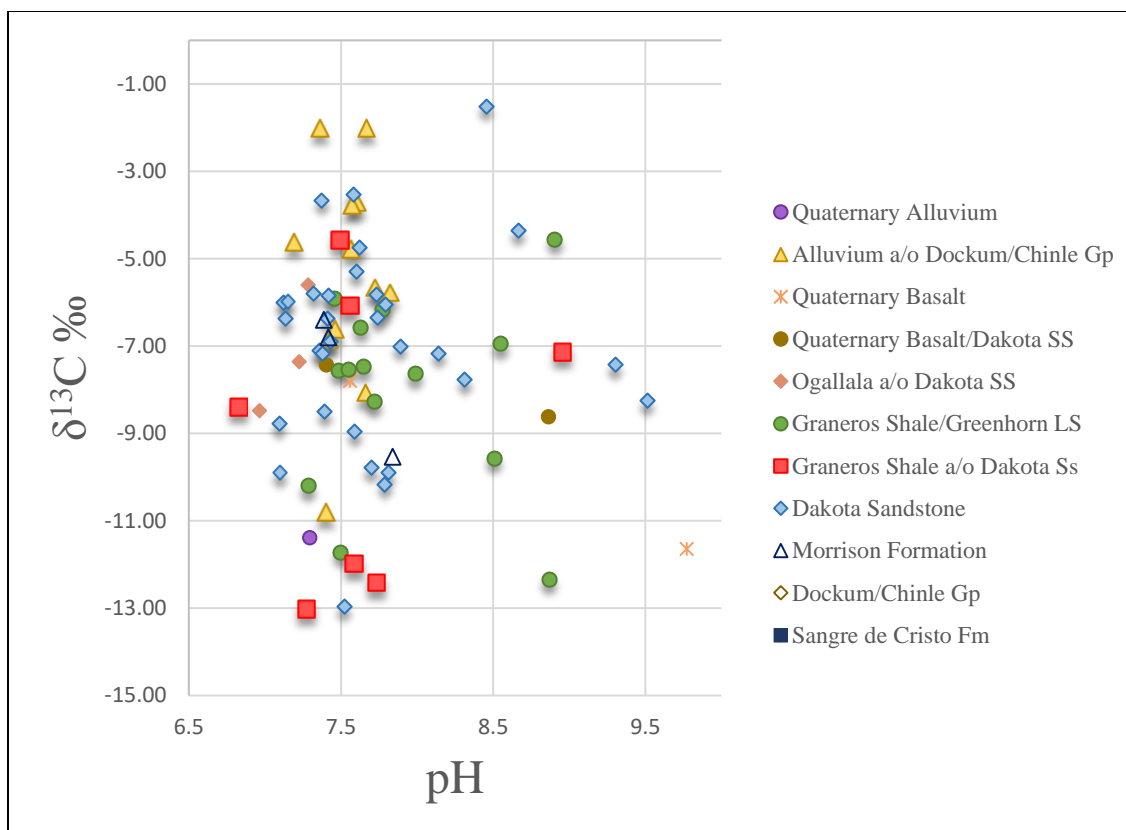
Figure 51: Scatterplot of δ¹³C-DIC vs. calculated pH (derived from alkalinity and DIC concentration) plotted by hydrostratigraphic unit.
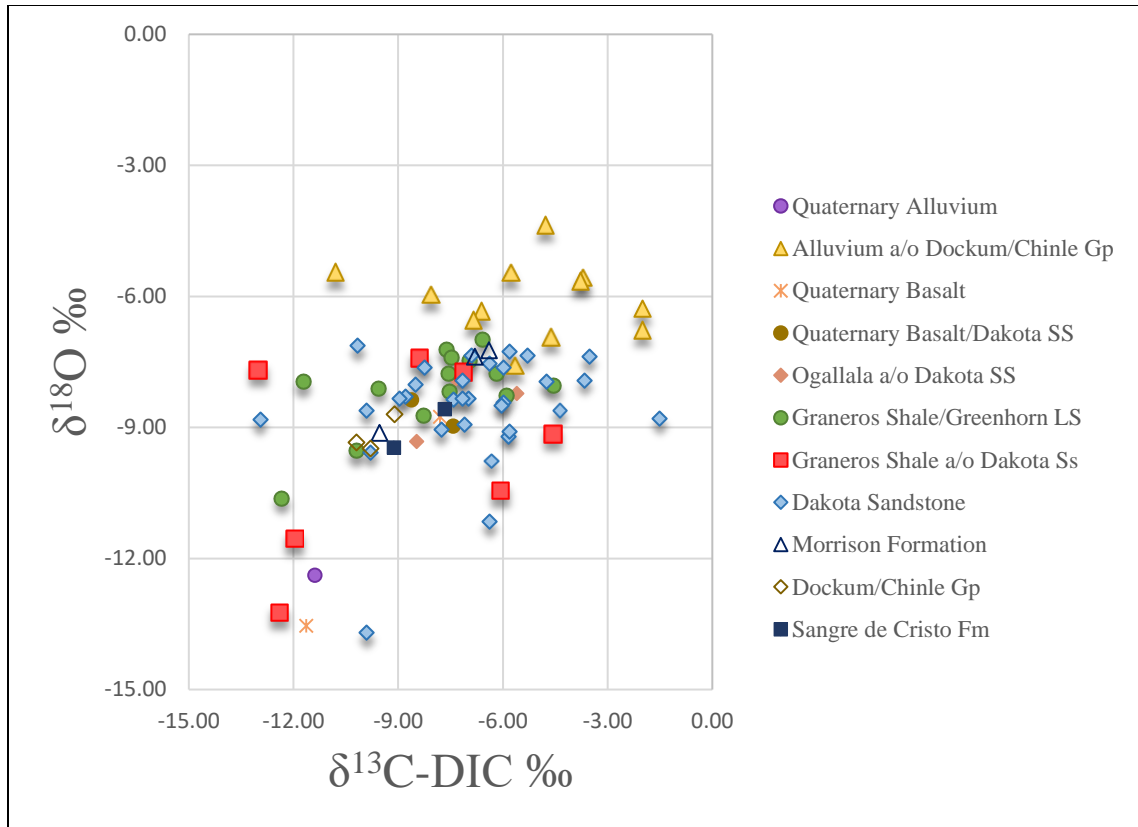
Figure 52: Scatterplot of δ¹⁸O vs. δ¹³C-DIC, plotted by hydrostratigraphic unit.

4.4   Tritium

Locations for tritium analysis were based on preliminary results of the study. U10 and C15 were chosen because of their very negative $\delta^{18}O$ and δD values, shown in Table 2. C16 was chosen as a point of reference to provide a data point close to a watercourse (hypothesized to be a site of focused recharge) and of interest for long-term water supply sustainability. U10 and C15 are considered to be tritium-free with tritium units (TU) below 0.8, while C16 has a much higher value of 4.40 TU (Table 2).

Table 2: Results of tritium analysis performed at the Tritium Laboratory at Miami University.

Location	$\delta^{18}O$ (‰)	δD (‰)	Tritium Units (TU)	Hydrostratigraphic Unit
U10	-11.16	-82.9	0.00	Dakota Sandstone
C15	-10.62	-78.3	0.04	Graneros Shale LS/Greenhorn LS
C16	-8.26	-56.9	4.40	Graneros Shale LS/Greenhorn LS

5   Discussion

5.1.1   Spatial distribution of isotopes

When considering the isotope data from all hydrostratigraphic units (Figure 18 and Figure 19), it appears that there is a general southeast to northwest trend from more isotopically enriched to more isotopically depleted samples. Likewise, Dutton (1995) found that both δD and δ18O decrease along a lateral south-to-north trajectory in both unconfined and confined aquifers in the southern and central High Plains regions. This trajectory is evidence of the continental effect – increasing distance over land, and away from the vapor source, results in increasingly depleted precipitation (Clark and Fritz, 1997). Although the findings of this study are somewhat consistent with the pattern observed by Dutton (1995), the study area covers less than two degrees of latitude and it is unlikely that continentality would be observed at this scale. It is more likely that the southeast to northwest trend found in the study area is the result of changes in elevation, discussed in section 5.1.3.

Dutton (1995) also found that δD and δ18O become increasingly negative along a vertical depth gradient between shallow unconfined aquifers and the deeper confined Triassic Dockum in the southern High Plains and between unconfined aquifers and the confined Dakota Sandstone beneath the Central High Plains. The data provided in this study also exhibit a vertical gradient from more enriched groundwater in younger hydrostratigraphic units (-7.58 to -4.37‰ in the alluvium and/or Dockum/Chinle Group unit and -10.62 to -6.99‰ in the Graneros Shale/Greenhorn Limestone unit) to more depleted groundwater in older hydrostratigraphic units (-13.23 to -7.41‰ in the Graneros Shale and/or Dakota Sanstone unit and -13.70 to -7.13‰ in the Dakota Sandstone unit).

Spatial distribution analysis is dependent on the distribution of data points. As seen in Figure 17, Figure 18, and Figure 19, the distribution of samples is not uniform across the study area. Sample locations were determined by landowner permission, the presence of springs, or the presence of developed wells, reflecting the nature of human patterns of land development. Spatial

analysis in future studies can be improved by filling the gaps in central and southern Union County, western Harding County, western Colfax County, and western Mora County.

5.1.2   Relationship of groundwater to the GMWL

A well-known method of analyzing the isotopic composition of water samples is to compare to the Global Meteoric Water Line, which is a composite average of local meteoric water lines from around the world. Because of regional variability, analysis is more accurate when groundwater samples are compared to local Meteoric Water Lines (LMWL) if precipitation data are available. Unfortunately, not all regions have had in-depth precipitation isotopic analysis performed, making the GMWL the default starting point for groundwater comparison and analysis (section 1.2).

While precipitation is used to define a LMWL, some regional and local studies have defined meteoric water lines using river water data as a proxy when it is difficult to collect precipitation samples. One such study, conducted by Kendall and Coplen (2001), found a national meteoric water line of $\delta^2H = 8.16\delta^{18}O‰ + 9.63‰$ VSMOW and a New Mexico meteoric water line of $\delta^2H = 6.70\delta^{18}O‰ -5.5‰$ VSMOW, inferred from river water samples. While the study conducted by Kendall and Coplen (2001) is included in this discussion, it is worth noting that although Kendall and Coplen (2001) justify the use of surface water as a proxy for local/regional precipitation, this practice is debated by Dutton et al. (2005). Dutton et al. (2005) found that rivers fed by snowmelt at high elevations and areas with high evapotranspiration in the summer months can have a very different isotopic composition than local meteoric waters. As a result, the regional MWL supplied by Kendall and Coplen (2001) may be inaccurate in regions with steep elevation gradients and/or high evapotranspiration rates in the summer – all conditions that are present in the study area. Therefore, the primary GMWL equation used for this analysis is $\delta^2H = 8.13\delta^{18}O‰ + 10.8‰$ VSMOW (Clark and Fritz, 1997).

The majority of the data shown in Figure 20 fall along the GMWL, with a posts-precipitation evaporation trend recorded only in the most enriched waters. The slope of water lines is controlled by evaporative processes. If precipitation accumulates at the surface prior to recharge, it is subject to evapotranspiration. Clark and Fritz (1997) found that samples collected where precipitation accumulated in liquid form, and subsequently evaporated, generally produce a lower slope, around 5. In areas where precipitation accumulates as snow and subsequently evaporates (sublimates), an evaporation trend is still present, but the slope is steeper (Clark and Fritz, 1997). This is the result of snow melting at the surface, partially evaporating, and mixing enriched surface waters with underlying depleted snow before contributing to recharge (Clark and Fritz, 1997).

The slope of the MWL can also be affected by evaporation that occurs as precipitation falls to the surface. This process leads to enrichment prior to collection and results in lower slopes of the MWL (Clark and Fritz, 1997; Kendall and Coplen, 2001; Dutton et al, 2005). This evaporation trend is most common in arid environments and has produced a slope of 6.7 in New Mexico (Kendall and Coplen, 2001). Although Kendall and Coplen's (2001) methodology is contested, studies in Bahrain and Oman found similarly low slopes of 6.3 and 5.2 respectively, indicating that Kendall and Coplen's slope is slightly higher, but acceptable to use for comparisons (Clark and Fritz, 1997). Eastoe and Rodney (2014) also found a low slope of 5.6 in samples of groundwater from the Sacramento Mountains. Further evidence of this phenomenon was found in a study conducted by Dutton et al. (2005). The authors calculated expected $\delta^{18}O$ values using latitude and elevation for comparison to actual values. They concluded that the actual $\delta^{18}O$ values were more positive than the expected $\delta^{18}O$ values because of enrichment during rainfall (Dutton et al., 2005). Unfortunately, as Kendall and Coplen (2001) point out, when comparing groundwater samples to a MWL, evaporation during rainfall cannot always be distinguished from evaporation on the land surface or in the soil zone before recharge. It can,

however, be said that "waters with isotopic signatures that fall near the GMWL have not been affected by evaporation" (Stotler et al., 2015).

An evaporation trend is most prominent in the samples from the alluvium and/or Dockum/Chinle Group unit (Figure 23). These samples are geographically clustered (Figure 21) and behave similarly. The slope of 2.37 for the alluvium and/or Dockum/Chinle Group, calculated from the samples that lie below and to the right of the GMWL (Figure 23), is much lower than the slopes discussed above (Clark and Fritz, 1997; Kendall and Coplen, 2001; Dutton et al., 2005; Eastoe and Rodney, 2014), indicating high levels of evaporation prior to recharge and a lack of mixing with more depleted waters after recharge.

The other three primary hydrostratigraphic units in the study area, the Graneros Shale/Greenhorn Limestone, Graneros Shale and/or Dakota Sandstone, and the Dakota Sandstone units, produced slopes of 7.52, 7.62, and 7.23, respectively. These slopes are all closer to the GMWL than other regional studies in semi-arid and arid climates would lead one to expect, if the aquifer contained highly evaporated summer (rain) or winter (snow) precipitation. The equations for these three units are, however, very close to the equation generated by Plummer et al. (2004) for alluvial basin groundwater in the Rio Grande Basin, shown as $\delta^2 H = 7.62\delta^{18}O‰ + 2.48‰$ VSMOW in Figure 4. The data for these three units vary geographically, spanning a range of elevations and hydrogeologic settings, but fall on or just below the GMWL. Slopes close to the GMWL slope of 8 imply fairly direct recharge of precipitation with little evaporation at the land surface or in the soil zone.

5.1.3 Relationship of groundwater to precipitation isotopic composition – elevation

Elevation is known to affect the isotopic composition of meteoric waters because air masses cool adiabatically as they uplift, raining out as they rise and eventually bringing isotopically depleted precipitation to higher elevations (Clark and Fritz, 1997). A steep elevation gradient within the study area should result in a large shift toward more negative $\delta^{18}O$ values of precipitation with increasing elevation, a shift that should also be reflected in groundwater. The

study area has an elevation range of 1,065m to 4,016m, totaling 2,951m change in elevation. Therefore, using an estimated lapse rate of -0.29‰ for every 100m rise in elevation (Dutton et al., 2005), $\delta^{18}O$ can be expected to change by roughly -8.56‰. $\delta^{18}O$ values in the study area range from -4.42‰ to -13.71‰, resulting in an actual change of -9.29‰, or -0.31‰ per every 100m rise in elevation. This slightly higher rate is likely the result of possible outliers circled in green and red in Figure 33. Excluding these outliers, an estimated line of best fit is included in Figure 33 and has a slope of -0.27‰.

The outlying data deviating from the elevation- $\delta^{18}O$ relationship are divided into two groups shown in Figure 33 and Figure 34. Group 1 (green) is more enriched than expected, with $\delta^{18}O‰$ values falling above and to the left of the overall trendline. Group 1 is comprised of six samples from the alluvium and/or Dockum/Chinle Group unit, and one sample from the Dockum/Chinle Group unit (U1, H15, H12, H2, H5, H7, and H9). Figure 34 demonstrates that these samples are grouped together near ephemeral water courses. With respect to the GMWL, the more enriched samples that correspond with the lowest elevations all fall at the least negative points and display an evaporative trend (Figure 20). The presence of overly enriched groundwater at lower elevations along ephemeral water courses is consistent with evaporation found in groundwater in arid and semi-arid environments (Clark and Fritz, 1997).

Samples in group 2 (red in Figure 33 and Figure 34) are more depleted than expected, with $\delta^{18}O‰$ values falling below and to the right of the line in Figure 33. Group 2 consists of seven samples from varying hydrostratigraphic units; M8, C4, and C5 and from the Graneros Shale and/or Dakota Sandstone unit, U10 and U2 are from the Dakota Sandstone unit, U9 is from the Quaternary alluvium unit, and C17 is from the Quaternary Basalt unit. Because cooler temperatures occur at higher elevations, the lowest points on the GMWL would represent the highest elevations if elevation were the only factor affecting isotopic composition. This group of samples does represent the lowest points along the GMWL in Figure 20, but does not represent

the highest elevations (Figure 33). More depleted δ^{18}O‰ values occurring at lower elevations than expected suggests that some other process is affecting these locations.

Six of the seven samples in group 2 are located along a steep elevation gradient (e.g. at the base of escarpments) illustrated in Figure 34. One possible explanation for these samples deviating from the elevation- δ^{18}O relationship is that these samples are the result of present-day or recent recharge and/or runoff from much higher, but geographically near, elevations, often referred to as mountain system recharge (MSR) (Meixner et al., 2016). The mountains also receive much more precipitation, so contributions of mountain runoff would create disproportionately depleted waters. The one exception to this is M8, found just south of the Mora County line. This location is not along a steep elevation gradient and therefore cannot be explained by proximity to higher elevations.

Figure 35 exhibits a much more defined relationship between elevation and δD, with several points falling far enough from the estimated line of best fit to be considered outliers. This scatterplot places Group 1 from Figure 33 and Figure 34 within the normal data distribution. This scatterplot also shows sample M8 within normal data distribution. With M8 excluded from the outliers in Figure 35 and falling on the edge of outlying data in Figure 33, it is possible that this data point is not in fact an outlier. If this is the case, M8 would behave similarly to the overall elevation effect observed in the study area. As per Figure 35, U9, C17, C9, C15, C4, C5, U10, U11, and U2 noticeably deviate from the pattern.

To further investigate the possibility of mountain front recharge, potential elevations that are necessary to produce these depleted δ^{18}O samples were calculated using the equation in Figure 33. Using this equation, the expected elevation at which precipitation would have fallen to produce depleted values in these groundwater samples ranged from 2,723 – 3,930m. The highest elevation in the area north of the bulk of the outliers is 2,650m. Excluding these outliers, the average error using the equation given in Figure 33 is ±275m. The only sample to fall within the range of error is M8 and this is the only outlying sample that is not in close proximity to higher

elevations. The remaining six samples, which are clustered in the northern part of the state, all fall outside of the range of error. These findings indicate that while mountain front recharge may occur in the study area, there is another variable affecting isotopic composition of groundwater. It is likely that seasonal variations, specifically the heavy influence of winter precipitation, is responsible for the overly depleted groundwater samples.

5.1.4   Relationship of groundwater to precipitation isotopic composition – seasonality

In general, summer precipitation in the study area originates in the Gulf of Mexico, whereas winter precipitation originates in the Pacific (Nativ and Riggio, 1989; Kendall and Coplen, 2001; Vachon, 2010). Because the isotopic composition of precipitation is dependent on conditions present at the source of vapor as well as conditions at the sampling location, summer and winter precipitation in this region will have different isotopic compositions. Although Nativ and Riggio (1989) found that two thirds of annual precipitation falls during summer months, summer precipitation is often entirely removed from recharge processes due to high rates of evapotranspiration in the soil zone (Clark and Fritz, 1997). As a result, recharge in semi-arid and arid regions is often dominated by winter precipitation that is first stored as snow, eventually melts, and is either lost to surface runoff, evaporates, or contributes to recharge (Clark and Fritz, 1997). Winter precipitation in the form of rain also has a higher infiltration rate due to lower rates of evapotranspiration (Clark and Fritz, 1997).

Despite a lack of corresponding precipitation data, comparisons to groundwater datasets from other studies can be made. Figure 53 is a histogram of $\delta^{18}O$ data from the central San Juan Basin, New Mexico (Phillips et al., 1986), the southern High Plains (Dutton, 1995), the central High Plains (McMahon et al., 2004), the Middle Rio Grande Basin, New Mexico (Plummer et al., 2004), and the southern Sacramento Mountains in New Mexico (Eastoe and Rodney, 2014), plotted along with the data from this study. Data in Figure 53 have been normalized to represent the percentage of total samples in each study. Data from this study is shown to have the largest range of values, most likely due to the amount of topographic relief in the study area. Data

74

frequencies for each value most closely resemble the studies conducted by McMahon et al. (2004) and Eastoe and Rodney (2014).

The study by Phillips et al. (1986) was conducted in the western part of New Mexico. The authors found significantly depleted waters, but concluded that those samples were paleowaters. The study conducted by Plummer et al. (2004) in the central part of New Mexico also concluded that depleted waters were paleowaters. To the east of the present study area, Dutton (1995) found evidence of paleowaters but did not discuss seasonality of precipitation, and McMahon et al. (2004) also neglected to consider seasonality. Eastoe and Rodney (2014), however, noted that winter precipitation is considered to be the dominant source of recharge in several mountain ranges in the southwestern USA. Eastoe and Rodney (2014) found this to be the case in their study, but did observe increases in summer recharge during years of higher monsoon precipitation.

Because of the high mountains that exist between the Pacific Ocean and the study area, winter precipitation that originates in the Pacific is isotopically depleted compared to precipitation originating in the Gulf of Mexico (Phillips et al., 1986). Where there is a heavy bias in seasonal recharge, the isotopic composition of groundwater will vary from the weighted averages of annual precipitation that comprise the MWL (Clark and Fritz, 1997). In the case of winter-dominated recharge, the mean isotopic composition of groundwater would be depleted relative to the mean isotopic composition of precipitation (Phillips et al., 1986). Seasonal variations can be attenuated in the unsaturated zone if summer precipitation does in fact contribute to groundwater, but the expectation is for groundwater to more closely resemble winter precipitation (Clark and Fritz, 1997). The mean $\delta^{18}O$ value for this study was -8.33‰, falling closer to -8.15‰ (McMahon et al., 2004) and -8.98‰ (Dutton, 1995), which were both to the west and did not discuss whether or not winter precipitation was a dominant source of recharge.

Although the data distribution shown in Figure 53 does not yield many clues, the slopes shown in Figure 26, Figure 29, and Figure 32 might highlight the influence of seasonality. It is

possible that steep slopes and slight evaporation trends are indicative of the pattern seen in snow melt recharge discussed by Clark and Fritz (1997) in which $\delta^{18}O$ values initially fall near the GMWL and deviate as they become more enriched due to evaporation or sublimation. In order to adequately assess seasonal contributions to recharge in the study area, more in-depth research should be conducted on precipitation (i.e. precipitation sampling at multiple locations and elevations).
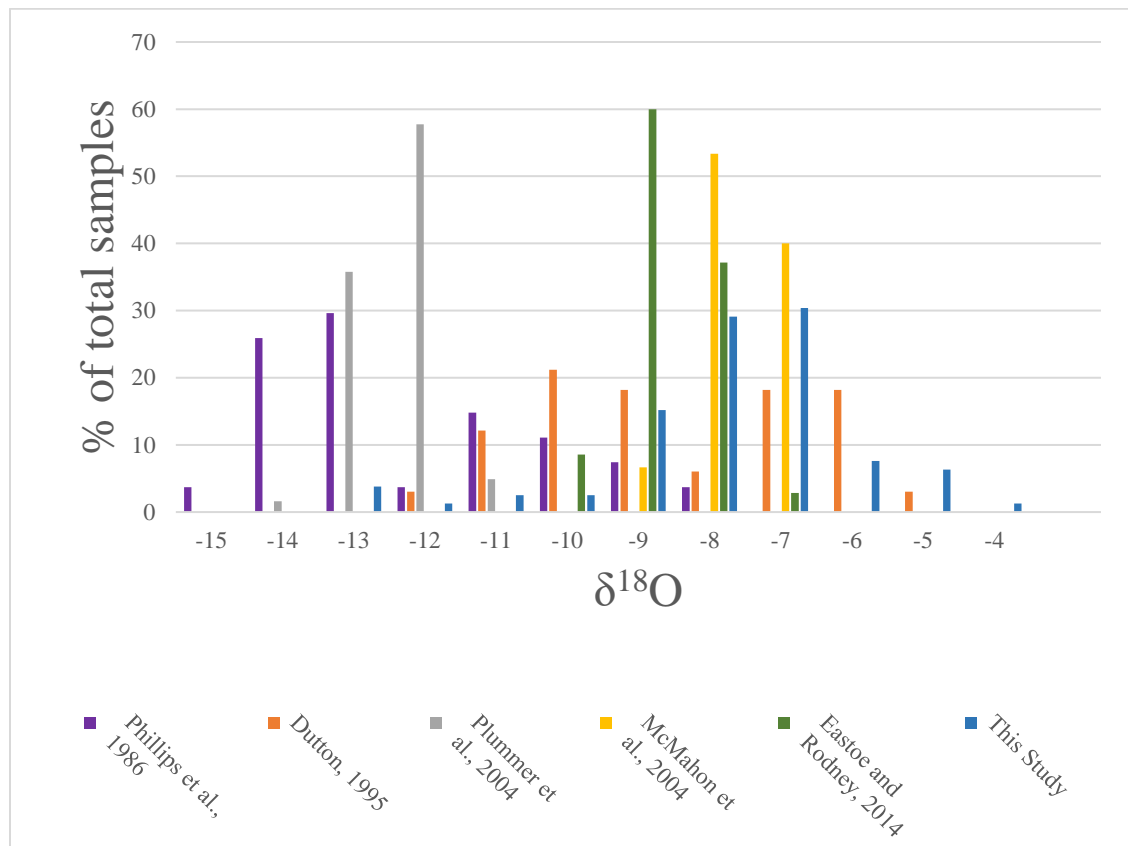
Figure 53: Histogram comparing the data distribution of $\delta^{18}O$ values from this study to $\delta^{18}O$ values from other studies conducted in the surrounding areas. Values have been normalized to reflect the percentage of total samples that fall within each category (Phillips et al., 1986; Dutton, 1995; Plummer et al., 2004; McMahon et al., 2004; Eastoe and Rodney, 2014).

5.2   Paleowaters

Until this point in the discussion, comparisons of groundwater to the GMWL have assumed that recharge had a similar isotopic composition to today's precipitation. This might not be the case if groundwater actually recharged under a past climate with conditions different from

those of today. Within the Quaternary period there have been two epochs – the Pleistocene, lasting from ~2.5 million years to ~11 thousand years ago, followed by the Holocene, which has lasted from ~11,000 years ago to the present day. The Pleistocene epoch featured an ice age ~1.8Ma and mean surface temperatures ~1.7ºC cooler than current temperatures (Hiscock and Bense, 2014). A transition to warmer surface temperatures occurred approximately 9,000 years ago (Rozanski et al., 1993; McMahon et al., 2004).

Because isotopic composition is influenced by temperature, it is easy to confuse the elevation effect with a climatic effect (Phillips et al., 1986; Clark and Fritz, 1997). Two studies conducted near this study area, one in the central San Juan Basin, New Mexico (Phillips et al., 1986) and one in Kansas (McMahon et al., 2004) had very little relief and were able to rule out elevation as a factor. Phillips et al. (1986) found that paleowaters averaged $\delta^{18}O$ values 3.0‰ lighter and δD values averaged 25‰ lighter than modern recharge and McMahon et al. (2004) found that average $\delta^{18}O$ values for paleowaters were depleted by 2-3‰ with respect to modern recharge. Findings from those two studies are in agreement with Dutton (1995), which found that δD paleowater values in confined aquifers in the central High Plains are 12-28‰ more depleted than unconfined aquifers.

The presence of identifiable paleowaters around the study area (Phillips et al., 1986; Dutton, 1995; McMahon et al., 2004; Plummer et al., 2004) suggests that paleowaters are present in northeastern New Mexico, although they are not necessarily being utilized by wells currently in existence. The majority of the data collected in this study falls near the average $\delta^{18}O$ value, -8.28‰, shown in Figure 20. If this average value represents Holocene recharge, potential paleowaters in the study area, recharged under cooler conditions, would have $\delta^{18}O$ values roughly -10.28‰ or lower, based on the 2-3‰ depletion found by Phillips et al. (1986) and MacMahon et al. (2004). By this metric, seven samples fall in this range of values.

Given the amount of elevation change in this study area, elevation must be considered as a possible explanation for the seven samples that fall at least 2‰ below the average. Figure 33 is

77

a scatterplot of the relationship between elevation and $\delta^{18}O$. Using the estimated line of best fit equation of y=-0.0027x – 3.0878, expected $\delta^{18}O$ values were calculated and compared with their corresponding actual $\delta^{18}O$ values. In total, seven samples are at least 2‰ below the expected value based on the elevation effect (M8, C4, C5, U9, U2, U10, and C17). These seven samples are the same seven samples that were considered to be potential outliers in section 5.1.3 (Figure 33, and Figure 34). The possible explanation given in that section is that these samples could represent runoff from higher elevations, known as mountain front recharge. Another possible explanation is that these samples represent paleowaters.

5.3   Groundwater evolution

Ca^{2+} $Mg^{2+}HCO_3^-$ waters typically exist in shallow, unconfined aquifers and indicate that relatively little water-rock interaction has taken place, resulting in the interpretation that these waters have shorter residence times. Na^+ HCO_3^- waters indicate cation exchange with clays, commonly include CO_2 from microbial respiration, and are somewhat more evolved than Ca^{2+} $Mg^{2+}HCO_3^-$ waters. Water chemistry is also dependent on aquifer material, as silicate and carbonate minerals contribute to the overall ion composition.

Of the samples that were analyzed for cations and anions, 42 samples were the Ca^{2+} $Mg^{2+}HCO_3^-$ type, making this most common type in the study area, followed by the Na^+ HCO_3^- type with 25 samples. Plummer et al. (2004) also found these to be the most common water types in the Rio Grande Basin, along with mixed cation HCO_3^- waters. Although the number of data points is small, five hydrostratigraphic units were shown to only contain the Ca^{2+} $Mg^{2+}HCO_3^-$ water type: Quaternary alluvium, Quaternary Basalt, Quaternary Basalt and/or Dakota Sandstone, Ogallala, and the Sangre de Cristo Formation. The other water types each had only a few samples: Ca^{2+} Mg^{2+} SO_4^{2-} (*n*=6), $Ca^{2+}Mg^{2+}$-Mixed anion (*n*=2), Na^+-mixed anion (*n*=2), Na^+ SO_4^{2-} (*n*=1), and Na^+ Cl^- NO_3^- (*n*=1).

Another indicator of recent recharge is the presence of high nitrate concentrations, since the main source of nitrate is agricultural land use activity (McMahon et al., 2004; Hiscock and

Bense, 2014). In total, only three samples had elevated nitrate concentrations: H15 from the alluvium and/or Dockum/Chinle Group unit, U5 from the Dakota Sandstone unit, and U6 from the Dockum/Chinle Group. Sample H15 is a Na^+ Cl^- NO_3^- water type, while U5 and U6 are both $Ca^{2+}Mg^{2+}$-Mixed anion water types. The high nitrate concentration in sample H15, coupled with high salinity suggests that this is highly evaporated recharge along ephemeral watercourses, with possible contributions from irrigation return flow. Unfortunately, high nitrate could be the result of aquifer material and these samples require further investigation as to the source of nitrate.

Two hydrostratigraphic units that are not discussed below must be mentioned, as they both had samples that were identified previously as potential paleowaters in sections 5.1.3 and 5.2. These samples are U9 from the Quaternary alluvium unit and C17 from the Quaternary Basalt unit. Both samples were found to have a Ca^{2+} $Mg^{2+}HCO_3^-$ water type, suggesting that although their $\delta^{18}O$ values are more depleted than expected due to elevation, these could be younger waters that have undergone relatively little water-rock interaction (Hiscock and Bense, 2014).

Each of the main hydrostratigraphic units is discussed in further detail below, but water chemistry can also be the result of mixing of waters from different recharge zones (Dutton, 1995; Clark and Fritz, 1997), or mixed waters in wells that access multiple aquifers (Clark and Fritz, 1997). Three of the main hydrostratigraphic units are known to access one or two geologic units, so mixing is assumed. Future research should include depth-to-water measurements to aid in analyzing groundwater evolution patterns.

5.3.1   Alluvial and/or Dockum/Chinle Group

Stable isotope and chemical analysis of this hydrostratigraphic unit indicates that the groundwater is young and highly evaporated. Twelve samples were successfully analyzed for their cation and anion concentrations, resulting in Ca^{2+} $Mg^{2+}HCO_3^-$ ($n=3$), Na^+ HCO_3^- ($n=6$), mixed Na^+-mixed anion ($n=2$), and Na^+ Cl^- NO_3^- types ($n=1$) (Table 1; Figure 38). All of these samples were taken at low elevations near water courses (Figure 17). This unit is higher in salinity than the other main units, and nine of the twelve samples are Na^+ dominated.

79

Groundwater in this hydrostratigraphic unit is highly enriched and evaporation is the likely cause

of high levels of sodium. The one sample with high NO_3^- is indicative of infiltration from

agricultural land use.

5.3.2   Graneros Shale and/or Greenhorn Limestone

Samples from the Graneros Shale/Greenhorn Limestone unit are Ca^{2+} $Mg^{2+}HCO_3^-$ ($n=8$),

Ca^{2+} Mg^{2+} SO_4^{2-} ($n=2$), and $Na^+HCO_3^-$ water types ($n=4$) (Table 1; Figure 39). Relative to the

GMWL, this unit was shown to be less influenced by evaporative processes (Figure 26), therefore

the high Na^+ concentrations are more likely the result of cation exchange deeper in the aquifer, or

other water rock interaction processes such as mineral weathering. This unit appears to be

following the typical pattern of groundwater evolution from young, shallow Ca^{2+} $Mg^{2+}HCO_3^-$

waters, to deeper and older $Na^+HCO_3^-$ waters (Hiscock and Bense, 2014). This unit has two

samples with high sulfate values, C8 and C9 (Appendix B), which is commonly found when

gypsum is present (Hiscock and Bense, 2014).

5.3.3   Graneros Shale and/or Dakota Sandstone

The Graneros Shale and/or Dakota Sandstone samples were characterized as Ca^{2+}

$Mg^{2+}HCO_3^-$ ($n=2$), mixed Ca^{2+} Mg^{2+} SO_4^{2-} ($n=1$), $Na^+HCO_3^-$ ($n=6$), and Na^+ SO_4^{2-} water types

($n=1$) (Table 1; Figure 40). Relative to the GMWL, this unit was also shown to be less influenced

by evaporative processes (Figure 29). Therefore, the high Na^+ concentrations are more likely the

result of cation exchange deeper in the aquifer, or other water rock interaction processes such as

mineral weathering. This unit also appears to follow the typical pattern of groundwater evolution

from young, shallow Ca^{2+} $Mg^{2+}HCO_3^-$ waters, to deeper and older $Na^+HCO_3^-$ waters (Hiscock and

Bense, 2014). In contrast to the Graneros Shale and/or Greenhorn Limestone and Dakota

Sandstone units, however, this unit has a higher percentage of samples that appear to be older.

This unit also has two sulfate values over 500mg/L, C1 and C7 (Appendix B). This is the only

main hydrostratigraphic unit that exhibits a strong positive correlation between increases in Mg^{2+}

and Ca^{2+}, and an inverse correlation between Ca^{2+} and DIC concentration, which McMahon et al. (2004) found to be evidence of dedolomitization.

From the previous discussion on paleowaters in section 5.2, three samples from this unit were highlighted as potential paleowaters: M8, C4, and C5 (Appendix A, Figure 20, Figure 33, Figure 34). Sample C4 was found to be a Ca^{2+} $Mg^{2+}HCO_3^-$ type, indicating that this sample might have undergone relatively little water-rock interaction (Hiscock and Bense, 2014). Samples M8 and C5 are both $Na^+HCO_3^-$ water type, indicating higher levels of water-rock interaction (Hiscock and Bense, 2014) and suggests that both of these samples are still potentially paleowaters.

5.3.4 Dakota Sandstone

Samples from this unit are comprised mostly of Ca^{2+} $Mg^{2+}HCO_3^-$ type (*n*=18), with one sample of $Ca^{2+}Mg^{2+}$-Mixed anion type, one sample of Ca^{2+} Mg^{2+} SO_4^{2-} type, and eight samples of $Na^+HCO_3^-$ type (Table 1; Figure 41). Relative to the GMWL, this unit was also shown to be less influenced by evaporative processes (Figure 32), therefore the high Na^+ concentrations are more likely the result of cation exchange deeper in the aquifer, or other water rock interaction processes such as mineral weathering. This unit also appears to follow the typical pattern of groundwater evolution from young, shallow Ca^{2+} $Mg^{2+}HCO_3^-$ waters, to deeper and older $Na^+HCO_3^-$ waters (Hiscock and Bense, 2014). A high percentage of samples reflect young waters with little water-rock interaction (Hiscock and Bense, 2014). Sulfate values remain mostly low within this unit and it has the least salinity of the four main hydrostratigraphic units. The Dakota Sandstone unit does have one location, U5, with a high level of nitrate, suggesting modern infiltration from agricultural land use.

From the previous discussion on paleowaters in section 5.2, two samples from this unit were identified as potential paleowaters: U10 and U2 (Appendix A, Figure 20, Figure 33, Figure 34). Both of these samples were found to have Ca^{2+} $Mg^{2+}HCO_3^-$ water type, indicating that these samples might have undergone relatively little chemical evolution (Hiscock and Bense, 2014).

81

5.4   Dissolved inorganic carbon

5.4.1   DIC and alkalinity

DIC is comprised of the carbon species H_2CO_3 (carbonic acid), HCO_3^- (bicarbonate), and CO_3^{2-} (carbonate) (Clark and Fritz, 1997). Of these four, HCO_3^- and CO_3^{2-} contribute to alkalinity and are the dominant carbon species present at higher pH levels (Clark and Fritz, 1997). Carbonic acid contributes to DIC, but not to alkalinity. Therefore, analyzing the relationship between DIC and alkalinity can reveal the presence of small amounts of carbonic acid in DIC, which can assist in drawing conclusions about residence time (Clark and Fritz, 1997). Groundwater with a significant contribution from carbonic acid is indicative of waters recharging at the water table, whereas groundwater with high alkalinity typically has undergone more downward flow evolution (Clark and Fritz, 1997).

Each of the main hydrostratigraphic units has some amount of carbonic acid present, as evidenced by points that fall below the 1:1 relationship shown in Figure 44. Data points for the alluvium and/or Dockum/Chinle Group unit are all below the line (Figure 45), indicating a constant contribution of carbonic acid and therefore water from this sample is likely relatively young. Samples from the Graneros Shale/Greenhorn Limestone unit adhere closely to the 1:1 relationship (Figure 46). One of the four samples with the highest alkalinity concentration, C13, is from this unit, indicating that these waters likely have longer residence times. Samples from the Graneros Shale and/or Dakota Sandstone unit do not adhere closely to the 1:1 relationship, indicating large contributions of carbonic acid (Figure 47). In fact, the sample with the largest component of carbonic acid, C1, was taken from this unit. However, three of the four samples with the highest alkalinity (C2, C3, and C10) were also all taken from this unit. Waters from the Graneros Shale and/or Dakota Sandstone unit appear to be a mix of different residence times and further investigation is necessary. Samples from the Dakota Sandstone unit fall mostly below the line, with a few exceptions (Figure 48). Based solely on proximity to the 1:1 line, this unit

appears to be between samples from the Graneros Shale and/or Dakota Sandstone unit and samples from the Graneros Shale/Greenhorn Limestone unit in residence time.

5.4.2 δ^{13}C-DIC

McMahon et al. (2014) recorded δ^{13}C-DIC values ranging from -4.6‰ to -8.0‰ in the Central High Plains. Dutton (1995) recorded δ^{13}C-DIC values ranging from -9.7‰ to -3.8‰ in the Southern High Plains. Although geologically similar to those studies, this study produced a much larger range of δ^{13}C-DIC values, -13.01 to -1.50‰ (Appendix B, Figure 50). Water reaching the water table has very negative values of δ^{13}C-DIC (Clark and Fritz, 1997). As carbonic acid dissolves aquifer material with δ^{13}C-DIC values close to 0‰, δ^{13}C-DIC values increase (Clark and Fritz, 1997). Groundwater with less negative δ^{13}C-DIC values indicates high levels of dissolution of aquifer material (Clark and Fritz, 1997). Very negative values transitioning to more positive values enables the use of δ^{13}C-DIC as a tracer of groundwater evolution along flowpaths.

Plummer et al. (2004) also found that δ^{13}C-DIC values can be used to infer ages of relatively young water by comparing them to ^{14}C data. Plummer et al. (2004) found that waters with δ^{13}C-DIC values of -11.9 ± 2.0‰ were less than roughly 200 years old, whereas waters with δ^{13}C-DIC values of -8.2 ± 1.4‰ were greater than 200 years old (Figure 8). Plummer et al. (2004) also found that δ^{13}C-DIC values averaged -7.9 ± 2.0‰ and remained relatively constant throughout their study area. Although the average for this study is -7.41‰ and is very close to the average found by Plummer et al. (2004), δ^{13}C-DIC values appear to behave more similarly to findings by Wahi et al. (2008), in which more negative values occurred near the mountain front and increased with proximity to the center of the basin (Figure 50).

For the purpose of this study, δ^{13}C-DIC values can be used to further investigate samples that were previously identified as potential paleowaters (M8, C4, C5, U9, U2, U10, and C17). Of these samples, C4, C5, U9, U2, and C17 fall within the -11.9 ± 2.0‰ range found by Plummer et al. (2004) to represent waters that are less than a few hundred years old. As such, these samples

are not likely to be paleowaters. Samples M8 and U10 have higher δ^{13}C-DIC values, falling at -6.07‰ and -6.37‰, respectively. Samples M8 and U10 cannot be labeled as paleowaters using this method only, but it is possible that they are over a few hundred years old.

Groundwater with very enriched values for δ^{13}C-DIC are present in the western and south-western parts of the study area, shown in Figure 50. For the purpose of this study, δ^{13}C-DIC values were used to rule out potential paleowaters, so enrichment was not further investigated.

5.5 Groundwater residence time: Water isotopes, tritium, and carbon-14

5.5.1 Tritium

It was hypothesized that modern recharge could be found using tritium analysis in locations near watercourses and points of accumulated runoff such as mountain fronts. To test this hypothesis, locations U10 and C15 were selected near the mountain front, and C16 was selected because of its proximity to a watercourse (Canadian River). These three samples revealed the absence of tritium in the mountain front with levels below 0.5 TU (Gurdak and Qi, 2006), and the presence of tritium near a watercourse. To expand the discussion, previously unpublished data from ZGC LLC has been incorporated into Table 3, Figure 54, Figure 55, and Figure 56. Generally speaking, tritium is present in groundwater near watercourses, but not present in the groundwater taken from higher locations on the escarpments surrounding the water courses or near the mountain front.

Of particular interest here is a very depleted δ^{18}O value for sample U10, which was previously identified as a potential paleowater. This sample does not have any tritium present, indicating groundwater with a residence time of over ~70 years. Preliminary results shown in Figure 54 and Figure 55 seem to suggest that samples with δ^{18}O values below -9.0‰ and δD values below 60.0‰ are tritium-free. Further testing of relatively shallow groundwater along watercourses can help expand our knowledge of modern recharge flowpaths, but it may not be helpful in elucidating recharge processes at the mountain front.

Table 3: Table of stable isotopes (this study) and tritium units from this study combined with unpublished data from the study area (Zeigler Geologic Consulting, unpublished data).

Location	$\delta^{18}O$	δD	Tritium (TU)	Hydrostratigraphic Unit
H11	-6.33	-46.9	1.55	Alluvium a/o Dockum/Chinle Group
H13	-6.76	-46.1	2.69	Alluvium a/o Dockum/Chinle Group
H14	-6.28	-43.5	2.93	Alluvium a/o Dockum/Chinle Group
H2	-5.95	-46.8	1.77	Alluvium a/o Dockum/Chinle Group
H4	-6.53	-50.1	3.53	Alluvium a/o Dockum/Chinle Group
H5	-5.56	-44.6	5.68	Alluvium a/o Dockum/Chinle Group
H6	-6.93	-48.4	0.10	Alluvium a/o Dockum/Chinle Group
H7	-5.45	-42.9	3.62	Alluvium a/o Dockum/Chinle Group
H10	-9.32	-59.5	0.07	Ogallala a/o Dakota SS
H3	-7.88	-53.8	0.00	Ogallala a/o Dakota SS
C15	-10.62	-78.3	0.04	Graneros Shale/Greenhorn LS
C16	-8.26	-56.9	4.40	Graneros Shale/Greenhorn LS
U10	-11.16	-82.9	0.00	Dakota Sandstone
H8	-7.23	-53.0	0.05	Morrison Formation
U1	-5.69	-41.7	4.14	Dockum/Chinle Group
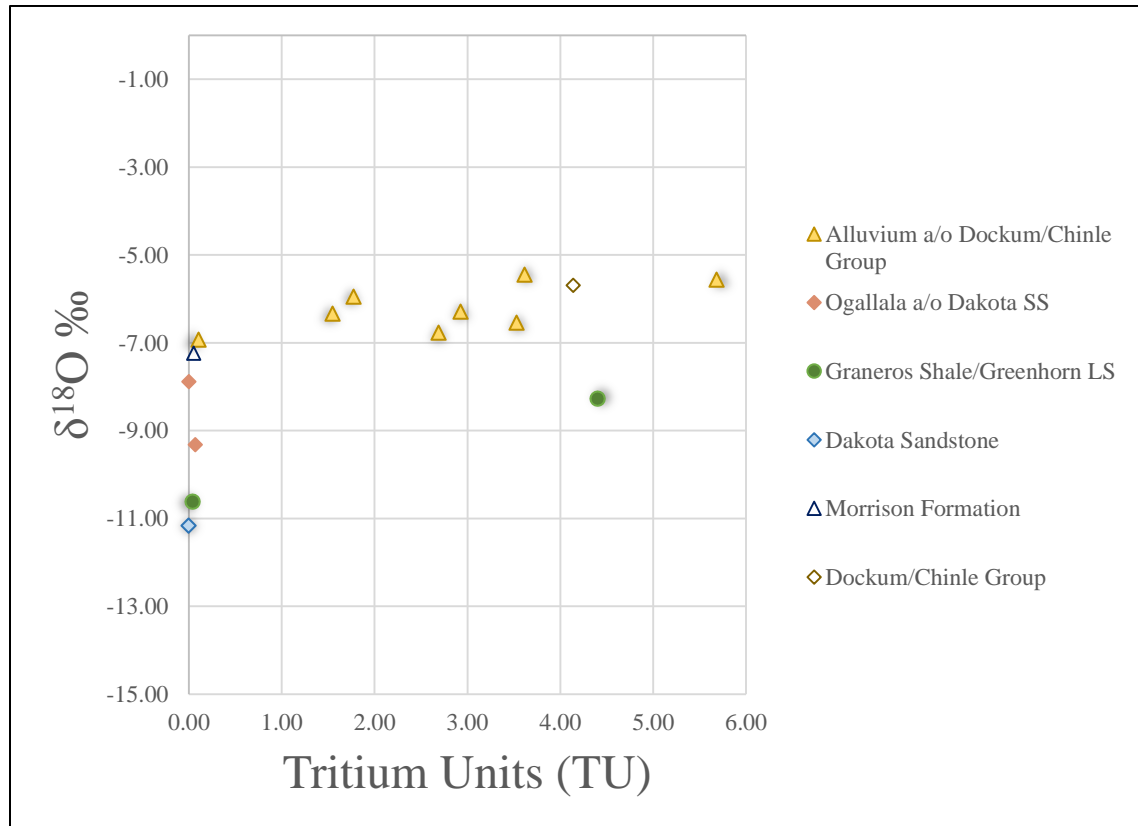
Figure 54: Scatterplot of $\delta^{18}O$ vs. Tritium Units. Data is combination of results from this study and unpublished data from the study area (Zeigler Geologic Consulting, unpublished data).
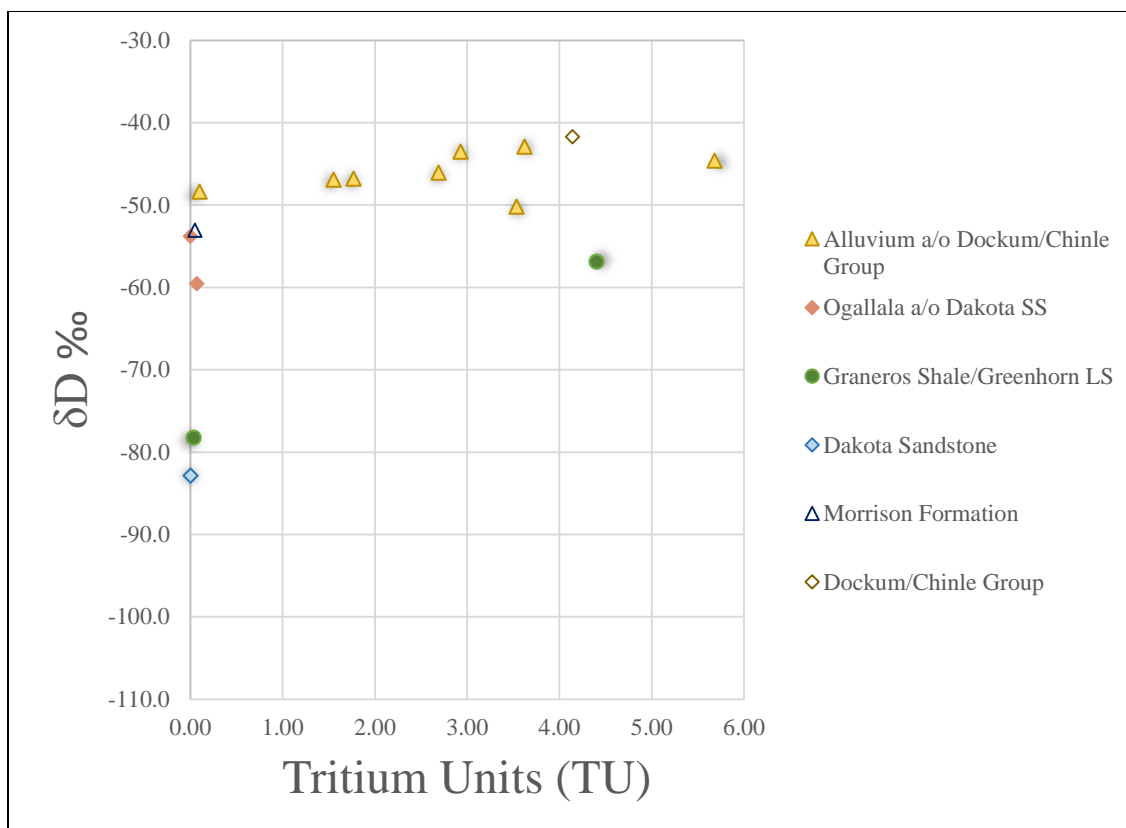
Figure 55: Scatterplot of δD vs. Tritium Units. Data is combination of results from this study and unpublished data from the study area (Zeigler Geologic Consulting, unpublished data).
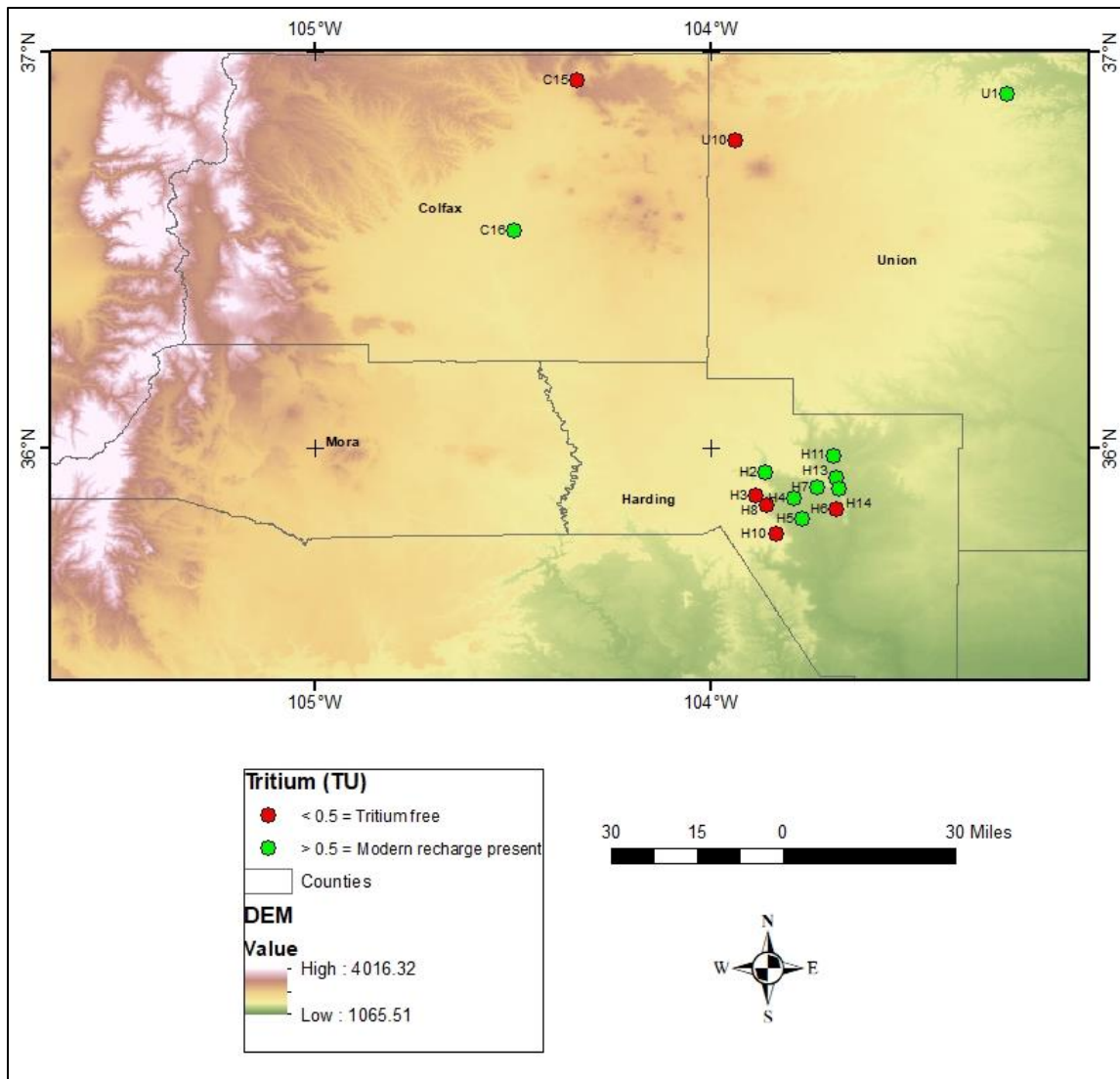
Figure 56: Map of tritium analysis locations, depicted as tritium-free or having modern recharge present.

5.5.2 Carbon-14

While tritium can identify modern waters that are less than ~70 years old, the majority of the study area is comprised of Holocene waters that are a few hundred to a few thousand years old. These waters can be identified using carbon-14 analysis. No carbon-14 analysis was performed as part of this study, but previously unpublished data from ZGC LLC are presented here in Table 4, Figure 57, Figure 58, and Figure 59 for discussion. The sample most depleted in $\delta^{18}O$, U2, was found to have 89.20 pMC, placing it at roughly 1,000 years old. The sample with the lowest pMC, H3, is roughly 12,000 years old, placing it at the transition from the Pleistocene

to the Holocene. Although "old", sample H3 is not isotopically distinct from the other samples in this study and therefore does not appear to have recharged under different climatic conditions. In fact, the oldest samples do not have very depleted $\delta^{18}O$ values, indicating that older is not necessarily more depleted.

It was hypothesized that $\delta^{13}C$-DIC values could be used as a pre-screening tool for carbon-14 dating, based on the findings of Plummer et al. (2004). Figure 60 shows that the relationship between $\delta^{13}C$-DIC values and estimated residence times from pMC data seems to match the relationship found by Plummer et al. (2004), shown in Figure 8. However, this concept does not hold true throughout the study area. An example is sample C15, which has a $\delta^{13}C$-DIC value of -12.34. Using $\delta^{13}C$-DIC values as a pre-screening tool, this sample would not be identified as a candidate for carbon-14 analysis. Unfortunately, sample C15 does not have any detectable tritium, therefore indicating the carbon-14 analysis is needed to get a more accurate estimate of residence time at this location. Alternatively, $\delta^{13}C$-DIC enriched groundwater in the southeast portion of the study area identifies locations that would benefit from carbon-14 analysis, but several of these samples have tritium present. It may not hold true that $\delta^{13}C$-DIC values can be used to estimate ages using the threshold discussed in section 5.4.2. However, very negative $\delta^{13}C$-DIC values are found near the water table (Clark and Fritz, 1997), indicating water that has not been present long enough to have recharged under paleoclimate conditions.

The sample size for these data points is small relative to the elevation range, hydrogeologic settings, and hydrostratigraphic units present in the study area. Future studies could incorporate carbon-14 dating to provide a more accurate analysis of the relationship between stable isotopes and ^{14}C in the study area. As this dataset is filled, the value of using $\delta^{13}C$-DIC as a pre-screening tool can be reevaluated.

Table 4: Table of stable isotopes (this study) and percent of modern carbon (pmC) from this study combined with unpublished data from the study area (Zeigler Geologic Consulting, unpublished data).

Location	$\delta^{18}O$	δD	pMC	TU	Hydrostratigraphic Unit
H11	-6.33	-46.9	90.70	1.55	Alluvium a/o Dockum/Chinle Group
H13	-6.76	-46.1	92.50	2.69	Alluvium a/o Dockum/Chinle Group
H14	-6.28	-43.5	80.10	2.93	Alluvium a/o Dockum/Chinle Group
H2	-5.95	-46.8	98.20	1.77	Alluvium a/o Dockum/Chinle Group
H4	-6.53	-50.1	104.70	3.53	Alluvium a/o Dockum/Chinle Group
H6	-6.93	-48.4	83.20	0.10	Alluvium a/o Dockum/Chinle Group
H7	-5.45	-42.9	83.60	3.62	Alluvium a/o Dockum/Chinle Group
H10	-9.32	-59.5	66.50	0.07	Ogallala a/o Dakota SS
H3	-7.88	-53.8	23.30	0.00	Ogallala a/o Dakota SS
M4	-8.01	-56.5	55.10	- -	Dakota Sandstone
U2	-13.70	-99.4	89.20	- -	Dakota Sandstone
M15	-9.12	-67.7	84.50	- -	Morrison Formation
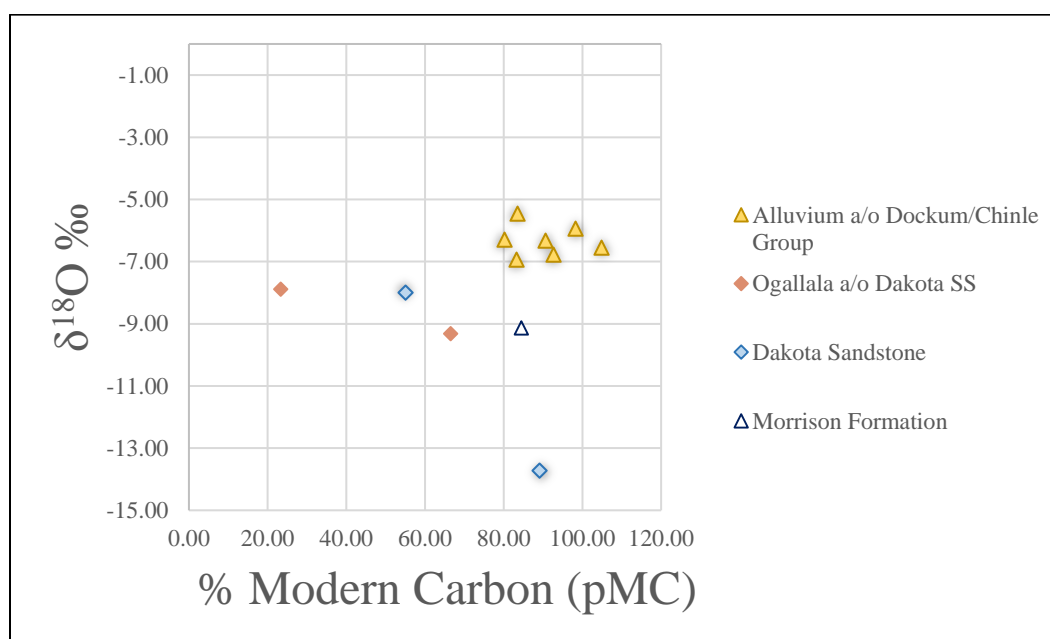
Figure 57: Scatterplot of $\delta^{18}O$ vs. percent modern carbon. PMC data are unpublished from Zeigler Geologic Consulting.
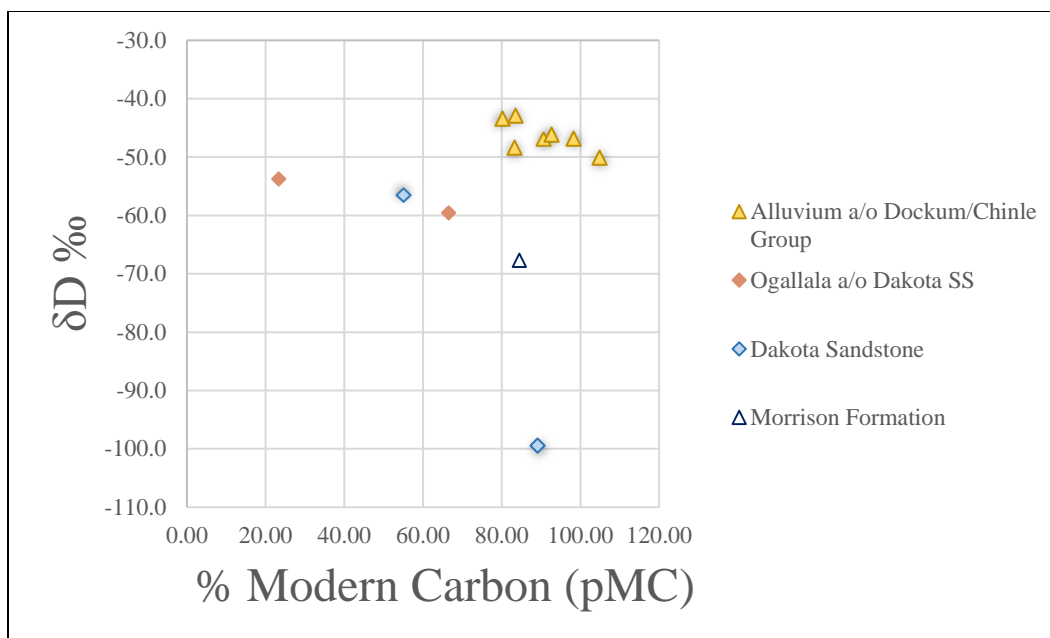
Figure 58: Scatterplot of δD vs. percent modern carbon. PMC data are unpublished from Zeigler Geologic Consulting.
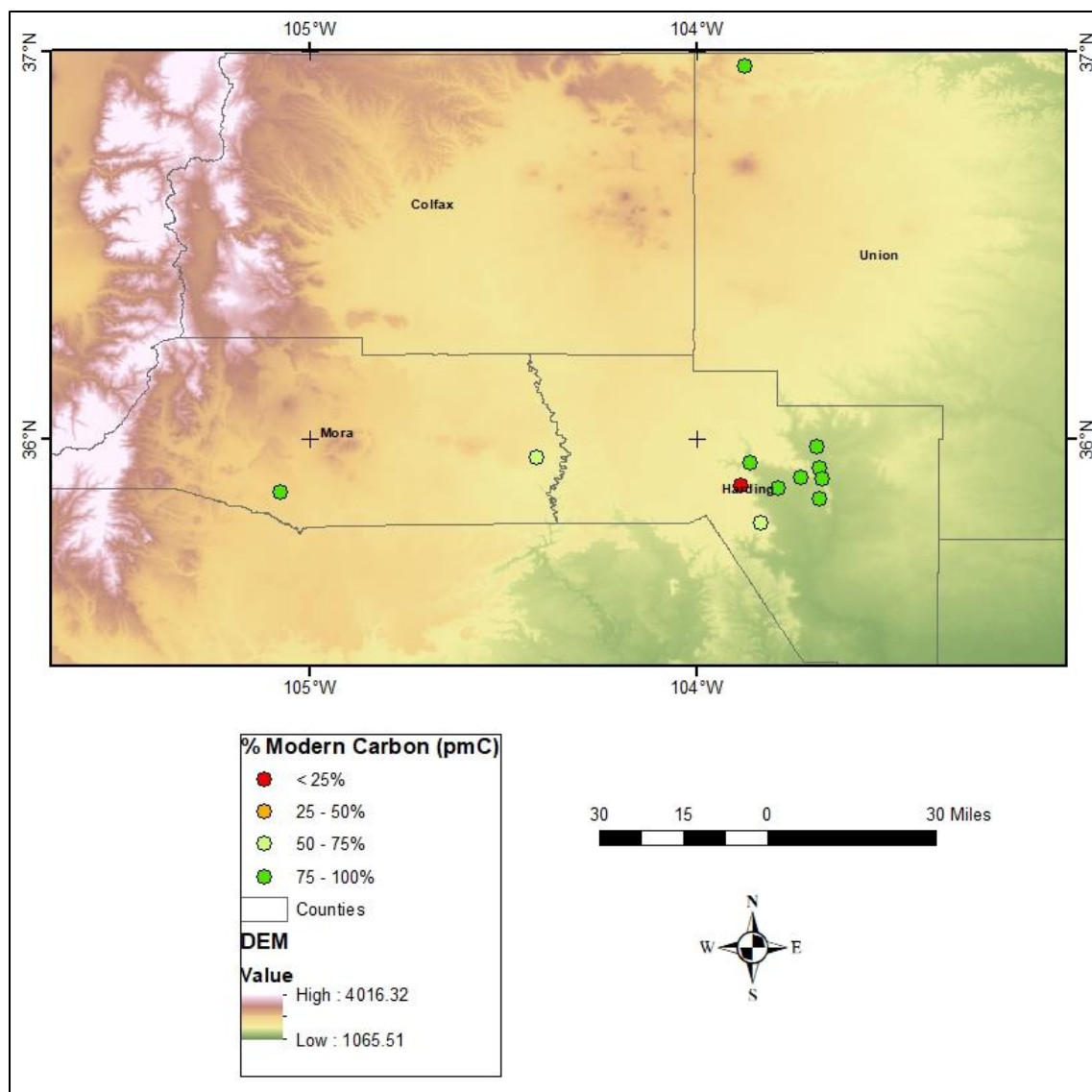
Figure 59: Map of percentages of modern carbon (pMC) based on previously unpublished data from Zeigler Geologic Consulting, LLC.
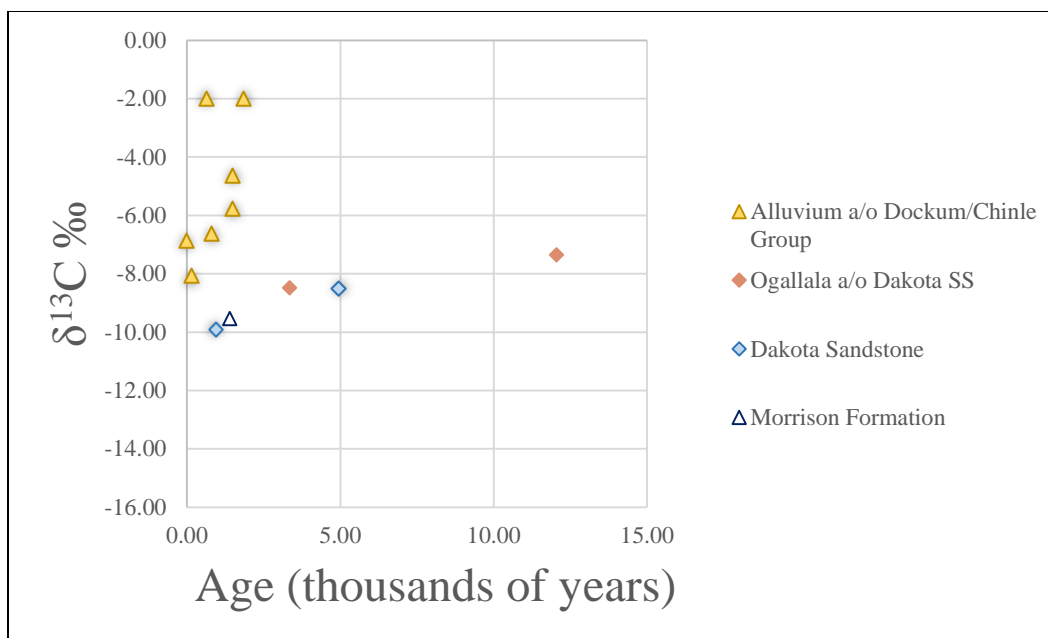
Figure 60: δ¹³C ‰ vs age estimation, calculated using pMC data provided by Zeigler Geologic Consulting, LLC.

6   Conclusions

$\delta^{18}O$ values range from -13.71 to -4.42‰ and δD values range from -104.85 to -41.85‰ within the study area, following a general spatial trend of less depleted waters in the southeast and more depleted waters in the northwest. A slight overall vertical gradient was observed as well, with less depleted waters in the younger alluvium and/or Dockum/Chinle Group unit, and more depleted waters in the older Dakota Sandstone unit.

The isotopic composition of groundwater for this study somewhat resembles the seasonal pattern found in another study in this region. With relation to the GMWL, slopes of three main hydrostratigraphic units indicate possible evaporative patterns of winter precipitation. The likelihood of high contributions of winter precipitation is also indicated by the inability to explain depleted groundwaters using elevation alone. Future studies that incorporate stable isotope analysis of precipitation will make it possible to accurately determine seasonal contributions to recharge in this area.

The isotopic composition of groundwater samples seems to most closely match the elevation effect, found to be approximately -0.31‰ per every 100m rise in elevation, or -0.27‰ per every 100m rise in elevation without data points that were identified as outliers. Seven samples, M8, C4, C5, U2, U9, U10, and C17, were found to have $\delta^{18}O$ values that are more depleted than expected, based on their elevation. Of these seven samples, U9, C17, C4, U10, and U2 were found to have the Ca^{2+} $Mg^{2+}HCO_3^-$ water type, suggesting low levels of water-rock interaction. M8 and C5 were found to have the $Na^+HCO_3^-$ water type, indicating that these are more evolved groundwaters with higher levels of water-rock interaction. Samples C4, C5, U9, U2, and C17 have $\delta^{13}C$-DIC values indicating that they are less than a few hundred years old. Two samples, M8 and U10, have $\delta^{13}C$-DIC values suggesting that they are less evolved waters.

Using these parameters, it is unlikely that U9, C17, C4, and U2 are paleowaters because their water type suggests little groundwater evolution and their $\delta^{13}C$-DIC values indicate they are younger than a few hundred years old. C5 has a more evolved water type, but a $\delta^{13}C$-DIC value indicating that it is younger than a few hundred years old. U10 has a $\delta^{13}C$-DIC value indicating that it is over a few hundred years old, but has a less evolved water type. M8 has a more depleted $\delta^{18}O$ value than expected for its elevation, has a more evolved water type, and a high $\delta^{13}C$-DIC value, indicating that this sample is the most likely sample to resemble paleowaters. Despite the uncertainty, it is highly unlikely that all of these seven samples are paleowaters. Therefore, it was determined that this study did not find evidence of a unique isotopic composition reflecting that of waters recharged under a paleoclimate. Although paleowaters have been identified to the south and east of the study area, it is possible that they have already been flushed out of this area, are not currently being accessed by wells in these counties, or do not have distinctive properties.

Major ions were analyzed to determine water types, yielding 42 samples of the Ca^{2+} $Mg^{2+}HCO_3^-$ type, making this the most common type in the study area, followed by the Na^+ HCO_3^- type with 25 samples. Nitrate was found in H15, U5, and U6, indicating modern recharge from agricultural land use activity. The alluvium and/or Dockum/Chinle Group unit was found to

have high salinity, matching the evaporation trend of stable isotope enrichment that was observed. Samples from this unit and in south-eastern and western portions of the study area were found to have enriched δ^{13}C-DIC values that may require further investigation. Water chemistry and stable isotope composition within the Graneros Shale/Greenhorn Limestone, Graneros Shale and/or Dakota Sandstone, and Dakota Sandstone units is highly variable. This is likely due to heterogeneity throughout the study area and the discontinuity of the hydrostratigraphic units.

It was hypothesized that tritium analysis conducted at targeted locations near watercourses and points of accumulated runoff such as mountain fronts will identify locations of probable modern-day recharge. Tritium analysis conducted by this study confirmed the presence of tritium along a watercourse, but not along the mountain front. Additional data also confirms the presence of tritium along watercourses in the southeastern portion of the study area.

^{14}C data appears to contradict tritium data in some locations, yielding age estimations in the hundreds to low thousands of years, while tritium indicates the presence of recharge that is less than ~70 years old. This indicates mixing of old and young water in these locations. Future analysis could focus on calculating recharge estimates to determine the level of mixing.

It was hypothesized that δ^{13}C-DIC values could be used as a pre-screening tool for carbon-14 dating. Available tritium data indicates that this is not supported; depleted locations were found to lack tritium, indicating a need for carbon-14 analysis, while enriched locations were found to have tritium present, indicating that carbon-14 analysis is less necessary there. While it may not hold true that δ^{13}C-DIC values can be used to identify ideal locations for ^{14}C testing, it does still hold true that low δ^{13}C-DIC values are indicative of recharge that is too recent to be deemed paleowater. This study highlights the dilemma in choosing between tritium and ^{14}C analysis and would benefit from the development of a more adequate way of estimating intermediate aged groundwater.

It does not appear as though any paleowaters were identified by this study, with groundwater ranging from a few hundred to a few thousand years old instead. Tritium was not found the along

the mountain front in the northern part of the study area. Locations that did have measurable tritium also had properties that are indicative of young water mixing with old water. If no portion of the groundwater sample reflects water recharged in the last ~70 years, that location is not receiving recharge during the average human lifespan. In terms of sustainability, any location that is not receiving recharge during the average human lifespan is not functioning on a human timescale and any use is therefore unsustainable. Locations that do have tritium are potentially sustainable, if the amount of abstraction and loss to streams is balanced with the amount of recharge. Additional tritium and ^{14}C testing throughout the study area in the future can assist with distinguishing between potentially sustainable groundwater and groundwater that is being mined. Furthermore, targeted, in-depth, multi-tracer studies at sites where tritium is found can be used to estimate recharge, assisting in water management efforts.

References Cited

Becker, M. F., Bruce, B. W., Pope, L. M., and Andrews, W. J., 2002, Ground-water quality in the Central High Plains Aquifer, Colorado, Kansas, New Mexico, Oklahoma, and Texas, 1999, U.S. Geological Survey Water-Resources Investigations Report, 2002-4112

Bethke, C.M., and Johnson, T.M., 2002, Ground water age: Ground Water, v. 40, p.337-339

Butler, J., Stotler, R., Whittemore, D., and Reboulet, E., 2013, Interpretation of water level changes in the High Plains aquifer in western Kansas: Ground Water, v. 51, p. 180–190, doi: 10.1111/j.1745-6584.2012.00988.x.

Castro, M.C., Goblet, P., 2005, Calculation of ground water ages – A comparative analysis: Ground Water, v. 43, p. 368-380

Clark, I.D., and Fritz, P., 1997, Environmental Isotopes in Hydrogeology: Boca Raton, Lewis Publ.

Craig, H., 1961, Isotopic variations in meteoric waters, Science, v. 133, p. 1702-1703, doi:10.1126/science.133.3465.1702.

Crosbie, R.S., Scanlon, B.R., Mpelasoka, F.S., Reedy, R.C., Gates, J.B., and Zhang, L., 2013, Potential climate change effects on groundwater recharge in the High Plains Aquifer, USA: Water Resources Research, v. 49, p. 3936–3951, doi: 10.1002/wrcr.20292

Dennehy, K.F., Litke, D.W., and McMahon, P.B., 2002, The High Plains Aquifer, USA: Groundwater development and sustainability. In: *Sustainable Groundwater Development*, K.M. Hiscock, M.O. Rivet and R.M. Davison (eds.), Geological Society, London, Special Publications, v. 193, p. 99–119, doi: 10.1144/gsl.sp.2002.193.01.09.

Drever, J.I., 1997. The Geochemistry of Natural Waters: Surface and Groundwater Environments, 3rd ed. ed. Prentice Hall, Upper Saddle River, N.J.

Dutton, A.R., 1995, Groundwater isotopic evidence for paleorecharge in U.S. High Plains aquifers: Quaternary Research, v. 43, p. 221–231, doi: 10.1006/qres.1995.1022.

Dutton, A., Wilkinson, B.H., Welker, J.M., Bowen, G.J., and Lohmann, K.C., 2005, Spatial distribution and seasonal variation in $^{18}O/^{16}O$ of modern precipitation and river water across the conterminous USA: Hydrological Processes, v. 19, p. 4121-4146, doi: 10.1002/hyp.5876.

Eastoe, C.J., Rodney, R., 2014, Isotopes as tracers of water origin in and near a regional carbonate aquifer: The southern Sacramento Mountains, New Mexico: Water, v. 6, p. 301-323, doi: 10.3390/w6020301.

Esnault, L., Gleeson, T., Wada, Y., Heinke, J., Gerten, D., Flanary, E., Bierkens, M.F.P., and Beek, L.P.H.V., 2014, Linking groundwater use and stress to specific crops using the groundwater footprint in the Central Valley and High Plains aquifer systems, U.S.: Water Resources Research, v. 50, p. 4953–4973, doi: 10.1002/2013wr014792.

Geologic Map of New Mexico, New Mexico Bureau of Geology and Mineral Resources, 2003, Scale 1:500,000.

Gurdak, J.J., and Qi, S.L., 2006, Vulnerability of recently recharged ground water in the High Plains aquifer to nitrate contamination: U.S. Geological Survey Scientific Investigations Report 2006-5050, 39 p.

Gurdak, J.J., and Roe, C.D., 2010, Recharge rates and chemistry beneath playas of the High Plains aquifer, USA: Hydrogeology Journal, v. 18, p. 1747–1772, doi: 10.1007/s10040-010-0672-3.

Gutentag, E.D., Heimes, F.J., Krothe, N.C., Luckey, R.R., and Weeks, J.B., 1984, Geohydrology of the High Plains aquifer in parts of Colorado, Kansas, Nebraska, New Mexico, Oklahoma, South Dakota, Texas, and Wyoming: U.S. Geological Survey Professional Paper 1400-B, 63 p.

Haacker, E.M.K., Kendall, A.D., and Hyndman, D.W., 2016, Water level declines in the High Plains Aquifer: Predevelopment to resource senescence: Groundwater, v. 54, p. 231–242, doi: 10.1111/gwat.12350.

Harrington, L., Harrington, J., and Kettle, N., 2007, Groundwater depletion and agricultural land use change in the High Plains: A case study from Wichita County, Kansas*: The Professional Geographer, v. 59, p. 221–235, doi: 10.1111/j.1467-9272.2007.00609.x.

Hiscock, K.M., and Bense, V.F., 2014, Hydrogeology: Principles and Practice: Chichester, Wiley Blackwell.

IAEA (International Atomic Energy Agency), 2009. Laser spectroscopic analysis of liquid water samples for stable hydrogen and oxygen isotopes, IAEA-TCS-35. Vienna: IAEA.

Kendall, C., Coplen, T.B., 2001, Distribution of oxygen-18 and deuterium in river waters across the United States: Hydrological Processes, v. 15, p. 1363-1393, doi: 10.1002/hyp.217.

Koeniger, P., Gaj, M., Beyer, M., and Himmelsbach, T., 2016, Review on soil water isotope-based groundwater recharge estimations: Hydrological Processes, v. 30, p. 2817–2834, doi: 10.1002/hyp.10775.

Meixner, T., Manning, A.H., Stonestrom, D.A., Allen, D.M., Ajami, H., Blasch, K.W., Brookfield, A.E., Castro, C.L., Clark, J.F., Gochis, D.J., Flint, A.L., Neff, K.L., Niraula, R., Rodell, M., Scanlon, B.R., Singha, K., Walvoord, M.A., 2016. Implications of projected climate change for groundwater recharge in the western United States. Journal of Hydrology 534, 124–138.

McGuire, K.J., McDonnell, J.J., Weiler, M., Kendall, C., McGlynn, B.L., Welker, J.M., and Siebert, J., 2005, The role of topography on catchment-scale water residence time: Water Resources Research, v. 41, W05002, doi:10.1029/2004WR003657.

McMahon, P.B., Bohlke, J.K., and Christenson, S.C., 2004, Geochemistry, radiocarbon ages, and paleorecharge conditions along a transect in the central High Plains aquifer, southwestern

Kansas, USA: Applied Geochemistry, v. 19, p. 1655-1686, doi: 10.1016/j.apgeochem.2004.05.003

Nativ, R., and Riggio, R., 1989, Meteorologic and isotopic characteristics of precipitation events with implications for groundwater recharge, Southern High Plains: Atmospheric Research, v. 23, p. 51–82, doi: 10.1016/0169-8095(89)90058-6.

Ng, G.-H. C., McLaughlin, D., Entekhabi, D., Scanlon, B.R., 2010, Probabilistic analysis of the effects of climate change on groundwater recharge, Water Resources Research, v. 46, W07502, doi:10.1029/2009WR007904.

Phillips, F.M., Peeters, L.A., Tansey, M.K., and Davis, S.N., 1986, Paleoclimatic inferences from an isotopic investigation of groundwater in the central San Juan Basin, New Mexico: Quaternary Research, v. 26, p.179-193.

Plummer, L,B., Bexfield, L., Anderholm, S., Sanford, W., and Busenberg, E., 2004, Hydrochemical tracers in the middle Rio Grande Basin, USA: 1. Conceptualization of groundwater flow: Hydrogeology Journal, v. 12, doi: 10.1007/s10040-004-0324-6.

Reilly, T.E., Dennehy, K.F., Alley, W.M., and Cunningham, W.L., 2008, Ground-Water Availability in the United States: U.S. Geological Survey Circular 1323, 70 p., also available online at http://pubs.usgs.gov/circ/1323/

Richey, A.S., Thomas, B.F., Lo, M.-H., Reager, J.T., Famiglietti, J.S., Voss, K., Swenson, S., and Rodell, M., 2015, Quantifying renewable groundwater stress with GRACE: Water Resources Research, v. 51, p. 5217–5238, doi: 10.1002/2015wr017349.

Robson SG, Banta ER. 1995. Ground-water atlas of the United States, segment 2, Arizona, Colorado, New Mexico, and Utah. U.S. Geological Survey Hydrologic Investigations Atlas HA-730C

Rosenberg, N.J., Epstein, D.J., Wang, D., Vail, L., Srinivasan, R., Arnold, J.G., 1999, Possible impacts of global warming on the hydrology of the Ogallala aquifer region, Climatic Change, v. 42, p. 677-692.

Rozanski, K., Araguás-Araguás, L., and Gonfiantini, R., 1993, Isotopic patterns in modern global precipitation. In Climate Change in Continental Isotopic Record, ed. PK Swart, KL Lohwan, JA McKenzie, S Savin, Geophys. Monogr. 78, pp. 1-37. Washington, DC: Am. Geophys. Union

Sayre, W.O., and Ort, M.H., 2011, A geologic study of the Capulin Volcano National Monument and surrounding areas, Union and Colfax Counties, New Mexico, New Mexico Bureau of Geology and Mineral Resources Open-File Report 541

Scanlon, B.R., Faunt, C.C., Longuevergne, L., Reedy, R.C., Alley, W.M., Mcguire, V.L., and Mcmahon, P.B., 2012, Groundwater depletion and sustainability of irrigation in the US High Plains and Central Valley: Proceedings of the National Academy of Sciences, v. 109, p. 9320–9325, doi: 10.1073/pnas.1200311109.

Steward, D.R., and Allen, A.J., 2016, Peak groundwater depletion in the High Plains Aquifer, projections from 1930 to 2110: Agricultural Water Management, v. 170, p. 36–48, doi: 10.1016/j.agwat.2015.10.003.

Steward, D.R., Bruss, P.J., Yang, X., Staggenborg, S.A., Welch, S.M., and Apley, M.D., 2013, Tapping unsustainable groundwater stores for agricultural production in the High Plains Aquifer of Kansas, projections to 2110: Proceedings of the National Academy of Sciences, v. 110, p. E3477–E3486, doi: 10.1073/pnas.1220351110.

Stotler, R.L., Whittemore, D.O., Smith, J.J., Katz, B.S., Yoerg, A., Butler, J.J., Ludvigson, G.A., and Hirmas, D.R., 2015, Isotopic composition of the Ogallala-High Plains aquifer and vadose zone: Procedia Earth and Planetary Science, v. 13, p. 39-42, doi: 10.1016/j.proeps.2015.07.009

Suckow, A., 2014, The age of groundwater – Definitions, models and why we do not need this term: Applied Geochemistry, v. 50, p. 222-230, doi:10.1016/j.apgeochem.2014.04.016.

Thomas, B., Behrangi, A., and Famiglietti, J., 2016, Precipitation intensity effects on groundwater recharge in the southwestern United States: Water, v. 8, doi: 10.3390/w8030090.

Vachon, R.W., Welker, J.M., White, J.W.C., and Vaughn, B.H., 2010, Monthly precipitation isoscapes (δ^{18}O) of the United States: Connections with surface temperatures, moisture source conditions, and air mass trajectories: Journal of Geophysical Research, v. 115, D21126, doi: 10.1029/2010JD014105.

Wahi, A.K., Hogan, J.F., Ekwurzel, B., Baillie, M.N., and Eastoe, C.J., 2008, Geochemical quantification of semiarid mountain recharge: Ground Water, v. 46, p. 414–425, doi: 10.1111/j.1745-6584.2007.00413.x.

Wood, W.W., and Sanford, W.E., 1995, Chemical and isotopic methods for quantifying ground-water recharge in a regional, semiarid environment: Ground Water, v. 33, p. 458–468, doi: 10.1111/j.1745-6584.1995.tb00302.x.

APPENDIX A: Isotope hydrology and cation data

Unit refers to the hydrostratigraphic unit: 11 = Quaternary alluvium, 10 = alluvium and/or Dockum/Chinle Group, 9 = Quaternary Basalt, 8 = Quaternary Basalt and/or Dakota Sandstone, 7 = Ogallala and/or Dakota Sandstone, 6 = Graneros Shale/Greenhorn Limestone, 5 = Graneros Shale and/or Dakota Sandstone, 4 = Dakota Sandstone, 3 = Morrison Formation, 2 = Dockum/Chinle Group, 1 = Sangre de Cristo Formation.

Sample	Unit	elevation (m)	dD	d18O	Na	K	Mg	Ca
U9	11	1835	-93.6	-12.38	38.2	1.8	29.8	79.4
H11	10	1393	-46.9	-6.33	226.7	3.3	28.5	25.8
H12	10	1390	-44.3	-5.44	153.0	3.4	64.6	64.2
H13	10	1372	-46.1	-6.76	315.1	3.3	43.8	41.6
H14	10	1360	-43.5	-6.28	364.4	2.7	33.3	19.1
H15	10	1373	-42.7	-4.37	289.0	3.5	19.3	96.0
H16	10	1361	-50.0	-7.58	232.6	2.2	3.6	6.1
H2	10	1419	-46.8	-5.95	64.0	6.4	36.0	45.7
H4	10	1362	-50.1	-6.53	119.4	5.2	42.1	28.5
H5	10	1337	-44.6	-5.56	197.2	5.6	45.9	22.7
H6	10	1394	-48.4	-6.93	73.1	2.6	15.3	42.7
H7	10	1381	-42.9	-5.45	111.4	4.6	17.2	11.3
H9	10	1369	-46.5	-5.64	319.8	4.6	40.3	18.9
C17	9	2402	-105.0	-13.54	17.1	3.8	10.7	29.3
M39	9	2275	-62.1	-8.76	13.6	2.0	13.6	34.3
M28	8	1992	-59.4	-8.37	18.2	2.2	11.8	57.7
U8	8	2079	-66.3	-8.97	32.6	2.5	27.3	72.1
U3	7	1431	-52.4	-8.22	17.3	2.7	14.8	46.9
H10	7	1622	-59.5	-9.32	75.8	4.6	19.8	48.6
H3	7	1656	-53.8	-7.88	65.5	6.2	26.0	36.4
M22	6	2153	-58.1	-8.10	50.5	4.4	41.1	75.8
C9	6	1893	-75.7	-9.53	186.5	1.1	77.5	207.8
C10	6	1975	-57.0	-8.04	19.7	2.2	17.2	39.3
C8	6	1839	-62.0	-7.96	610.3	3.2	416.0	640.7
M37	6	1927	-56.5	-7.77	78.2	2.4	25.7	102.2
C11	6	1949	-53.2	-7.21	43.6	3.5	15.4	62.2
C12	6	2021	-52.5	-7.40	52.2	0.2	11.7	18.1
C13	6	1832	-67.1	-9.46	1241.6	10.1	4.3	7.4
C14	6	2084	-55.4	-7.46	25.3	0.4	14.8	58.7
M32	6	1905	-59.7	-8.73	36.4	40.1	8.6	25.1
M36	6	1950	-51.8	-6.99	26.9	2.6	19.1	75.3
C15	6	2227	-78.3	-10.62	152.0	0.8	2.2	4.7
C16	6	1842	-56.9	-8.26	39.2	1.0	15.9	68.7
M21	6	2172	-58.2	-7.76	17.6	2.0	7.9	63.2
M14	6	1886	-58.8	-8.18	45.5	-	-	-

Sample	Unit	elevation (m)	dD	d18O	Na	K	Mg	Ca
M11	5	1966	-69.0	-9.14	78.1	6.3	22.1	47.3
M5	5	1905	-57.2	-7.68	110.3	2.3	26.4	41.8
M8	5	1936	-71.1	-10.44	198.7	3.9	3.7	10.8
C2	5	1855	-58.7	-7.74	853.7	3.3	1.8	3.0
C1	5	1785	-50.7	-7.41	310.6	10.6	82.9	135.5
C3	5	1787	-57.3	-7.86	871.8	14.4	8.4	11.5
C6	5	1895	-52.9	-7.73	117.1	4.8	37.8	109.9
C7	5	1844	-52.0	-7.54	826.5	9.7	5.9	7.1
C4	5	2026	-87.8	-11.54	55.1	1.6	22.2	55.1
C5	5	2069	-96.5	-13.23	97.8	2.4	18.8	51.2
M10	4	2035	-67.3	-9.20	56.4	4.2	19.6	55.5
M16	4	2080	-54.8	-7.54	37.4	-	-	-
M17	4	2043	-56.7	-7.63	-	-	-	-
M2	4	1814	-59.4	-8.93	67.1	4.4	19.0	53.2
M3	4	1924	-55.9	-7.36	57.1	4.0	15.2	66.8
M4	4	1786	-56.5	-8.01	66.2	2.8	18.3	74.6
M6	4	1955	-54.1	-7.27	44.5	2.4	24.3	41.2
M7	4	1979	-59.8	-8.35	20.6	2.3	12.4	49.3
M9	4	1986	-56.0	-7.63	45.8	3.7	21.7	63.6
U4	4	1553	-61.4	-8.61	164.3	6.0	20.5	28.8
U5	4	1517	-54.4	-8.80	16.1	4.2	24.0	46.2
M26	4	2171	-58.4	-7.95	85.7	4.0	14.5	44.6
M23	4	2159	-63.5	-9.06	71.1	1.6	19.8	19.8
M24	4	2149	-63.6	-8.82	69.4	1.5	21.3	22.4
M18	4	2138	-54.7	-7.92	52.5	2.4	22.1	29.7
M20	4	2147	-58.8	-8.29	22.5	1.4	10.5	67.5
M38	4	1854	-65.8	-9.09	170.8	6.0	13.5	31.1
M19	4	2159	-61.3	-8.37	185.3	1.0	4.8	7.2
M29	4	1945	-59.1	-8.42	13.6	2.0	13.6	34.3
M33	4	1843	-59.3	-8.35	46.8	5.5	31.3	42.2
M30	4	1978	-68.7	-9.56	100.0	2.3	12.5	36.1
M31	4	1871	-59.6	-8.33	37.9	3.5	16.0	71.4
M34	4	2084	-58.7	-8.61	81.5	2.5	8.5	23.7
U10	4	2062	-82.9	-11.16	32.0	3.9	17.1	33.6
H17	4	1650	-54.0	-7.38	24.9	4.0	18.1	33.3
H18	4	1677	-56.3	-7.92	19.1	4.2	18.8	35.9
U11	4	1935	-73.1	-9.77	76.2	4.5	24.1	50.5
M13	4	1881	-51.1	-7.13	43.3	-	-	-
M1	4	2155	-53.5	-7.34	39.5	4.2	28.7	46.9
U2	4	1934	-99.4	-13.70	56.7	1.6	36.2	108.4
M27	4	1984	-60.7	-8.49	26.6	3.2	20.0	36.9
H1	3	1353	-49.3	-7.38	107.3	5.9	31.4	62.2

Sample	Unit	elevation (m)	dD	d18O	Na	K	Mg	Ca
H8	3	1577	-53.0	-7.23	162.7	9.7	72.6	42.5
M15	3	2026	-67.7	-9.12	109.1	2.3	26.8	38.6
U1	2	1466	-41.7	-5.69	49.4	-	-	-
U6	2	1635	-62.9	-8.70	92.9	4.5	51.8	134.8
U7	2	1670	-62.4	-9.34	81.6	4.1	79.0	207.1
M25	2	2223	-66.7	-9.48	16.2	1.6	18.9	52.3
M12	1	2291	-67.0	-9.46	32.3	-	-	-
M35	1	2223	-59.6	-8.58	22.8	2.6	11.6	31.6

APPENDIX B: Anion and inorganic carbon data

Unit refers to the hydrostratigraphic unit: 11 = Quaternary alluvium, 10 = alluvium and/or Dockum/Chinle Group, 9 = Quaternary Basalt, 8 = Quaternary Basalt and/or Dakota Sandstone, 7 = Ogallala and/or Dakota Sandstone, 6 = Graneros Shale/Greenhorn Limestone, 5 = Graneros Shale and/or Dakota Sandstone, 4 = Dakota Sandstone, 3 = Morrison Formation, 2 = Dockum/Chinle Group, 1 = Sangre de Cristo Formation. Values for pH were calculated using alkalinity and DIC.

Sample	Unit	elevation (m)	F	Cl	NO3 as NO3	SO4	Alkalinity (meq/L)	DIC (mM)	pH	d13C-DIC
U9	11	1835	0.3	5.4	0.3	16.2	6.40	7.18	7.29	-11.39
H11	10	1393	2.3	39.2	1.7	154.2	8.95	9.69	7.46	-6.61
H12	10	1390	1.2	41.6	0.1	260.0	8.56	9.38	7.40	-10.80
H13	10	1372	1.7	108.6	1.1	348.4	9.22	10.18	7.36	-2.00
H14	10	1360	2.6	72.4	2.5	333.0	9.70	10.20	7.67	-2.00
H15	10	1373	0.3	254.6	12.5	304.4	4.62	4.92	7.57	-4.77
H16	10	1361	2.1	35.2	0.2	173.4	5.92	6.19	7.72	-5.66
H2	10	1419	1.4	19.0	0.4	59.6	6.46	6.80	7.66	-8.06
H4	10	1362	2.0	21.1	0.7	145.4	6.38	6.96	7.43	-6.85
H5	10	1337	2.6	26.8	0.3	254.6	7.41	7.85	7.61	-3.71
H6	10	1394	0.4	46.8	0.0	47.4	4.33	5.00	7.19	-4.62
H7	10	1381	0.7	17.1	0.0	54.7	5.18	5.37	7.82	-5.77
H9	10	1369	2.9	45.0	1.4	398.0	8.26	8.79	7.57	-3.77
C17	9	2402	0.2	2.5	4.7	4.6	3.15	2.63	9.77	-11.64
M39	9	2275	0.2	2.6	0.4	1.3	3.18	3.39	7.56	-7.80
M28	8	1992	0.8	11.7	0.1	78.5	4.52	4.39	8.86	-8.62
U8	8	2079	0.7	32.0	3.2	14.3	4.75	5.20	7.40	-7.43
U3	7	1431	0.7	6.4	2.8	21.7	3.45	3.88	7.28	-5.60
H10	7	1622	2.1	16.0	1.6	101.8	4.69	5.91	6.96	-8.48
H3	7	1656	2.6	8.9	0.0	67.9	5.18	5.92	7.23	-7.36
M22	6	2153	0.3	11.0	0.6	182.6	5.34	5.38	8.51	-9.56
C9	6	1893	0.7	18.7	0.0	874.2	6.43	7.23	7.29	-10.20
C10	6	1975	0.8	9.2	3.3	19.7	3.33	3.34	8.90	-4.55
C8	6	1839	0.1	138.4	0.0	4512.8	12.21	13.14	7.50	-11.72
M37	6	1927	0.6	57.3	2.8	131.4	4.92	5.31	7.48	-7.55
C11	6	1949	2.8	6.2	-	31.4	5.65	5.79	7.99	-7.63
C12	6	2021	3.1	2.6	0.0	26.7	3.33	3.51	7.65	-7.47
C13	6	1832	2.4	756.6	0.0	1.4	29.64	-	-	-
C14	6	2084	1.7	3.2	0.0	94.3	3.50	3.45	8.55	-6.95
M32	6	1905	0.4	57.0	0.3	1.4	2.62	2.74	7.72	-8.27
M36	6	1950	0.4	9.7	1.2	20.0	4.64	4.90	7.63	-6.57
C15	6	2227	0.5	5.2	0.0	4.2	6.16	6.18	8.87	-12.34
C16	6	1842	0.5	10.7	1.4	21.3	4.18	4.53	7.46	-5.90
M21	6	2172	0.3	4.9	0.9	20.1	4.06	4.05	7.77	-6.17

Sample	Unit	elevation (m)	F	Cl	NO3 as NO3	SO4	Alkalinity (meq/L)	DIC (mM)	pH	d13C-DIC
M14	6	1886	0.4	13.2	0.7	38.5	4.80	5.13	7.55	-7.53
M11	5	1966	0.7	18.7	0.1	72.8	5.84	6.29	7.49	-4.57
M5	5	1905	1.0	23.0	0.0	1.0	8.13	9.17	7.27	-13.01
M8	5	1936	1.0	13.6	0.0	97.5	6.85	7.31	7.56	-6.07
C2	5	1855	1.8	45.2	0.0	128.0	33.73	-	-	-
C1	5	1785	0.9	35.4	0.0	1038.0	5.67	7.69	6.83	-8.39
C3	5	1787	2.2	83.5	0.0	107.8	37.57	-	-	-
C6	5	1895	0.5	4.1	0.3	483.2	3.77	3.78	8.96	-7.13
C7	5	1844	1.3	32.7	0.0	668.4	21.92	-	-	-
C4	5	2026	0.2	6.9	0.3	120.6	4.35	4.62	7.59	-11.97
C5	5	2069	0.3	15.3	0.4	97.4	5.85	6.11	7.73	-12.41
M10	4	2035	0.7	24.5	0.2	65.0	5.01	5.47	7.42	-5.84
M16	4	2080	0.8	18.1	0.8	74.0	4.13	4.86	7.14	-6.37
M17	4	2043	-	-	-	-	5.57	4.97	9.51	-8.25
M2	4	1814	0.9	11.6	0.1	50.1	5.78	6.39	7.36	-7.10
M3	4	1924	1.0	26.0	0.6	66.2	5.09	5.54	7.43	-6.90
M4	4	1786	0.8	42.2	0.4	117.6	4.54	4.98	7.39	-8.50
M6	4	1955	1.0	15.1	0.0	49.3	4.38	4.88	7.32	-5.80
M7	4	1979	0.7	10.2	0.9	30.8	3.55	3.66	7.89	-7.00
M9	4	1986	1.1	26.1	0.7	48.3	5.22	6.17	7.12	-6.00
U4	4	1553	2.1	15.7	0.1	159.2	6.87	6.74	8.66	-4.36
U5	4	1517	0.6	31.2	6.7	29.9	3.08	3.04	8.45	-1.50
M26	4	2171	0.8	19.2	1.5	52.0	5.42	5.73	7.62	-4.75
M23	4	2159	0.4	3.8	0.1	26.8	5.17	5.23	8.32	-7.77
M24	4	2149	0.3	3.7	0.1	23.8	5.27	5.65	7.52	-12.96
M18	4	2138	0.4	8.5	0.5	31.4	4.63	4.71	8.14	-7.16
M20	4	2147	0.4	5.7	0.6	14.0	4.82	5.75	7.09	-8.78
M38	4	1854	0.6	31.8	2.1	44.2	8.13	8.49	7.73	-5.82
M19	4	2159	1.2	6.8	0.1	62.1	6.29	5.84	9.30	-7.43
M29	4	1945	0.5	8.4	0.3	27.9	3.67	4.29	7.15	-5.99
M33	4	1843	0.8	10.0	0.0	29.9	5.69	6.04	7.59	-8.96
M30	4	1978	0.3	13.4	0.0	109.2	4.58	4.80	7.70	-9.79
M31	4	1871	1.0	21.5	0.0	60.4	4.76	5.24	7.38	-7.16
M34	4	2084	0.4	7.2	-	46.6	4.30	4.46	7.81	-9.90
U10	4	2062	0.7	10.5	2.8	7.0	3.33	3.64	7.41	-6.37
H17	4	1650	0.9	8.3	1.1	4.8	3.34	3.55	7.58	-3.53
H18	4	1677	0.8	11.7	1.2	4.6	3.24	3.57	7.37	-3.66
U11	4	1935	1.4	10.6	0.0	85.8	5.72	5.97	7.74	-6.34
M13	4	1881	0.7	11.2	0.9	35.0	6.36	6.61	7.79	-10.16
M1	4	2155	0.7	12.5	0.1	33.5	5.47	5.80	7.60	-5.30
U2	4	1934	0.6	14.9	0.0	286.6	4.88	5.81	7.10	-9.90
M27	4	1984	0.6	5.1	0.1	27.9	3.89	4.04	7.79	-6.04

104

Sample	Unit	elevation (m)	F	Cl	NO3 as NO3	SO4	Alkalinity (meq/L)	DIC (mM)	pH	d13C-DIC
H1	3	1353	0.7	21.5	1.0	133.2	6.35	6.93	7.42	-6.80
H8	3	1577	4.8	50.0	0.4	380.0	5.70	6.26	7.39	-6.40
M15	3	2026	0.3	11.6	0.0	59.5	4.45	4.60	7.84	-9.54
U1	2	1466	0.5	27.4	-	68.3	7.82	-	-	-
U6	2	1635	0.3	10.0	12.6	389.6	6.24	7.18	7.20	-9.11
U7	2	1670	0.6	17.2	4.8	648.2	6.76	7.94	7.14	-10.20
M25	2	2223	0.2	3.7	0.4	12.5	4.59	4.56	8.20	-9.79
M12	1	2291	0.3	5.0	1.6	10.1	5.63	5.80	7.91	-9.13
M35	1	2223	0.3	4.6	1.0	8.8	3.15	3.01	9.07	-7.67